THE HIGH RESOLUTION ELECTRONIC SPECTRUM OF PROPYNAL

A thesis submitted to the University of London
in partial fulfilment of the regulations for
the degree of Doctor of Philosophy
by

Simon Anthony Edwards

Department of Chemistry
University College London

February 1991

ACKNOWLEDGEMENTS

I would like to thank Dr. J.E. Parkin for his advice and guidance throughout this work and also Prof. J.H. Callomon for numerous helpful discussions and the gift of his sample of propyn-1-ol-2d_1. I would also like to thank Mr. K. Tavladorakis for communicating the results of his analysis of the infrared spectra of propynal-d_1 and propynal-d_1,d_2 prior to publication. I am indebted to Dr. M. Dworetsky for his assistance with the microdensitometry and to Dr. C. Cossart and Dr. D. Cossart for their hospitality and the use of the comparator at the Université Paris-Sud.

Finally I would like to thank the Science and Engineering Research Council for their financial support.

ABSTRACT

The one photon ultraviolet absorption spectra of propynal (HCCCHO) and the three deuterated compounds have been recorded under a higher resolution than has previously been reported. The spectrum arising from the $\tilde{A}^1A'' \leftarrow \tilde{X}^1A'$ ($S_1 \leftarrow S_0$) transition has been studied in detail and the existing vibrational analysis has been extended. Rotational analyses of many of the vibrational bands in this spectrum have been carried out. Several vibrational and rotational perturbations have been observed and for many of these coupling matrix elements have been calculated. Where possible perturbing levels have been suggested.

Existing studies on the ground electronic states of these compounds have been correlated and improved values of the molecular constants have been obtained. These values have been further enhanced from rotational analyses of the origin and lower vibrational bands of the $S_1 \leftarrow S_0$ spectrum by weighted least squares fits to both lower and excited states.

On excitation of higher vibrational levels in the S_1 state of propynal an overall broadening and diffuseness of rotational structure is observed. This has been charted throughout the spectrum and lifetimes of the levels concerned have been estimated from the linewidths. These observations are compared to previous fluorescence studies and interpreted in terms of vibrationally and rotationally

dependent predissociation.

The origin band of the $T_1 \leftarrow S_0$ transition is reported for the molecules HCCCDO and DCCCDO for the first time and partial rotational analyses are attempted.

The kinetics and mechanisms of energy decay from the S_1 and T_1 states of propynal are discussed on the basis of the results of this and previous studies.

CONTENTS

	PAGE
CHAPTER I INTRODUCTION.	12
I.1 Electronic spectroscopy.	12
I.1.1 Propynal.	12
I.2 Electronic transitions.	13
I.2.1 Electronic energy levels.	14
I.2.2 Vibronic energy levels.	15
I.2.3 Vibrational perturbations.	19
I.2.4 Rovibronic energy levels.	20
I.2.5 Rotational perturbations.	25
I.2.6 Singlet-triplet interactions.	28
CHAPTER II EXPERIMENTAL.	31
II.1 Materials.	31
II.2 Ultraviolet spectra.	32
II.3 Microdensitometry.	33
II.4 Least squares fitting.	34
II.5 Spectral simulations.	36
CHAPTER III ELECTRONIC GROUND STATE.	38
III.1 Vibrationless levels.	38
III.2 Vibrationally excited levels.	46

PAGE

CHAPTER IV THE ULTRAVIOLET SPECTRUM. 49

IV.1 General structure of the ultraviolet spectrum. 49

IV.2 The $\tilde{A}^1A''$ ⟵ $\tilde{X}^1A'$ transition. 52

IV.2.1 Vibrational analysis. 52

IV.2.2 General rotational structure. 53

IV.2.3 Rotational analyses of the origin bands. 61

IV.2.4 Fundamentals, overtones and combination bands. 70

IV.2.5 Hot bands. 111

IV.2.6 Sequences and cross sequences. 113

IV.3 The $\tilde{a}^3A''$ ⟵ $\tilde{X}^1A'$ transition. 116

CHAPTER V ENERGY DECAY OF THE EXCITED ELECTRONIC STATES. 121

V.1 Energy decay from the S_1 electronic state. 122

V.2 Energy decay from the T_1 electronic state. 135

V.3 Coupling between the S_1 and T_1 electronic states. 136

CHAPTER VI DISCUSSION. 138

APPENDIX 1 Additions to the vibrational analyses of HCCCHO, DCCCHO and HCCCDO. 142

APPENDIX 2 Vibrational analysis of DCCCDO. 145

PAGE

APPENDIX 3 Zero order frequencies and anharmonicity coefficients of the S_1 state. 150

APPENDIX 4 The dependence of $(A-\bar{B})$ on vibrational level in the S_1 state. 154

REFERENCES 155

TABLES

	PAGE
1.1 Character table for the C_s point group.	15
1.2 Rotational selection rules for asymmetric rotors.	25
1.3 Vibrational and rotational selection rules for Coriolis interactions.	28
3.1 Molecular constants of HCCCHO in the $\tilde{X}^1A'$ state.	40
3.2 Molecular constants of DCCCHO in the $\tilde{X}^1A'$ state.	41
3.3 Molecular constants of HCCCDO in the $\tilde{X}^1A'$ state.	42
3.4 Molecular constants of DCCCDO in the $\tilde{X}^1A'$ state.	42
3.5 Fundamental frequencies of propynal in the $\tilde{X}^1A'$ state.	47
4.1 Fundamental frequencies of propynal in the $\tilde{A}^1A''$ state.	54
4.2 Molecular constants of HCCCHO in the $\tilde{A}^1A''$ state.	62
4.3 Molecular constants of DCCCHO in the $\tilde{A}^1A''$ state.	63
4.4 Molecular constants of HCCCDO in the $\tilde{A}^1A''$ state.	64
4.5 Molecular constants of DCCCDO in the $\tilde{A}^1A''$ state.	65
4.6 Calculated frequencies and intensities of 1_0^1.	71
4.7 Molecular constants of the 4^1 level of HCCCDO.	81
4.8 Molecular constants of the 4^3 level of HCCCDO.	82
4.9 Molecular constants of the 4^2 level of DCCCDO.	83
4.10 Molecular constants of the 4^3 level of DCCCDO.	84
4.11 The levels 4^4 of HCCCDO and DCCCDO.	85
4.12 ν_4' of HCCCDO and DCCCDO.	87
4.13 Rotational constants of band 1 of HCCCHO.	93

PAGE

4.14 Rotational constants of band 2 of HCCCHO. 93

4.15 Rotational constants of band 3 of HCCCHO. 94

4.16 Fermi resonance of ν_4' and $\nu_5' + \nu_9'$ of HCCCHO. 99

4.17 Molecular constants of the 6^1 level of HCCCDO. 101

4.18 Molecular constants of the 6^1 level of DCCCDO. 102

4.19 Fermi resonance between ν_6' and $2\nu_{10}'$ of HCCCHO. 105

4.20 The calculated energy levels of the vibronic levels 6^1 and 10^2 of HCCCHO. 106

4.21 The levels 10^1. 109

4.22 The levels 12^1. 110

4.23 Coriolis coupling of ν_9'' and ν_{12}''. 112

4.24 Fundamental frequencies of propynal in the $\tilde{a}^3A''$ state. 118

4.25 Partial analyses of the $T_1 \leftarrow S_0$ origin bands. 119

4.26 Molecular constants of HCCCHO in the $\tilde{a}^3A''$ state. 120

FIGURES

	PAGE
3.1 Ground state structure of HCCCHO.	45
4.1 The 0_0^0 band of HCCCHO.	55
4.2 The 10_0^1 band of HCCCHO.	56
4.3 The 12_0^1 band of HCCCHO.	57
4.4 The 10_0^1 band of DCCCDO.	58
4.5 The 0_0^0 band of HCCCDO.	67
4.6 The bands 2_0^1 and $4_0^1 6_0^1$ of HCCCDO.	72
4.7 Perturbation in the 2_0^1 band of HCCCDO.	73
4.8 Energy level diagram for the levels 2^1 and $4^1 6^1$ of HCCCDO.	74
4.9 Perturbation in the 2_0^1 band of DCCCDO.	77
4.10 Perturbation in the $2_0^1 4_0^1$ band of DCCCDO.	78
4.11 Perturbation in the 3_0^1 band of HCCCHO.	80
4.12 The 4_0^1 band of HCCCDO.	86
4.13 Perturbation in the 4_0^2 band of HCCCDO.	88
4.14 Fluorescence spectrum of the bands 1, 2 and 3.	91
4.15 The absorption spectrum of HCCCHO in the 4_0^1 region.	92
4.16 Plot of $\bar{B}' - D'_{JK} K'^2$ against K'^2 for band 1.	96
4.17 The 6_0^1 band of HCCCDO.	103
4.18 The bands 6_0^1 and 10_0^2 of HCCCHO.	104
4.19 The 0_0^0 band of the $T_1 \leftarrow S_0$ transition of HCCCDO.	117
5.1 Energy level diagram for the decay of the S_1 and T_1 states.	121

PAGE

5.2 Linebroadening in the 4_0^n progression of HCCCDO. 124

(a) $^PQ_7$ to $^PQ_9$ of the 0_0^0 band of HCCCDO. 124

(b) $^PQ_7$ to $^PQ_9$ of the 4_0^1 band of HCCCDO. 125

(c) $^PQ_7$ to $^PQ_9$ of the 4_0^2 band of HCCCDO. 126

(d) $^PQ_7$ to $^PQ_9$ of the 4_0^3 band of HCCCDO. 127

(e) $^PQ_7$ to $^PQ_9$ of the 4_0^4 band of HCCCDO. 128

5.3 Plot of linewidth against excess vibrational energy of the S_1 state. 130

(a) HCCCHO. 130

(b) DCCCHO. 130

(c) HCCCDO. 131

(d) DCCCDO. 131

5.4 Plot of quantum yield of fluorescence, phosphorescence and photodissociation against excess vibrational energy. 132

(a) Fluorescence. 132

(b) Phosphorescence. 132

(c) Photodissociation. 133

CHAPTER I INTRODUCTION

I.1 ELECTRONIC SPECTROSCOPY

Electronic spectroscopy is the most direct method of obtaining information about the various electronic states of a molecule and as such is important to our understanding of its chemical and physical properties. The energy of a photon absorbed or emitted during an electronic transition gives directly the energy difference between the molecular energy levels involved. These energy levels can be described by quantum mechanics although for even relatively small molecules we have to use approximations in order to simplify the problem. The study of an electronic spectrum is therefore a test for the reliability of these approximations and can give information on how and when they break down.

I.1.1 PROPYNAL

The propynal molecule (figure 3.1, page 45) is structurally the simplest conjugated carbonyl compound and its chemical properties are typical of those of conjugated aldehydes. The electronic spectrum of the molecule is of interest because the π^* orbital can delocalise over the whole C≡C-C=O chain and it is to be expected that the

structures and force fields of the carbonyl group and the ethynyl group will be affected by electronic excitation.

Propynal is generally favourable for spectroscopic analysis since, as the molecule has only six atoms, the spectra are relatively simple and may be fairly well described in standard spectroscopic terms. The rotational analyses of the spectra are simplified since propynal is only slightly asymmetric and therefore only levels with low K are appreciably displaced from symmetric top values.

The dynamics of energy decay from the excited electronic states of propynal are of particular interest because it is an "intermediate case" molecule [1] and therefore features both quantum and statistical aspects of intramolecular coupling.

I.2 ELECTRONIC TRANSITIONS

The total energy of a polyatomic molecule can be expressed by the Schrödinger equation $H\psi = E\psi$. To a good approximation [2], neglecting the effects of spin, the energy E can be separated into the terms

$$E = E_e + E_v + E_r + E_t \qquad (1.1)$$

where the terms are due to the electronic, vibrational, rotational and translational energies respectively. Similarly we can factorise the eigenfunction into the parts

$$\psi = \psi_e \psi_v \psi_r \psi_t . \qquad (1.2)$$

For the present discussion we do not need to consider the translational energy.

I.2.1 ELECTRONIC ENERGY LEVELS

For molecules of C_s symmetry such as propynal there are only two types of electronic state, those whose eigenfunctions are symmetric and those whose eigenfunctions are antisymmetric with respect to reflection in the plane of symmetry. These symmetry species are designated $^{2S+1}A'$ and $^{2S+1}A''$ respectively where 2S + 1 is the multiplicity of the state.

The general selection rule for transitions between the two electronic states ψ'_e and ψ''_e is

$$R_e = \int \psi'^{*}_e \mathbf{M} \, \psi''_e d\tau_e \neq 0 \qquad (1.3)$$

where ψ'' denotes the lower state, ψ' denotes the upper state and $\mathbf{M}$ is the electric dipole moment vector. It can be shown that this requirement is met only if $\Gamma(\psi'_e) \times \Gamma(\psi''_e)$ belongs to the same species as one of the components of $\mathbf{M}$. The components of $\mathbf{M}$ transform in the same way as the coordinates x,y,z which for the C_s point group corresponds to either A' or A'' symmetry (see table 1.1). Thus for propynal all electronic transitions are allowed by the above selection rule.

If the spin-orbit interaction is small the spin selection rule is $\Delta S = 0$, that is only transitions between

Table 1.1. Character table for the C_s point group

C_s	E	σ_{xy}		
A'	+ 1	+ 1	x, y, R_z	$\begin{cases} x^2, y^2 \\ z^2, xy \end{cases}$
A"	+ 1	- 1	z, R_x, R_y	yz, xz

states of the same multiplicity are formally allowed. This rule does not hold if the spin-orbit coupling is not negligibly small but the previously forbidden transition would be expected to be weak. Spin-orbit coupling is discussed in more detail in section I.2.6.

I.2.2 VIBRONIC ENERGY LEVELS

The twelve normal modes of vibration of the propynal molecule divide into the symmetry species 9A' + 3A".

The vibrational term values of a slightly anharmonic oscillator [3] are given by

$$G(v_1,v_2,v_3,\ldots) = \sum_i \omega_i(v_i + d_i/2) + \sum_{i\le k}\sum x_{ik}(v_i + d_i/2)(v_k + d_k/2) + \sum_{i\le k}\sum g_{ik}l_i l_k + \text{higher terms} \qquad (1.4)$$

where ω_i are the zero order vibrational frequencies, v_i and v_k are the vibrational quantum numbers, x_{ik} and g_{ik} are comparatively small anharmonicity constants, d_i and d_k are the degeneracies of the vibrations and l_i and l_k are

angular momentum quantum numbers for the degenerate vibrations. For non-degenerate vibrations $l_i = g_{ik} = 0$.

Referring the vibrational levels to the zero point level, we have for non-degenerate vibrations

$$G_0(v_1, v_2, v_3, \ldots) = \sum_i \omega_i^c v_i + \sum_{i \leq k} \sum x_{ik}^c v_i v_k \qquad (1.5)$$

where $\omega_i^c = \omega_i + x_{ii} + \frac{1}{2}\sum_{k \neq i} x_{ik}$ and $x_{ik}^c \simeq x_{ik}$.

The transition moment for a transition between vibrational levels of different electronic states is given by

$$R_{ev} = \int \psi'^{*}_{ev} \, \mathbf{M} \, \psi''_{ev} d\tau_{ev} \qquad (1.6)$$

and the requirement for a transition to be allowed is that $R_{ev} \neq 0$. Using the approximation that the electronic transition moment is independent of nuclear motion we can write $\psi_{ev} = \psi_e \psi_v$ and hence we obtain

$$R_{ev} = \iint \psi'^{*}_e \psi'^{*}_v \, \mathbf{M} \, \psi''_e \psi''_v d\tau_e d\tau_v \qquad (1.7)$$

$$= R_e \int \psi'^{*}_v \psi''_v d\tau_v + \int \psi'^{*}_e \psi''_e d\tau_e \int \psi'^{*}_v \mathbf{M} \, \psi''_v d\tau_v .$$

For transitions between vibrational levels of the same electronic state we have $\int \psi'^{*}_v \psi''_v d\tau_v = 0$ and $\int \psi'^{*}_e \psi''_e d\tau_e = 1$ and thus the transition moment is given by $\int \psi'^{*}_v \mathbf{M} \, \psi''_v d\tau_v$.

Again from table 1.1 we see that no purely vibrational transition is symmetry forbidden in propynal and that the transitions $A' \leftrightarrow A'$ and $A'' \leftrightarrow A''$ have transition moments

lying in the molecular plane and the transitions A' ↔ A" have moments perpendicular to the plane. For purely vibrational transitions the harmonic selection rule is $\Delta v_i = \pm 1$ and for an anharmonic oscillator vibrational overtone transitions, although allowed, are generally weak. In addition we have the selection rules that for transitions to be allowed in the infrared spectrum there must be a change of the dipole moment of the molecule, and in the Raman spectrum there must be a change in the amplitude of the induced dipole moment.

For vibrational transitions between different electronic states $\int \psi_e'^* \psi_e'' d\tau_e = 0$ and the transition moment is given by $R_{ev} = R_e \int \psi_v'^* \psi_v'' d\tau_v$. The first factor is in general a constant for a given electronic transition and has been discussed above. The second factor is the Condon integral for the vibrational levels and is non-zero if $\psi_v'^* \psi_v''$ is totally symmetric. These integrals together with the relative populations of the levels determine the relative intensities of the vibrational bands observed in the electronic spectrum. The normal Boltzmann distribution means that under thermal equilibrium the most intense transitions will normally originate from the ground vibrational level. Extending the Franck-Condon principle [4] to polyatomic molecules it follows that, if there is a significant change in molecular geometry on electronic excitation, bands due to transitions from the same initial level will be most intense for transitions to vibrational states where the particular vibrations distort the molecular configuration into a configuration similar to

that of the initial state. This will lead to a progression in the corresponding vibration and the intensity maximum of the progression will in general be at a non-zero value of ν'.

From the above discussion we would expect the vibrational structure of the absorption spectrum of an allowed electronic transition of a polyatomic molecule to be characterised by an intense origin band, progressions in one or more of the symmetrical vibrations and weaker sequences from the low frequency vibrations of the initial state. The low frequency vibrations are mostly nontotally symmetric and are generally observed in $\Delta\nu = 0$ sequences. Cross sequences from a low frequency vibration ν_i'' to a vibration ν_k' in the excited state can occur if there is some reorganization of the normal coordinates on electronic excitation. Duschinsky [5] has pointed out that in general symmetry considerations restrict the mixing of normal modes between two electronic states to modes of the same symmetry species.

It can happen that transitions to vibrational levels occur which contravene the selection rule that $\psi_v'^{*}\psi_v''$ is totally symmetric. This is due to the break down of the approximation that the vibronic eigenfunction is separable into electronic and vibrational parts. The forbidden vibronic bands can acquire their intensity by interaction with other allowed electronic levels [6]. An improved approximation of R_{ev} is obtained by expanding the electronic transition moment as a Taylor series in the normal coordinates Q_i of the vibrations:

$$R_e = (R_e)_o + \sum_i \left[\frac{\partial R_e}{\partial Q_i} \right]_o Q_i + \frac{1}{2!} \sum_{i,k} \left[\frac{\partial^2 R_e}{\partial Q_i \partial Q_k} \right]_o Q_i Q_k + \cdots \qquad (1.8)$$

where the subscript 0 refers to the equilibrium configuration of the molecule. Truncating at the second term we obtain

$$R_{ev} = (R_e)_o \int \psi'_v \psi''_v d\tau_v + \sum_s \left[\frac{\partial R_e}{\partial Q_s} \right]_o \int \psi'_v Q_s \psi''_v d\tau_v + \sum_a \left[\frac{\partial R_e}{\partial Q_a} \right]_o \int \psi'_v Q_a \psi''_v d\tau_v \qquad (1.9)$$

where the vibrations have been separated into those which are totally symmetric (s) and those which are non-totally symmetric (a). The third term in this expansion accounts for the occurrence of non-totally symmetric vibrations in an electronically allowed spectrum.

I.2.3 VIBRATIONAL PERTURBATIONS

The treatment given above breaks down if two vibrational levels would be nearly degenerate. In this case the two levels can interact such that the lower level is pushed down in energy and the higher one is pushed up. The interaction is called a Fermi resonance [7] and there is a mixing of the wave functions of the unperturbed states such that in a Fermi diad the wave functions of the perturbed states ψ_i, ψ_k are linear combinations of those of the unperturbed states ψ_i^c, ψ_k^o. When the separation between the

unperturbed levels is zero the perturbed levels are equal mixtures of the two and we cannot distinguish between them. A further result of the mixing of states is that vibrational bands which would otherwise be weak may gain intensity from an interaction with a stronger band. Using first-order perturbation theory for the case of two close levels E_i^c and E_k^o we obtain the energy shift ΔE due to the interaction from the determinant

$$\begin{vmatrix} E_i^c - \Delta E & W \\ W & E_k^o - \Delta E \end{vmatrix} = 0$$

which gives $\Delta E = \frac{1}{2}(E_i^c + E_k^o) \pm \frac{1}{2}\sqrt{(4W^2 + \delta^2)}$ where δ is the separation between the unperturbed levels and W is the interaction energy.

I.2.4 ROVIBRONIC ENERGY LEVELS

The rotational Hamiltonian of a rigid molecule is given by $H_r(\text{rigid}) = B_x J_x^2 + B_y J_y^2 + B_z J_z^2$ where the rotational constants are given by $B_\alpha = \hbar^2/2hcI_\alpha$, with I_α the principal moments of inertia, and the J_α are the components of total angular momentum $\underset{\sim}{J}$ about the principal axes given by $\underset{\sim}{J}^2 = J_x^2 + J_y^2 + J_z^2$. The matrices of $\underset{\sim}{J}^2$ and J_z are diagonal with eigenvalues $J(J + 1)$ and k. For singlet states the allowed values of the quantum numbers are $J = 0, 1, 2, \cdots$ and $k = -J, -J + 1, \cdots, J - 1, J$. The molecular axes are usually labelled a, b and c where the rotational constants are in the order $A \geq B \geq C$. For an asymmetric top the energy

levels are labelled by considering the two limiting cases (1) the prolate symmetric top with A > B = C and (2) the oblate symmetric top with A = B > C. In case (1) the energy eigenfunction is an eigenfunction of $|J_a|$ with eigenvalue $K_a = |k|$, whereas in case (2) it is an eigenfunction of $|J_c|$ with eigenvalue K_c. For intermediate cases each level is characterised by the set of numbers J_{K_a,K_c} where the energy increases with K_a and decreases with K_c and $K_a + K_c = J$ or $J + 1$.

Slight deviations from this model arise from the non-rigidity of molecules and this is allowed for by introducing higher-order terms associated with centrifugal distortion into the Hamiltonian. The Hamiltonian can then be written as [8]

$$H_r = \sum_{\alpha} B_\alpha J_\alpha^2 + \sum_{\alpha\beta} T_{\alpha\beta} J_\alpha^2 J_\beta^2 + \sum_{\alpha} \Phi_{\alpha\alpha\alpha} J_\alpha^6 + \sum_{\alpha\neq\beta} \Phi_{\alpha\alpha\beta}(J_\alpha^4 J_\beta^2 + J_\beta^2 J_\alpha^4)$$

$$+ \Phi_{xyz}(J_x^2 J_y^2 J_z^2 + J_z^2 J_y^2 J_x^2) \qquad (1.10)$$

where the coefficients are real. This form of the rotational Hamiltonian is convenient for the calculation of the molecular constants from the structure and potential constants of the molecule. The quartic terms in equation 1.10 are related to the normal coordinates of the molecule by the expressions

$$T_{\alpha\alpha} = -\frac{\hbar^3}{8I_\alpha^4} \sum_k \left(\frac{a_k^{(\alpha\alpha)}}{\omega_k} \right)^2 \qquad (1.11a)$$

$$T_{\alpha\beta} = -\frac{\hbar^3}{8I_\alpha^2 I_\beta^2} \sum_k \left(\frac{a_k^{(\alpha\alpha)} a_k^{(\beta\beta)}}{\omega_k \omega_k} \right) - \frac{\hbar^3}{4I_\alpha^2 I_\beta^2} \sum_k \left(\frac{a_k^{(\alpha\beta)}}{\omega_k} \right)^2 \qquad (1.11b)$$

where $a_k^{(\alpha\alpha)}$ is the derivative of the instantaneous moment of inertia I_α along the α axis by the k^{th} normal coordinate and ω_k is the k^{th} vibrational wavenumber.

The rotational Hamiltonian for asymmetric rotor molecules has been expressed by Watson [8] in a form which is more convenient for empirical fits to observed spectra. Using the I^r representation that b = x, c = y and a = z the form of this A reduction of the Hamiltonian becomes

$$\tilde{H}_{rot}^{(A)} = B_x^{(A)} J_x^2 + B_y^{(A)} J_y^2 + B_z^{(A)} J_z^2 \qquad (1.12)$$

$$- \Delta_J (\underset{\sim}{J}^2)^2 - \Delta_{JK} \underset{\sim}{J}^2 J_z^2 - \Delta_K J_z^4$$

$$- \tfrac{1}{2} \left[\delta_J \underset{\sim}{J}^2 + \delta_K J_z^2 , J_+^2 + J_-^2 \right]_+$$

$$+ \Phi_J (\underset{\sim}{J}^2)^3 + \Phi_{JK} (\underset{\sim}{J}^2)^2 J_z^2 + \Phi_{KJ} \underset{\sim}{J}^2 J_z^4 + \Phi_K J_z^6$$

$$+ \tfrac{1}{2} \left[\phi_J (\underset{\sim}{J}^2)^2 + \phi_{JK} \underset{\sim}{J}^2 J_z^2 + \phi_K J_z^4 , J_+^2 + J_-^2 \right]_+$$

where $J_\pm = J_x \pm i J_y$. The expressions for the submatrices then have the form

$$E_{k,k} = \langle J,k | \tilde{H}_{rot}^{(A)} | J,k \rangle = \tfrac{1}{2} \left[B_x^{(A)} + B_y^{(A)} \right] J(J+1) \qquad (1.13a)$$

$$+ \left\{ B_z^{(A)} - \tfrac{1}{2} \left[B_x^{(A)} + B_y^{(A)} \right] \right\} k^2 - \Delta_J J^2 (J+1)^2$$

$$- \Delta_{JK} J(J+1) k^2 - \Delta_K k^4 + \Phi_J J^3 (J+1)^3 + \Phi_{JK} J^2 (J+1)^2 k^2$$

$$+ \Phi_{KJ} J(J+1) k^4 + \Phi_K k^6 ,$$

$$E_{k\pm2,k} = \langle J,k \pm 2|\tilde{H}^{(A)}_{rot}|J,k\rangle = \Big\{ \tfrac{1}{4}\left[B_x^{(A)} - B_y^{(A)}\right] \qquad (1.13b)$$

$$- \delta_J J(J+1) - \tfrac{1}{2}\delta_K\left[(k\pm2)^2 + k^2\right] + \phi_J J^2(J+1)^2$$

$$+ \tfrac{1}{2}\phi_{JK} J(J+1)\left[(k\pm2)^2 + k^2\right] + \tfrac{1}{2}\phi_K\left[(k\pm2)^4 + k^4\right]\Big\}$$

$$\times \Big\{\left[J(J+1) - k(k\pm2)\right]\left[J(J+1) - (k\pm1)(k\pm2)\right]\Big\}^{1/2}.$$

The relationships between the coefficients in equations 1.10 and 1.12 have been given by Watson [8]. For the present purposes we only consider equation 1.10 up to the second term where the relationships are

$$B_x - 2T_{yz} = B_x^{(A)} + 2\Delta_J + \Delta_{JK} - 2\delta_J - 2\delta_K \qquad (1.14a)$$

$$B_y - 2T_{zx} = B_y^{(A)} + 2\Delta_J + \Delta_{JK} + 2\delta_J + 2\delta_K \qquad (1.14b)$$

$$B_z - 2T_{xy} = B_z^{(A)} + 2\Delta_J \qquad (1.14c)$$

$$T_{xx} = -\Delta_J - 2\delta_J \qquad (1.14d)$$

$$T_{yy} = -\Delta_J + 2\delta_J \qquad (1.14e)$$

$$T_{zz} = -\Delta_J - \Delta_{JK} - \Delta_K \qquad (1.14f)$$

$$T_{yz} + T_{zx} + T_{xy} = -3\Delta_J - \Delta_{JK} \qquad (1.14g)$$

$$B_xT_{yz} + B_yT_{zx} + B_zT_{xy} = -(B_x^{(A)} + B_y^{(A)} + B_z^{(A)})\Delta_J - \tfrac{1}{2}(B_x^{(A)} + B_y^{(A)})\Delta_{JK}$$

$$+(B_x^{(A)} - B_y^{(A)})(\delta_J + \delta_K). \qquad (1.14h)$$

For a near-prolate symmetric top the off-diagonal elements in equation 1.12 are small and, neglecting sextic distortion effects, we can use the symmetric top approximation to the rotational term values

$$F(J,K) = (A - \bar{B})K^2 + \bar{B}J(J + 1) - D_J J^2(J + 1)^2 - D_{JK}J(J + 1)K^2 - D_K K^4 \qquad (1.15)$$

where $\bar{B} = (B + C)/2$. The degree of asymmetry is given by Ray's asymmetry parameter $\kappa = (2B - C - A)/(A - C)$ which takes the values -1 and +1 for prolate and oblate symmetric tops respectively. It is common to use this result to relabel the quantum numbers K_a and K_c as K_{-1} and K_{+1} respectively.

The vibrational dependence of the rotational constants is given by $B_v = B_e - \sum_i \alpha_i^B(v_i + \frac{1}{2})$ where the α_i are small vibration-rotation constants and the subscript e refers to the equilibrium configuration.

The general selection rule for rotational transitions in asymmetric rotors is $\Delta J = 0, \pm 1$. The selection rules for K_{-1} and K_{+1} depend on the direction of the dipole moment [9] and are summarised in table 1.2. These selection rules are very general and in practise for a prolate near-symmetric rotor only transitions with $\Delta K_{-1} = 0, \pm 1$ have significant intensity.

The result of the selection rules given in table 1.2 is that the rotational structure of the vibrational bands of an asymmetric rotor may be of type A, B, C or a hybrid depending on whether the dipole moment is along the a, b or

Table 1.2. Rotational selection rules for asymmetric rotors

Direction of dipole moment	K_{-1}	K_{+1}		K_{-1}	K_{+1}
a axis	even	even	⟷	even	odd
	odd	even	⟷	odd	odd
b axis	even	even	⟷	odd	odd
	odd	even	⟷	even	odd
c axis	even	even	⟷	odd	even
	even	odd	⟷	odd	odd

c inertial axes or between them. For a near-prolate symmetric rotor bands of type A are called parallel bands and bands of types B and C are called perpendicular bands.

I.2.5 ROTATIONAL PERTURBATIONS

Deviations from the energy level expressions given in the previous section can occur if the approximation that the vibrational and rotational energies can be separated breaks down. In particular the vibrational and rotational energies can be coupled by Coriolis forces set up by the rotating molecule.

Coriolis interactions can be discussed by considering the following approximate vibration-rotation Hamiltonian [10]:

$$H = \frac{(J_x - p_x)^2}{2I_x} + \frac{(J_y - p_y)^2}{2I_y} + \frac{(J_z - p_z)^2}{2I_z} + \frac{1}{2}\sum_r (P_r^2 + \lambda_r Q_r^2) \qquad (1.16)$$

where Q_r is the r^{th} normal coordinate with its conjugate momentum P_r, and p_α is the component of vibrational angular momentum about the α axis, given by

$$p_z = \sum_a -i\hbar \left[x_a(\partial/\partial y_a) - y_a(\partial/\partial x_a)\right] \qquad (1.17)$$

etc with cyclic permutations of x, y and z, where x_a is a mass adjusted Cartesian displacement coordinate of atom a.

The Hamiltonian (1.16) may be written in terms of the rigid rotor Hamiltonian H_r, an assembly of harmonic oscillators H_v and the vibrational angular momenta H' :

$$H = H_r + H_v + H', \qquad (1.18)$$

where

$$H' = - p_x J_x/I_x - p_y J_y/I_y - p_z J_z/I_z + p_x^2/2I_x + p_y^2/2I_y + p_z^2/2I_z \qquad (1.19)$$

can be treated as a perturbation.

Rotational perturbations mainly arise from the first three terms in H' and the matrix elements of these terms factorise into vibration-rotation products of the form: $\langle v;r| -p_z J_z/I_z |v';r'\rangle = (-1/I_z)\langle v|p_z|v'\rangle\langle r|J_z|r'\rangle$ and we can write $H' = H_r' H_v'$. For the symmetric top approximation the non-zero matrix elements of the components of total angular momentum are given by:

$$\langle J,K|J_z|J,K\rangle = \hbar K \qquad (1.20a)$$

$$\langle J,K|J_x \pm iJ_y|J,K \pm 1\rangle = \hbar \left[J(J+1)-K(K\pm1) \right]^{1/2} \qquad (1.20b)$$

Expressing the vibrational angular momenta in terms of the normal coordinates we obtain:

$$p_z = \sum_r \sum_s \zeta^z_{r,s}[Q_r P_s - Q_s P_r] \qquad (1.21)$$

where the Coriolis zeta constants are given by:

$$\zeta^z_{r,s} = \sum_\alpha [(\partial x_\alpha/\partial Q_r)(\partial y_\alpha/\partial Q_s) - (\partial x_\alpha/\partial Q_s)(\partial y_\alpha/\partial Q_r)]. \qquad (1.22)$$

Each zeta constant is real with $|\zeta^\alpha_{r,s}| \leq 1$, $\zeta^\alpha_{r,s} = -\zeta^\alpha_{s,r}$ and relates a pair of normal coordinates by rotation about one of the axes. According to the selection rule of Jahn [11] $\zeta^\alpha_{r,s}$ is non-zero only if the product of the symmetry species of Q_r and Q_s contains the species of rotation about the α axis.

If the vibrational basis functions are assumed to be products of harmonic oscillator functions in the normal coordinates the non-zero matrix elements of the vibrational angular momentum follow from equation (1.21)

$$\langle v_r+1, v_s | p_\alpha | v_r, v_s+1 \rangle = -i\hbar\zeta^\alpha_{r,s}[(v_r+1)(v_s+1)]^{1/2}\Omega_{rs} \qquad (1.23)$$

$$\langle v_r+1, v_s+1 | p_\alpha | v_r, v_s \rangle = -i\hbar\zeta^\alpha_{r,s}[(v_r+1)(v_s+1)]^{1/2}\Phi_{rs} \qquad (1.24)$$

where

$$\Omega_{rs} = \tfrac{1}{2}\left[\left(\frac{v_r}{v_s}\right)^{\frac{1}{2}} + \left(\frac{v_s}{v_r}\right)^{\frac{1}{2}}\right] \text{ and } \Phi_{rs} = \tfrac{1}{2}\left[\left(\frac{v_r}{v_s}\right)^{\frac{1}{2}} - \left(\frac{v_s}{v_r}\right)^{\frac{1}{2}}\right].$$

The overall selection rule is $\Delta J = 0$ and the specific rotational selection rules are given below in table 1.3.

Thus for propynal, neglecting asymmetry ($K = K_{-1}$), we have the following three types of interaction :

(1) coupling about the a axis, $H'_r = -J_\alpha$, giving the rotational selection rules $\Delta J = 0$, $\Delta K = 0$ for H'_r to be non-zero and the vibrational selection rule $^vA' \leftrightarrow {}^vA''$ for

Table 1.3. Vibrational and rotational selection rules for Coriolis interactions

vibrational operator	vibrational selection rule	rotational operator	rotational selection rule
p_a	$\Gamma(v)\times\Gamma(v')=\Gamma(R_a)$	J_a	$\Delta K_{-i} = 0$, $\Delta K_{+i} = \pm 1$
p_b	$\Gamma(v)\times\Gamma(v')=\Gamma(R_b)$	J_b	$\Delta K_{-i} = \pm 1$, $\Delta K_{+i} = \mp 1$
p_c	$\Gamma(v)\times\Gamma(v')=\Gamma(R_c)$	J_c	$\Delta K_{-i} = \pm 1$, $\Delta K_{+i} = 0, \mp 2$

H'_v non-zero. H'_r is proportional to K;

(2) coupling about the b axis, $H'_r = -J_b$ and therefore the selection rules are $\Delta J = 0$, $\Delta K = \pm 1$, $^vA' \leftrightarrow {}^vA''$ and H'_r is proportional to $[J(J+1)-K(K\pm1)]^{1/2}$;

(3) coupling about the c axis giving the selection rules $\Delta J = 0$, $\Delta K = \pm 1$, $^vA' \leftrightarrow {}^vA'$, $^vA'' \leftrightarrow {}^vA''$ and H'_r is proportional to $[J(J+1)-K(K\pm1)]^{1/2}$.

I.2.6 SINGLET-TRIPLET INTERACTIONS

The singlet and triplet electronic states of a polyatomic molecule can interact by first- or second-order mechanisms, where the first-order mechanism represents direct spin-orbit coupling between the different states [12]. The dominant second-order contributions are due to vibronic spin-orbit coupling (type I), spin-rotation coupling (type II) and spin-vibronic coupling (type III) [13].

In the zeroth order we can write the Hamiltonian as

$$H = H_e + H_v + H_r + H' \tag{1.25}$$

where the perturbation Hamiltonian is given by

$$H' = H_{so} + H_{ev} + H_{or}. \tag{1.26}$$

Here H_{so} denotes the spin-orbit operator, H_{ev} is the vibronic interaction operator and H_{or} is the operator coupling electronic orbital motion with the overall rotation of the molecule.

The operator $H_r = H_1 + H_2$, in equation (1.25) is given by

$$H_1 = AN_z^2 + \tfrac{1}{2}(B + C)(N_x^2 + N_y^2) \tag{1.27a}$$

$$H_2 = \tfrac{1}{2}(B - C)(N_x^2 - N_y^2) \tag{1.27b}$$

where N_α is the component of the resultant of the molecular rotation angular momentum R and the electronic orbital motion angular momentum L.

The operators in equation (1.26) take the following forms:

$$H_{ev} = \sum_k (\partial H_E/\partial Q_k)_o Q_k + \text{higher terms} \tag{1.28}$$

$$H_{or} = -2AN_z \cdot L_z - 2BN_x \cdot L_x - 2CN_y \cdot L_y \tag{1.29}$$

$$H_{so} = \sum_i A_i l_i \cdot s_i \tag{1.30}$$

where the sum is over all electrons and s_i is the spin angular momentum, l_i is the orbital angular momentum and A_i is a function of the electrical field [13].

The overall selection rule for first- and second-order

interactions is $\Delta J = 0$.

For direct spin-orbit coupling the perturbation term is simply given by H_{so} and we have the selection rules $\Delta N = \Delta K = 0, \pm 1$. The $\Delta K = 0$ interactions occur when ${}^{ev}\Gamma_S \, {}^{ev}\Gamma_T = R_z$ and the $\Delta K = \pm 1$ interactions occur when ${}^{ev}\Gamma_S \, {}^{ev}\Gamma_T = R_x$ or R_y. Here ${}^{ev}\Gamma_S$ refers to the vibronic wavefunction of the singlet state and ${}^{ev}\Gamma_T$ to that of the triplet state.

Type I second-order coupling is given by $H_{ev} + H_{so}$ with the selection rules $\Delta N = 0, \pm 1$ $\Delta K = 0$ for ${}^{ev}\Gamma_S \, {}^{ev}\Gamma_T = R_z$ or $\Delta K = \pm 1$ for ${}^{ev}\Gamma_S \, {}^{ev}\Gamma_T = R_x$ or R_y.

Type II coupling consists of the terms $H_{or} + H_{so}$ and has the selection rules $\Delta N = 0, \pm 1$ $\Delta K = 0, \pm 2$.

Type III coupling is due to a term of the form $(\partial H_{so}/\partial Q_k)_o Q_k$ and is expected to be small for molecules made up of light atoms.

In orthorhombic molecules, direct or first-order coupling between singlet and triplet states of the same electronic configuration is forbidden. In propynal the matrix elements for direct coupling of the ${}^1(n\pi^*)$ and ${}^3(n\pi^*)$ states is expected to be small and competitive with type I and type II second-order coupling [14].

CHAPTER II EXPERIMENTAL

II.1 MATERIALS

Propynal was prepared by the chromic acid oxidation of commercial propyn-1-ol under reduced pressure (40 torr) and temperature (5°C) according to the method of Sauer [15]. Initially the more recently published synthesis due to Veliev and Guseinov [16] was attempted but in this work, as reported by McNab [17], it was not found to be possible to separate the product from the solvents.

Propynol (40ml) was dissolved in a cooled mixture of sulphuric acid (45ml) and water (150ml). Nitrogen was introduced into the reaction vessel through a capillary and the pressure in the system was reduced to 40 mmHg. A solution of chromium trioxide (70g) in sulphuric acid (45ml) and water (130ml) was added dropwise over the course of 5 hours while the temperature of the reactants was kept at about 5°C.

The crude product was collected in three traps, the contents of which were combined and saturated with sodium chloride. The upper layer, consisting of nearly pure propynal, was removed and dried over anhydrous magnesium sulphate. The propynal was then vacuum-distilled, after which there were no traces of impurities when analysed both by n.m.r spectroscopy and by the high-resolution ultraviolet absorption spectrum. The pure propynal (12.6g =

35% yield) was stored under vacuum in solid CO_2 to prevent decomposition and was redistilled before use.
(^1H nmr H1 δ=9.22, H2 δ=3.55; 60 MHz; CCl_4).

Propynal-d_1 (HCCCDO) was prepared by the oxidation of propyn-1-ol-2d_1 ($HCCCD_2OH$) using the above method on a much reduced scale. The purity was ascertained from the high resolution ultraviolet absorption spectrum and the 200 MHz n.m.r spectrum, and no traces of impurities or of other isotopically substituted species were found.

Propynal-d_2 (DCCCHO) was prepared by the oxidation of $DCCCH_2OD$, as above, obtained from propyn-1-ol by repeated exchange with slightly alkaline D_2O. From the high-resolution ultraviolet spectrum it was estimated that the compound was contaminated by about 5% of the undeuterated compound. The direct deuteration of HCCCHO with alkaline D_2O was attempted but extensive polymerisation was observed and the yield of DCCCHO was greatly reduced.

Propynal-d_1,d_2 was prepared by the oxidation of $DCCCD_2OD$, obtained by repeated exchange of $HCCCD_2OH$ with D_2O and was estimated to be contaminated by about 5% of HCCCDO.

II.2 ULTRAVIOLET SPECTRA

A 2m multiple reflection cell was filled with 0.5 torr of propynal vapour and spectra were recorded using path-lengths of between 8m and 64m. The spectra were

photographed on Kodak Pan 2415 recording film with exposures ranging from 1 minute to 60 minutes, using the 15^{th} to 18^{th} orders of the University College 4m Czerny-Turner spectrograph [18], corresponding to a theoretical resolution of better than 0.05 cm^{-1}. The continuum source was provided by a high pressure Xenon arc. Spectra were calibrated from reference spectra of an iron hollow-cathode lamp using Edlén's formula to correct wavelengths in air to vacuum wavelengths and hence vacuum wavenumbers.

Films were measured on the Tomkins-Fred comparator at the Université Paris-Sud or on the University College Zeiss-Abbe comparator to an estimated relative accuracy of $\pm$ 0.001 cm^{-1}.

II.3 MICRODENSITOMETRY

Microdensitometer tracings were taken on the Joyce-Loebl MK III CS microdensitometer at University College. The tracings were recorded digitally and stored on magnetic tape. In all cases the minimum step size of 5μ between readings was used and thus a 10cm scan involved the recording of 20000 points. This corresponds to a resolution of between approximately 0.01 cm^{-1} and 0.005 cm^{-1} depending on the wavelength dispersion on the film.

The digitised spectra were manipulated and plotted by the use of two computer programs written by the author during the course of this work. The programs are written

in Fortran 77 using Gino subroutines and exist in both GEC and Pyramid compatible forms. The first program, MDPL1, simply allows a spectrum to be plotted as an x,y plot where x is distance and y is optical density. The second, MDPL2, is more versatile and allows the conversion of optical density D to relative intensity I by fitting to the equation $I = 10^{aD} + b$ when the constants a and b have been found from a calibration film. This program also allows the spectrum to be linearised in wavenumber once the calibration curve for the measured film has been obtained. Features in the spectrum can then be measured from the computer screen and the measurements have been found to be within $\pm$ 0.01 cm^{-1} of the measurements obtained at the Université Paris-Sud.

The digitised spectra were plotted either on the Benson continuous plotter or on the laser printer at the University College Computer Centre.

II.4 LEAST SQUARES FITTING

The theory of the least squares refinement of spectroscopic data to rotational constants has been described in considerable detail by Albritton *et al* [19].

The least squares fitting program, MAINUV, was originally written by Dr. J.E.Parkin and was extensively modified by the author. The program currently allows up to 2000 assigned and measured rotational transitions observed in a purely rotational spectrum and/or a rovibronic

spectrum to be fitted to the Hamiltonian given in equation 1.12 for either or both of the states. The relative weights of microwave and infrared (or ultraviolet) transitions are set to the square of the ratio of the estimated precisions and individual transitions can further be weighted relative to one and other. Lines which are assigned to unresolved transitions which are asymmetry doubled are treated as the mean of the two components. Up to 31 molecular constants (15 rotational and distortion constants for each state plus the vibrational origin) are fitted by a least squares method of repeated iterations to give the best fit values, their standard deviations, the correlation coefficients and the fit to the input transitions. Transitions which are more than three standard deviations from the calculated values are removed in successive iterations but may be restored if a further iteration brings them back into this range.

Calculations were carried out on the Amdahl 5890 model 300 mainframe computer at the University of London Computer Centre. A large fit of about 1000 observed transitions to both ground and excited states in three iterations took about 30 minutes computing time.

In reporting the results from least squares fits Albritton recommends that the coefficients and their standard errors and correlation coefficients are included together with the data, the weighting factors and the fit to the data. In this work however large numbers of transitions were fitted and it is impractical to include all of the data here although it is available at the

Department of Chemistry, University College London.

The best choice for the set of constants was determined individually for each data set by a method of trial and error taking account of the overall fit, the standard errors of the constants and the correlation coefficients.

It should be noted that in solving for excited electronic states there are occasions when the set of excited state constants include higher order centrifugal distortion constants for which the ground state counterpart is not known. These constants were included purely in order to improve the overall fit and obviously contain some contribution from the ground state.

II.5 SPECTRAL SIMULATIONS

The spectral simulation program, KONTUR90, was originally written by Dr. L.Pierce and was extensively modified by Dr. J.E.Parkin and the author. Currently the program only uses the symmetric rotor approximation given in equation 1.15 for the treatment of the centrifugal distortion corrections. The energy levels of the two states ($J < 130$) and transitions between them, together with their relative intensities, are calculated from the input molecular constants and specified selection rules. One version of the program can simulate hybrid bands given the percentage mixture of the band types. There are also two versions of KONTUR90 which simulate the effect of Coriolis interactions on the frequencies of transitions. The first

one due to Dr. J.E.Parkin is a first order treatment of coupling about the a axis described in section I.2.5 and the other, due to the author, is a first order treatment of coupling about either the b or c axes.

The simulated spectra were plotted at the University College Computer Centre.

CHAPTER III THE ELECTRONIC GROUND STATE

III.1 VIBRATIONLESS LEVELS

The microwave spectrum of propynal was first reported by Howe and Goldstein [20] who were able to fit the 7 observed transitions to the rotational constants B and C. By studying the Stark effect they also obtained values for the dipole moments μ_a, μ_b and hence the resultant μ. Later Costain and Morton [21] recorded the spectra of fifteen isotopically substituted species of propynal including the three deuterated compounds. They obtained reasonably accurate values of the rotational constants for each of these species. Unfortunately, as is often the case, the microwave spectrum does not contain enough information to obtain the centrifugal distortion constants.

The millimetre wave spectrum of HCCCHO was recorded by Winnewisser [22] and he was able to fit the data to include the five quartic and two of the sextic centrifugal distortion constants. More recently several new microwave transitions have been reported by Jones [23] and Takami and Shimoda [24] measured in the course of infrared-microwave double resonance experiments, and by Benson and co-workers [25] recorded during a study of the Zeeman effect.

As the previous work did not take account of the relative accuracies of the microwave and millimetre wave experiments it seemed of interest to repeat Winnewisser's

calculation with a proper weighting of the transitions, including the new data mentioned above. A least squares fit, weighted inversely by the squares of the estimated precisions, of all the now available data to Watson's Hamiltonian resulted in improved values for the constants quoted by Winnewisser. The standard deviation of the weighted fit was 11kHz compared to 87kHz obtained by Winnewisser. The revised constants, given to a sufficient number of digits to allow the calculation to be reproduced, and their standard deviations are compared to those derived by Winnewisser in table 3.1. In reporting the rotational constants $B_{\alpha}^{(A)}$ we have followed Watson's recommendation [8] and have omitted the superscript although it should be noted that all the least squares fits in this work are to the A reduction of the Hamiltonian.

The results from the fit show that the higher weighting given to the microwave data over the millimetre wave data improves the accuracy of the rotational constants B_x and B_y and the distortion constants δ_J and δ_K whereas the accuracy of the other distortion constants remains relatively unchanged. This is presumably because it is the lower J, K transitions that contain the most information on the asymmetry of the molecule on which these constants are dependent. The high correlations of B_z and Δ_K (0.94), and of B_x and B_y with δ_K (-0.93 and 0.93) quoted by Winnewisser have also been reduced, in the first case because of the additional data and in the second because of the weighting matrix.

The millimetre wave spectrum of DCCCHO was recorded by

Table 3.1. Molecular constants of HCCCHO in the $\tilde{X}^1A'$ state

	Winnewisser[a]	This work[b]
B_x / MHz	4826.3014 ± 0.0073	4826.28744 ± 0.0007
B_y / MHz	4499.5107 ± 0.0069	4499.52306 ± 0.0006
B_z / MHz	68035.299 ± 0.043	68035.24489 ± 0.024
Δ_J / kHz	1.917 ± 0.0012	1.9076 ± 0.0014
Δ_{JK}/ kHz	-148.102 ± 0.047	-148.049 ± 0.047
Δ_K / kHz	8991.240 ± 9.73	8988.136 ± 6.91
δ_J / kHz	0.3458 ± 0.0014	0.34488 ± 0.0003
δ_K / kHz	39.000 ± 3.18	32.8582 ± 0.09
Φ_{JK}/ Hz	-0.741 ± 0.059	-0.76299 ± 0.07
Φ_{KJ}/ Hz	-8.310 ± 0.13	-8.1561 ± 0.20
Δ_0/amuA^2	0.1770	0.1764
κ	-0.9897132	-0.9897140

(a) σ = 87 kHz, 92 transitions, from reference [22].

(b) σ = 11kHz, 139 transitions.

Correlation coefficients:

	B_x	B_y	B_z	Δ_J	Δ_{JK}	Δ_K	δ_J	δ_K	Φ_{JK}	Φ_{KJ}
B_x	1.00	0.57	0.50	0.79	0.27	0.44	0.60	0.12	0.36	-0.13
B_y		1.00	0.19	0.28	0.57	-0.14	-0.05	-0.35	0.34	0.25
B_z			1.00	0.43	0.12	0.80	0.49	-0.06	0.23	-0.17
Δ_J				1.00	0.23	0.64	0.79	-0.01	0.48	-0.31
Δ_{JK}					1.00	-0.21	0.06	-0.29	0.81	0.19
Δ_K						1.00	0.71	0.02	0.16	-0.48
δ_J							1.00	-0.18	0.48	-0.58
δ_K								1.00	-0.31	0.10
Φ_{JK}									1.00	-0.39
Φ_{KJ}										1.00

Table 3.2. Molecular constants of DCCCHO in the $\tilde{X}^1A'$ state

	Takami[a]	This work[b]
B_x / MHz	4463.8489 ± 0.0007	4463.83758 ± 0.0009
B_y / MHz	4177.7950 ± 0.0007	4177.81419 ± 0.0014
B_z / MHz	66778.016 ± 0.012	66778.00195 ± 0.017
Δ_J / kHz	1.5919 ± 0.0005	1.59710 ± 0.0009
Δ_{JK}/ kHz	-139.214 ± 0.013	-139.229 ± 0.024
Δ_K / kHz	9432.8 ± 1.8	9425.13 ± 2.75
δ_J / kHz	0.2885 ± 0.0004	0.28021 ± 0.0001
δ_K / kHz	30.69 ± 0.04	27.3363 ± 0.25
Φ_{JK}/ Hz	-0.817 ± 0.013	-0.73782 ± 0.03
Φ_{KJ}/ Hz	-9.62 ± 0.04	-10.0891 ± 0.06
Φ_K / Hz	2550 ± 80	1894.70 ± 108.9
ϕ_J / Hz	0.0047 ± 0.0003	0.00272 ± 0.0003
ϕ_{JK}/ Hz	-	-2.490 ± 0.25
Δ_o/amuÅ^2	0.1839	0.1830
κ	-0.9908609	-0.9908619

(a) σ = 70kHz, 139 transitions, from reference [26].

(b) σ = 27kHz, 157 Transitions.

Correlation coefficients:

	B_x	B_y	B_z	Δ_J	Δ_{JK}	Δ_K	δ_J	δ_K	Φ_{JK}	Φ_{KJ}	Φ_K	ϕ_J	ϕ_{JK}
B_x	1.00	0.40	0.29	0.52	0.34	-0.16	0.24	0.24	-0.01	0.45	-0.22	-0.18	0.14
B_y		1.00	0.72	0.89	0.16	0.53	-0.39	-0.73	-0.00	0.20	0.42	0.56	-0.59
B_z			1.00	0.54	0.26	0.75	-0.23	-0.41	0.04	0.27	0.65	0.30	-0.20
Δ_J				1.00	0.17	0.41	-0.21	-0.56	-0.01	0.25	0.30	0.47	-0.51
Δ_{JK}					1.00	-0.23	0.14	-0.05	0.81	0.27	-0.34	0.08	-0.15
Δ_K						1.00	-0.33	-0.43	-0.23	-0.01	0.95	0.30	-0.13
δ_J							1.00	0.38	0.12	0.03	-0.33	-0.10	0.21
δ_K								1.00	-0.14	0.16	-0.33	-0.82	0.88
Φ_{JK}									1.00	-0.32	-0.39	0.17	-0.28
Φ_{KJ}										1.00	0.08	-0.13	0.21
Φ_K											1.00	0.26	-0.03
ϕ_J												1.00	-0.93
ϕ_{JK}													1.00

Table 3.3. Molecular constants of HCCCDO in the $\tilde{X}^1A'$ state

	Costain et al[21]	This work
B_x/ MHz	4791.439	4791.528 ± 0.005
B_y/ MHz	4378.764	4378.846 ± 0.005
B_z/ MHz	51764.46	51768.01 ± 0.03
Δ_J/ KHz	-	1.833 ± 0.1
Δ_{JK}/ KHz	-	-49.78 ± 1.0
Δ_K/ KHz	-	2930.1 ± 30.0
Δ_o/amuÅ^2	0.1775	0.1780
κ	-0.982582	-0.982583

Table 3.4. Molecular constants of DCCCDO in the $\tilde{X}^1A'$ state

	Costain et al[21]	This work
B_x/ MHz	4429.099	4429.187 ± 0.01
B_y/ MHz	4069.604	4069.683 ± 0.01
B_z/ MHz	51074.93	51079.224 ± 0.07
Δ_J/ KHz	-	1.748 ± 0.2
Δ_{JK}/ KHz	-	-55.28 ± 5.0
Δ_K/ KHz	-	3667.8 ± 70
Δ_o/amuÅ^2	0.1847	0.1854
κ	-0.984704	-0.984705

Takami [26] and the ground state constants including four of the sextic distortion constants were obtained. These constants are given in table 3.2. Again this result did not use any weighting factors and more transitions have since been reported [27]. A weighted least squares fit of the existing microwave and millimeter wave data and the more recent microwave data was therefore attempted and this resulted in a value for the additional constant ϕ_{JK}. The constants obtained and their standard errors are given in table 3.2. The standard deviation of the fit was 27kHz compared to the 70kHz obtained by Takami.

The result of the fit is that there is in general a slight decrease in the quoted accuracies of the constants the only large discrepancy being for δ_K where it is due to correlation with ϕ_{JK}. It is difficult to make further comparisons since Takami does not quote any correlation coefficients.

The only ground state information available for the compounds HCCCDO and DCCCDO is that of Costain and Morton and hence good ground state distortion constants are not available for these molecules. In this work the ground state constants for these molecules have been revised by weighted least squares fits to the microwave data and the origin bands of the first singlet excited state spectra (see section IV.2.3). The rotational constants of these compounds are given in tables 3.3 and 3.4.

Comparing the results for the four molecules we see that there are the following trends with deuteration of the aldehyde group:

(i) decrease of B_z by about 24% whereas B_y is lowered by about 2.6% and B_x is reduced by only 0.7%, leading to a small increase in Δ_o. These changes can be understood from the position of the aldehydic hydrogen relative to the axes as shown in figure 3.1.

(ii) decrease of Δ_{JK} and Δ_K by about 60% whereas Δ_J is left relatively unchanged. We can see from equations 1.14 and 1.11 that for propynal $\Delta_K \sim -T_{zz} \propto 1/I_z^4$ and hence the decrease in Δ_K follows from the decrease in B_z and corresponding increase in I_z. Similarly we have $\Delta_{JK} \sim -T_{yz}-T_{zx}-T_{xy}$ which contains terms of the form $1/I_y^2I_z^2$ and again the decrease in Δ_{JK} follows from the increase in I_z. From equation 1.14 we also see that $-T_{yy} \sim \Delta_J \sim -T_{xx}$ and the small change in Δ_J reflects the small changes of B_x and B_y.

On deuteration of the ethynyl group we see:

(i) decrease of B_x by 7.5% and B_y by 7.1% whereas B_z is lowered by only 1.5%, leading to an increase in Δ_o of about 4 %. This is due to the fact that the ethynyl hydrogen lies close to the z axis and as we would expect, I_x and I_y increase on deuteration whereas I_z is only slightly changed.

(ii) increase of Δ_K whereas Δ_J is lowered by about 15% and Δ_{JK} about 5%. As explained above the decrease of Δ_J and Δ_{JK} follow from the increases in I_x and I_y. The increase in Δ_K has been explained by Takami [26] to be a result of the reduction of ν_7 and ν_{11} (see table 3.5) and increase of $a_7^{(zz)}$ and $a_{11}^{(zz)}$ on deuteration of the ethynyl group where, unlike the case of aldehydic deuteration, changes in these terms in equation 1.11 are not masked by an increase in I_z.

The structure of the normal compound of propynal as determined by Costain and Morton [21] is shown in figure 3.1. The estimated errors in the bond lengths and bond angles are ±0.001 Å and ±10' respectively.

Figure 3.1. Ground state structure of HCCCHO [21]

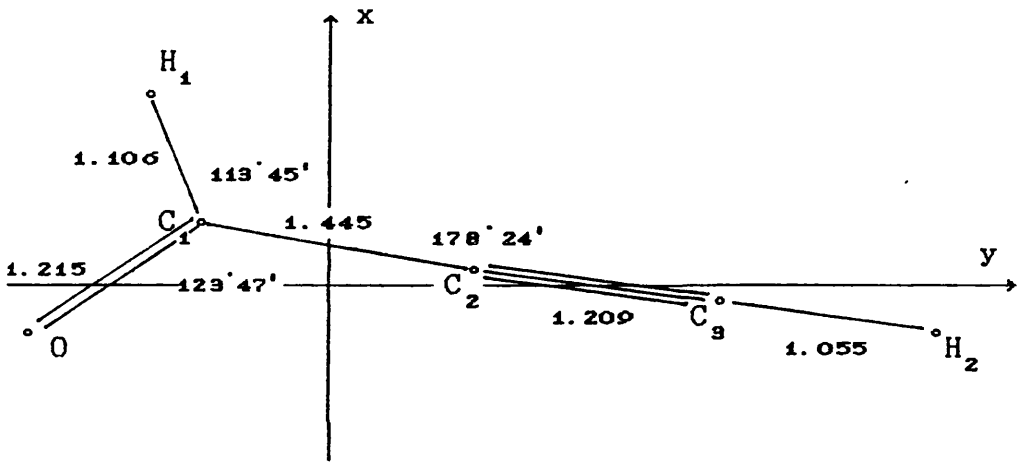

The dipole moment of HCCCHO in the ground electronic state has been redetermined by Brown and Godfrey [28] to be $\mu_a = (7.87 \pm 0.06)\times10^{-30}$Cm, $\mu_b = (4.90 \pm 0.07)\times10^{-30}$Cm and hence $\mu = (9.27 \pm 0.06)\times10^{-30}$Cm. From their study of the Zeeman effect Benson *et al* [25] have determined the molecular g values, magnetic susceptibility anisotropies and molecular quadrupole moments of HCCCHO.

III.2 VIBRATIONALLY EXCITED LEVELS

The infrared spectra of propynal and the compounds DCCCHO and HCCCDO have been studied by Brand and Watson [29,30] and vibrational analyses have been proposed. The Raman spectrum of the normal compound was investigated by King and Moule [31] and Klaboe and Kremer [32] and the assignments of the fundamental frequencies confirmed. The fundamental frequencies of these compounds in their electronic ground states are given in table 3.5.

Brand and Watson were also able to attempt partial rotational analyses for a few of the vibrational bands. Takami *et al* [24,27,33] have completed rotational analyses of the ν_2 bands of propynal and DCCCHO by using IR-MW double and triple resonance techniques. Jones [23] has similarly studied the three combination bands in the propynal spectrum arising from the transitions (ν_{11} = 1; ν_{12} = 1) $\longleftarrow$ 0, (ν_8 = 1; ν_6 = 1) $\longleftarrow$ (ν_8 = 1) and (ν_9 = 1; ν_6 = 1) $\longleftarrow$ (ν_9 = 1) giving the rotational constants A, B and C of the states involved. He also obtained B and C values from the a-type transitions to 12 other assigned states with vibrational energies up to 950 cm^{-1}.

Recently the mid-infrared spectrum of DCCCDO has been analysed by Tavladorakis under medium resolution [34] and the fundamental frequencies ν_2 to ν_6 and ν_{10} have been determined. The frequencies ν_7 to ν_{12} have been found from vibrational hot bands in the ultraviolet spectrum during the course of this work and are reported in table 3.5 (see section IV.2.5). Tavladorakis has also investigated the

Table 3.5. Fundamental frequencies of propynal in the $\tilde{X}^1A'$ state

mode/cm^{-1}		HCCCHO	DCCCHO	HCCCDO	DCCCDO
ν_1	a'	3326	2605	3325.42[c]	—
ν_2	a'	2858.231[a]	2857.888[b]	2119[c]	2110[c]
ν_3	a'	2106	1977	2104.5[c]	1984[c]
ν_4	a'	1696.9	1697.0	1678[c]	1689[c]
ν_5	a'	1389	1387.6	1078.96[c]	1071[c]
ν_6	a'	943.7	933.6	876.5	870[c]
ν_7	a'	650.0	507.9	651.17[c]	507.4[d]
ν_8	a'	613.7	609.0	611.9	607.0[d]
ν_9	a'	205.3	195.6	201.5	192.8[d]
ν_{10}	a"	981.2	980.9	848.0[c]	849.0[c]
ν_{11}	a"	692.7	548.6	692.67[c]	542.5[d]
ν_{12}	a"	260.6	248.5	249.9	237.1[d]

All frequencies from reference [30] except:
a [24], b [27], c [34], d This work.

infrared spectrum of HCCCDO under high resolution and has obtained more accurate values for many of the fundamental frequencies, as shown in table 3.5.

The assignments of the frequencies to vibrational modes in the propynal molecule of Brand and Watson has been confirmed by a normal coordinate analysis by Williams [35] and are given below on the basis of the numbering in figure 3.1.

(i) in plane vibrations:

ν_1 C_3- H_2 stretch, ν_2 C_1- H_1stretch, ν_3 $C_2\equiv C_3$stretch,

ν_4 C_1= O stretch, ν_5 C_1- H_1 rock, ν_6 C_1- C_2 stretch,

ν_7 C_3- H_2 rock, ν_8 C_2- C_1= O bend, ν_9 C_1- $C_2\equiv C_3$ bend,

(ii) out of plane vibrations:

ν_{10} C_1- H_1 wag, ν_{11} C_3- H_2 wag, ν_{12} C_1- $C_2\equiv C_3$ bend.

CHAPTER IV THE ULTRAVIOLET SPECTRUM

IV.1 GENERAL STRUCTURE OF THE ULTRAVIOLET SPECTRUM

Propynal shows three relatively intense absorption systems in the ultraviolet spectrum: (1) banded absorption between 3000 Å and 3900 Å centred on 3820 Å, which displays complex vibrational structure; (2) banded absorption in the 2600 Å to 2100 Å region centred on 2570 Å; (3) continuous absorption from 2200 Å to shorter wavelengths centred on 2140 Å. An additional group of very weak bands appear to the red of the 3820 Å system when high pressures of propynal are used. These bands , centred on 4140 Å, extend from 4180 Å towards the 3820 Å system.

The ultraviolet absorption spectrum of propynal vapour between 3000 Å and 3900 Å was examined under medium resolution by Howe and Goldstein [36] and a partial analysis was attempted. This spectrum has been the subject of a detailed analysis by Watson and co-workers [30,37,38,39] and they have assigned it as arising from the $\pi^* \longleftarrow n$, $^1A'' \longleftarrow {}^1A'$ ($S_1 \longleftarrow S_0$) transition. Their work has resulted in an extensive vibrational analysis [30] and 11 of the 12 excited state fundamental frequencies have been assigned (table 4.1). A rotational analysis of the 0-0 band [39] has given accurate values for the rotational constants of the vibrationless level of the singlet excited state S_1 (table 4.2) and has revealed a positive inertial

defect which is interpreted as indicating a planar or near planar structure in the excited state. This is in contrast to methanal which has been shown to be non-planar in the excited state [40]. The spectrum shows numerous perturbations, including Fermi and Coriolis interactions, many of which have been noted and analysed by Watson [30]. The 3820 Å system of propynal also shows a predissociation which is observed as a break in the sub-band structure and overall line broadening in the progression in ν_4' after $2\nu_4'$.

The 4140 Å system has been studied both in absorption [41,42] and emission [42,43] and has been assigned as due to the spin forbidden $\pi^* \longleftarrow n$, $^3A'' \longleftarrow {}^1A'$ ($T_1 \longleftarrow S_0$) transition. It is believed that the transition gains its intensity from an allowed $^1A' \longleftarrow {}^1A'$ transition. Nine fundamental vibration frequencies have been assigned in the triplet state and a rotational analysis of the 0-0 band [41] has resulted in accurate values for the rotational constants. An approximate Franck-Condon analysis [44] has given two possible structures for the triplet excited state. The phosphorescence of the triplet excited state, T_1, has been studied by Huber and co-workers [45,46,47] for both HCCCHO and HCCCDO. They explain their findings in terms of temperature sensitive radiative and radiationless processes with the vibrational temperature as the determining factor.

Several studies have been carried out on the energy decay from the $^1A''$ state. Brenner *et al* [48,49,50] and Lesiecki *et al* [51] have studied the vibrational relaxation

of hot bands in the singlet excited state S_1 spectrum following infrared-visible multiphoton absorption, under both collisionless and single collision conditions. Thayer and co-workers [52,53,54] monitored the energy flow from the vibrationless level of the S_1 state and suggested the 8 possible decay processes:

(1) $S_1 \xrightarrow{k0} S_0 + h\nu_F$	fluorescence;
(2) $S_1 \xrightarrow{k1} S_0^\dagger$	collision-free internal conversion;
(3) $S_1 \xrightarrow{k2} T_1^\dagger$	collision-free intersystem crossing;
(4) $S_1 + S_0 \xrightarrow{k3} T_1^\dagger + S_0 + E_{t,r}$	collision-induced intersystem crossing;
(5) $S_1 + S_0 \xrightarrow{k4} S_0^\dagger + S_0 + E_{t,r}$	collision-induced internal conversion;
(6) $T_1 \xrightarrow{k5} S_0 + h\nu_P$	phosphorescence;
(7) $T_1 \xrightarrow{k6} S_0^\dagger$	collision-free intersystem crossing;
(8) $T_1 + S_0 \xrightarrow{k7} S_0^\dagger + S_0 + E_{t,r}$	collision-induced intersystem crossing;

They conclude that the dominant collision-induced process is intersystem crossing (4).

In similar experiments Huber and co-workers [55] found that internal conversion (2) dominates in collision-free conditions with $\Phi_{IC} \geq 0.88$.

In various observations of quantum beats in the fluorescence decay of the S_1 state Huber and co-workers have been able to study the singlet-triplet excited state coupling and have calculated the matrix elements for the

coupling of two single rovibronic levels of the S_1 state with the T_1 state [56]. Their calculations favour vibronic spin-orbit coupling over direct coupling and Zeeman studies [57] agree with this conclusion.

Russegger and co-workers have performed calculations on the photochemistry of propynal [58,59] and have calculated the potential energy surface for photodissociation. They conclude that the lowest energy reaction channel is:

$$HC{\equiv}C\text{-}C(=O)H \xrightarrow{h\nu} HC{\equiv}CH + CO$$

IV.2 THE $\tilde{A}^1A'' \leftarrow \tilde{X}^1A'$ TRANSITION

IV.2.1 VIBRATIONAL ANALYSIS

The vibrational analyses of the $S_1 \leftarrow S_0$ absorption spectra of propynal and the two singly deuterated compounds have been reported by Watson [30]. In the course of our examination of the ultraviolet spectrum several new vibrational assignments have been made and these additions to the analyses are detailed in appendix A1.

The vibrational analysis of DCCCDO from this work is given in appendix A2. In both appendices A1 and A2 intensities, where quoted, are relative to the system origin which is arbitrarily given a value of 10.

The spectra of all four compounds are dominated by progressions in the symmetric carbonyl stretch ν_4', and the

vibrational structure close to the system origin is repeated with successive quanta of this mode. All of the out of plane vibrational modes are seen in the spectra, either as fundamentals or in combinations with each other. Of the in plane vibrations only the ethynyl hydrogen stretch ν_1' is not seen in any of the spectra and this is in good agreement with the intensity calculations of Williams [35] although he did not extend his work to the doubly deuterated compound. The in plane aldehydic bend ν_7' is not seen in the spectra of HCCCHO and HCCCDO but does occur in the other two compounds, which again agrees with the intensity calculations. The fundamental frequency for ν_7', quoted in table 4.1, for these two molecules was argued by Watson [30] to be close to the ground state value and this is also in agreement with the normal coordinate analysis.

The fundamental frequencies of the four compounds in the first singlet excited state are compared in table 4.1.

IV.2.2 GENERAL ROTATIONAL STRUCTURE

The moments of inertia of propynal are very close to those of a prolate symmetric top: $I_C \approx I_B \sim 10\, I_A$, $\kappa = -0.9897$. The spectrum of propynal consists of four types of vibrational bands: (1) C-type bands, which are out of plane perpendicular bands whose rotational structure has a central maximum close to the band origin, making up the majority of the spectrum; (2) in-plane B-type bands which

Table 4.1. Fundamental frequencies of propynal in the $\tilde{A}^1A''$ state

mode/cm^{-1}		HCCCHO	DCCCHO	HCCCDO	DCCCDO[a]
ν_1	a'	—	—	—	—
ν_2	a'	2952.5	2953.1	2204	2175.5
ν_3	a'	1945.8	1850.9	1947	1847.9
ν_4	a'	1304.0	1298.6	1267.6	1260.4
ν_5	a'	1119.5	1115.6	824	812.7
ν_6	a'	951.6	936.6	942.3	930.2
ν_7	a'	(650)[b]	529.3	(650)[b]	526.7
ν_8	a'	506.9	486.5	499.9	481.9
ν_9	a'	189.4	183.6	187.4	180.2
ν_{10}	a''	462.1	459.0	411.3	401.2
ν_{11}	a''	389.7	291	375	288.5
ν_{12}	a''	345.9	346.9	321.8	320.1

All frequencies from reference [30] except: a This work.
b see text.

are seen as perpendicular bands with a central minimum; (3) A-type parallel bands; and (4) AB hybrid bands. Examples of the four band types can be seen in figures 4.1, 4.2, 4.3 and 4.4 respectively. The K- and J-rotational structures of the bands are easily identified and it can be seen that the J-structure is only slightly degraded whereas the K-structure is strongly degraded to higher wavelengths. Thus each sub-band consists of a P- and an R-branch, composed of almost equally spaced lines, and an unresolved

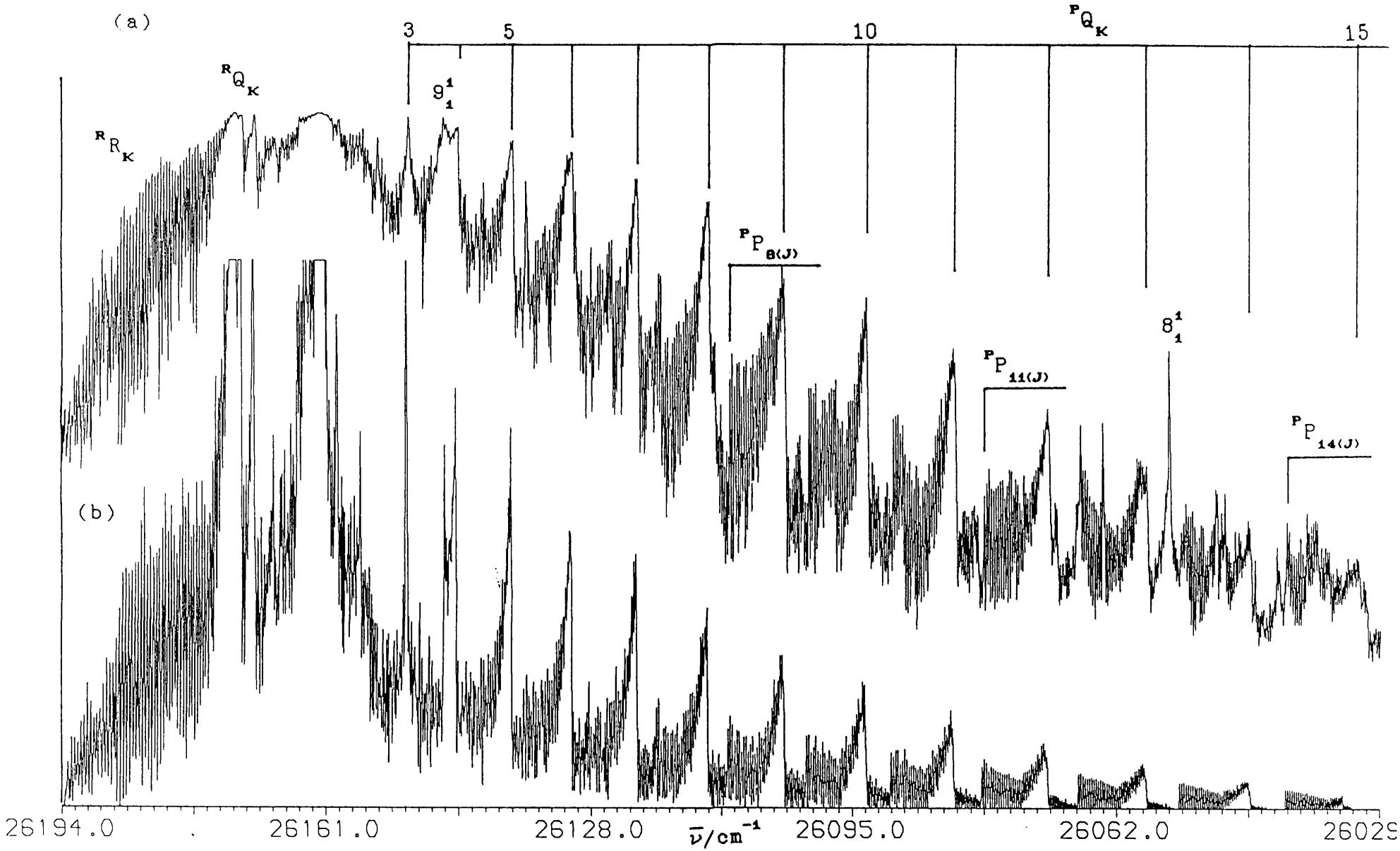

Figure 4.1. The 0^{o}_{o} band of HCCCHO (a) observed and (b) calculated

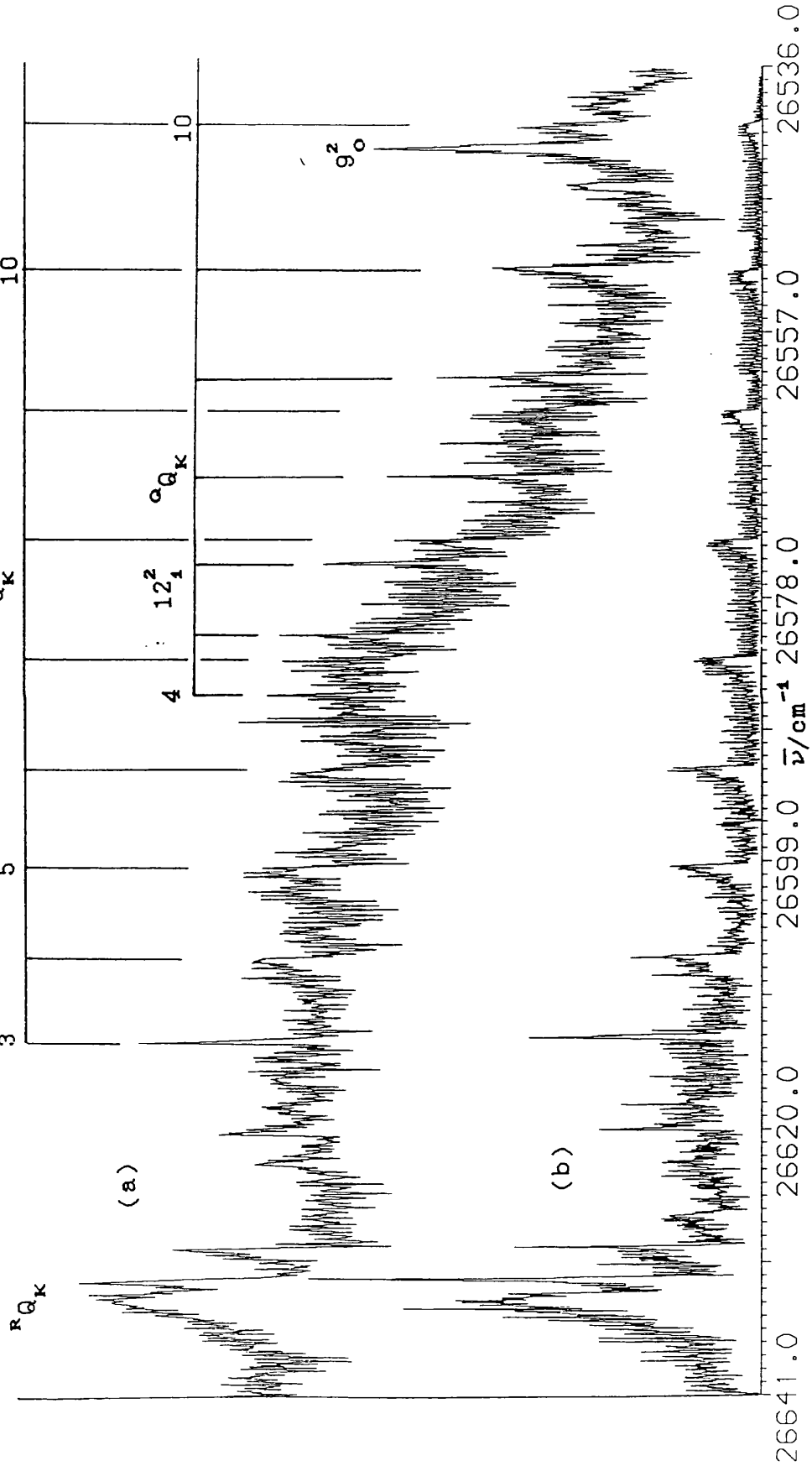

Figure 4.2. The 10_o^1 band of HCCCHO (a) observed and (b) calculated

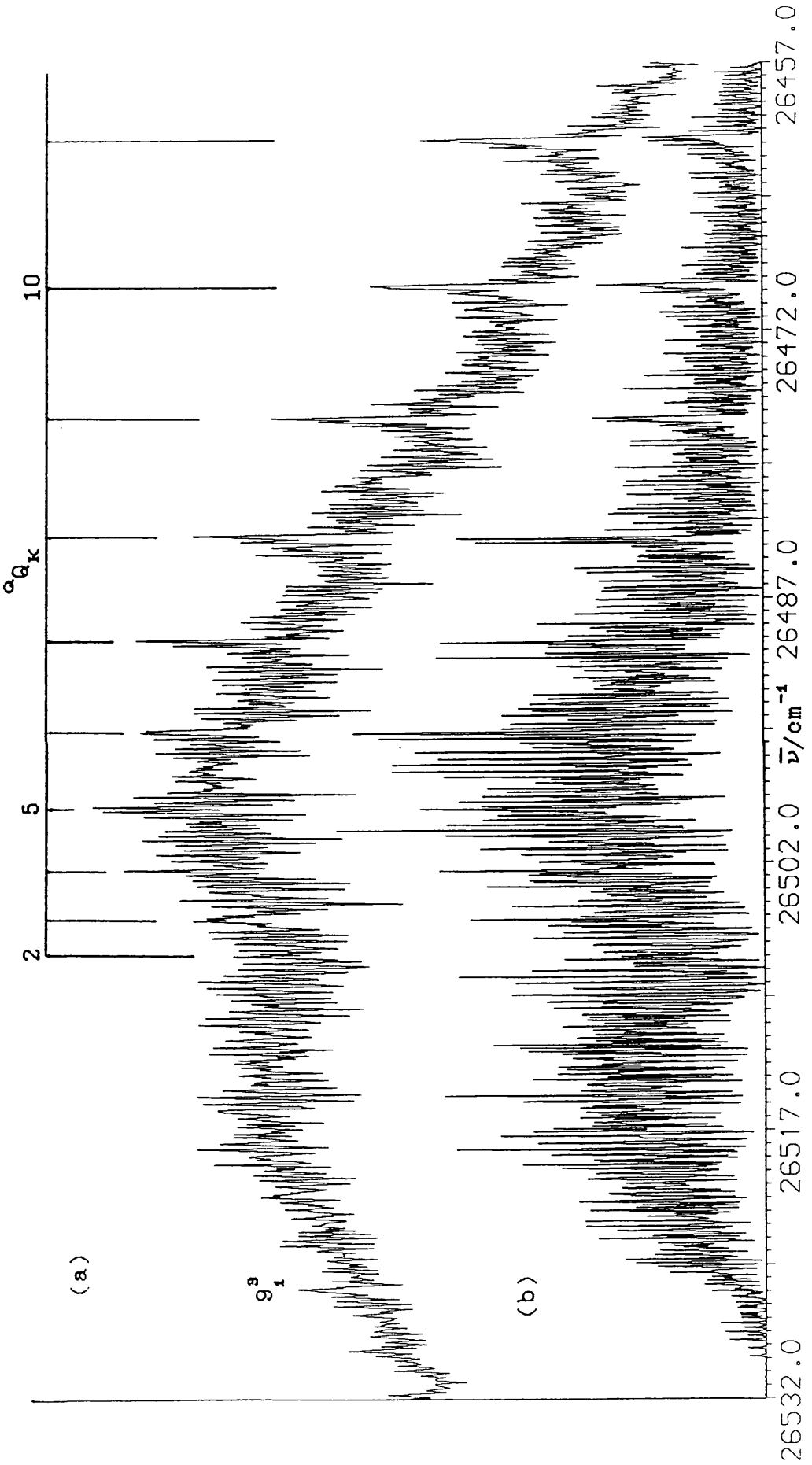

Figure 4.3. The 12^1_0 band of HCCCHO (a) observed and (b) calculated

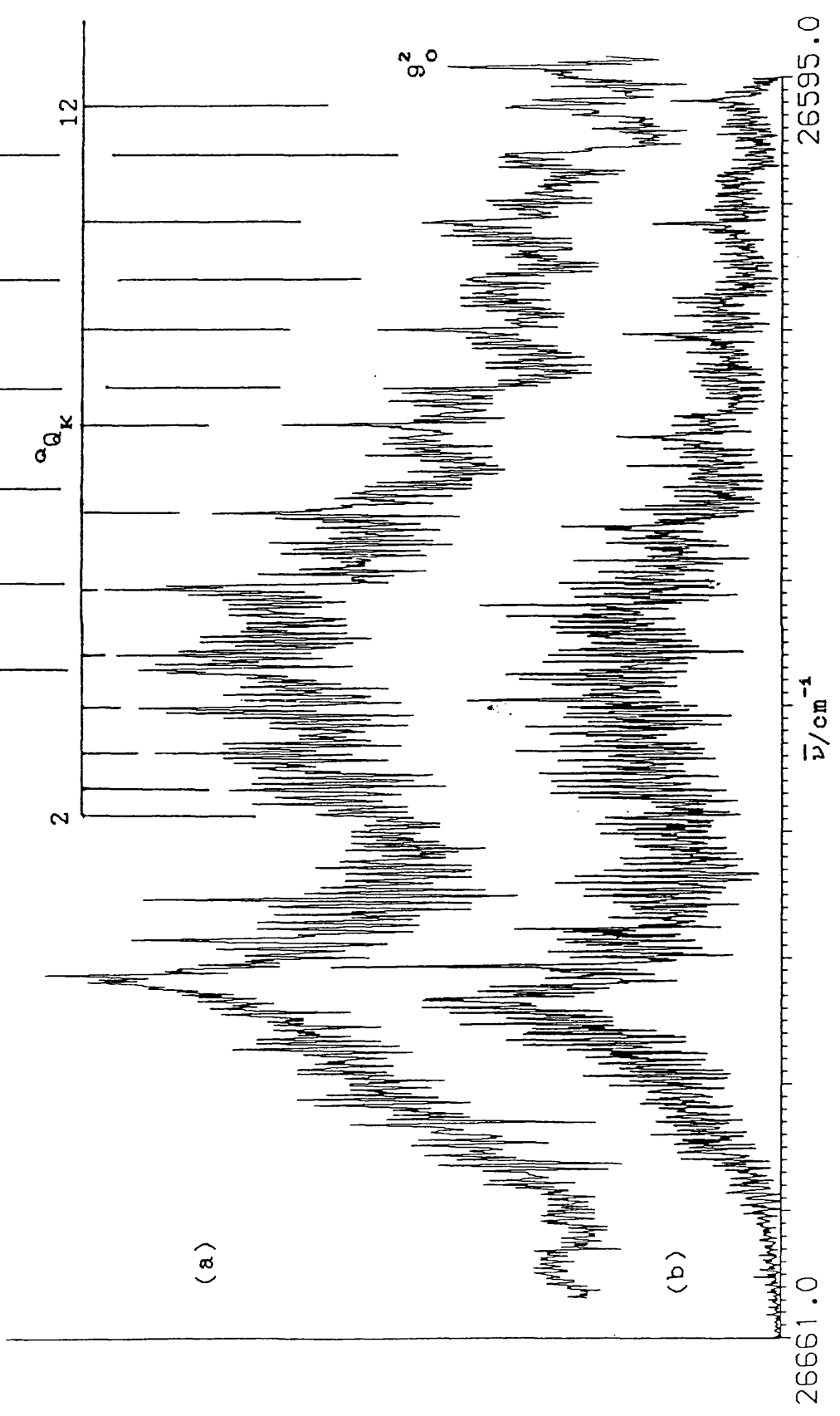

Figure 4.4. The 10^{1}_{o} band of DCCCDO (a) observed and (b) calculated

Q-branch forming a sharp peak on the low-frequency side. The degradation of the K-structure causes the R-type sub-bands of perpendicular bands to form a head on the high-frequency side of the band origin.

IV.2.2.1 PERPENDICULAR BANDS

The heads formed by the ^{P}Q branches and the individual ^{P}P lines are relatively easy to identify in perpendicular bands and thus form the starting point of any rotational analysis. The K numbering of the ^{P}Q sub-bands is relatively straightforward as the differences $^{P}Q_{K} - {}^{P}Q_{K+1}$ are nearly linear in K and extrapolate back to the known $2(A - \bar{B})''$ at K = $\frac{1}{2}$. The positions of ^{R}Q heads can be calculated from the combination differences:

$$\Delta_2 F''(K) = {}^{R}Q_{K-1} - {}^{P}Q_{K+1} = 4(A - \bar{B})''K - 8\Delta_K''K(K^2 + 1) \qquad (4.1)$$

if the ground-state constants are known. When the ^{R}Q bands are known, the differences

$$({}^{R}Q_{K-1} - {}^{P}Q_{K+1}) / 4K = (A - \bar{B})'' - 2\Delta_K''(K^2+1) \qquad (4.2)$$

$$({}^{R}Q_{K} - {}^{P}Q_{K}) / 4K = (A - \bar{B})' - 2\Delta_K'(K^2+1) \qquad (4.3)$$

are used to separate the lower and upper states. With these values for Δ_K'' and Δ_K' the band origin ν_o and an improved value of $\{(A - \bar{B})' - (A - \bar{B})''\}$ can be obtained from the combination sum:

$$^{R}Q_K + {}^{P}Q_{K+1} + (\Delta'_K - \Delta''_K)\{K^4 + (K+1)^4\} \qquad (4.4)$$

$$= 2\nu_o + \{(A - \bar{B})' - (A - \bar{B})''\}\{K^2 + (K+1)^2\}$$

For perpendicular bands arising from the zero point level of the ground state the differences

$$^{P}Q_{K+1}(v) - {}^{P}Q_{K+1}(0) = G_o(v) + \{(A - \bar{B})'_v - (A - \bar{B})'_o\}K^2$$

$$- \{D'_K(v) - D'_K(0)\}K^4 \qquad (4.5)$$

are normally linear in K^2 and give good values of $G_o(v)$ and $(A - \bar{B})'_v$.

Perpendicular hot bands due to transitions ending on the zero point level of the excited state can similarly be analysed by the equations

$$^{P}Q_K(0) - {}^{P}Q_K(v) = G_o(v) + \{(A - \bar{B})''_v - (A - \bar{B})''_o\}K^2$$

$$- \{D''_K(v) - D'_K(0)\}\,K^4 \qquad (4.6)$$

IV.2.2.2 PARALLEL BANDS

For parallel bands the $^{Q}Q_K$ heads can be fitted to the equation

$$^{Q}Q_K = \nu_o + \{(A - \bar{B})' - (A - \bar{B})''\}\,K^2 - (D'_K - D''_K)\,K^4 \qquad (4.7)$$

and parallel type hot bands can similarly be fitted to the equation

$$^{Q}Q_K = T_o - G_o(v) + \{(A - \bar{B})'_o - (A - \bar{B})''_v\}\,K^2$$

$$- \{D'_K(0) - D''_K(v)\}\,K^4. \qquad (4.8)$$

IV.2.3 ROTATIONAL ANALYSES OF THE ORIGIN BANDS

Brand and co-workers have published a complete rotational analysis of the electronic origin band of HCCCHO [39] and partial analyses for the three deuterated compounds. Since we now have a more complete ground state determination of HCCCHO and DCCCHO (section III.1) it seemed of interest to repeat the rotational analysis for HCCCHO and extend the DCCCHO analysis. More complete analyses have also been attempted for the molecules HCCCDO and DCCCDO.

The rotational analyses of the origin bands of the $S_1 \leftarrow S_o$ absorption spectra were carried out by a least squares refinement of the observed transitions to Watson's A reduction of the rotational Hamiltonian (equation 1.12). In the cases of HCCCHO and DCCCHO, where good ground state constants were available these constants were kept fixed throughout the analysis. The initial step was the fitting of the readily assignable ^{P}P branches, ^{P}Q and ^{R}Q heads to the constants of Brand *et al* [39]. From the refined constants other transitions were calculated, such as the blended ^{R}R lines and the weak ^{R}P and ^{P}R lines, and searched for. The accuracy of the new lines was checked by combination differences. When a calculated branch could be followed for several members this branch was added to the data set. This process was repeated several times until the assignments of calculated transitions became difficult. When several transitions were assigned to the same spectral line the weight of each was set to the inverse of the

Table 4.2. Molecular constants of HCCCHO in the $\tilde{A}^1A''$ state

	Brand et al[(a)]	This work[(c)]
T_o /cm^{-1}	26162.941 ± 0.002	26162.943 ± 0.002
B_x /cm^{-1}	0.163022 ± 0.000008	0.1631289 ± 0.000009
B_y /cm^{-1}	0.149840 ± 0.000008	0.1497486 ± 0.00001
B_z /cm^{-1}	1.88934 ± 0.0001	1.8899282 ± 0.00006
$\Delta_J \times 10^8$/cm^{-1}	10.4 ± 0.2	11.465 ± 0.07
$\Delta_{JK} \times 10^6$/cm^{-1}	-7.09 ± 0.03	-7.124 ± 0.03
$\Delta_K \times 10^4$/cm^{-1}	2.80 ± 0.02	2.85232 ± 0.007
$\delta_J \times 10^8$/cm^{-1}	[1.1535][(b)]	4.909 ± 0.1
$\delta_K \times 10^6$/cm^{-1}	[1.300][(b)]	7.9990 ± 0.4
$\Phi_{JK} \times 10^{10}$/cm^{-1}	-	-0.283 ± 0.09
$\Phi_K \times 10^8$/cm^{-1}	10.9 ± 0.7	1.101 ± 0.2
Δ_o/amuA^2	0.175 ± 0.008	0.3138 ± 0.01
κ	-0.9848439	-0.9846218

(a) σ = 0.013cm^{-1}; 530 transitions, from reference [39].

(b) constant fixed to ground state value.

(c) σ = 0.013cm^{-1}; 1222 transitions.

Correlation coefficients:

	B_x	B_y	B_z	Δ_J	Δ_{JK}	Δ_K	δ_J	δ_K	Φ_{JK}	Φ_K	ν_o
B_x	1.00	-0.81	0.05	0.08	0.16	-0.03	0.91	-0.11	0.13	-0.04	-0.21
B_y		1.00	-0.10	0.27	0.30	-0.15	-0.90	-0.29	0.13	-0.13	-0.16
B_z			1.00	0.05	0.00	0.89	0.09	0.14	0.11	0.81	-0.52
Δ_J				1.00	0.41	-0.06	-0.19	0.14	0.66	-0.05	-0.31
Δ_{JK}					1.00	-0.32	-0.04	-0.52	0.76	-0.32	-0.42
Δ_K						1.00	0.08	0.25	-0.11	0.98	-0.24
δ_J							1.00	-0.05	-0.05	0.06	-0.04
δ_K								1.00	0.07	0.21	0.29
Φ_{JK}									1.00	-0.13	-0.20
Φ_K										1.00	-0.18
ν_o											1.00

Table 4.3. Molecular constants of DCCCHO in the $\tilde{A}^1A''$ state

	Brand et al[a]	This work[b]
T_o /cm^{-1}	26191.82 ± 0.01	26191.879 ± 0.002
B_x /cm^{-1}	0.15094 ± 0.00003	0.1511078 ± 0.00001
B_y /cm^{-1}	0.13932 ± 0.00001	0.1391941 ± 0.00001
B_z /cm^{-1}	1.8433 ± 0.0002	1.8444880 ± 0.0001
$\Delta_J \times 10^8$/cm^{-1}	10.6 ± 0.4	5.210 ± 0.08
$\Delta_{JK} \times 10^6$/cm^{-1}	-6.39 ± 0.09	-5.7139 ± 0.03
$\Delta_K \times 10^4$/cm^{-1}	2.59 ± 0.1	2.83882 ± 0.02
$\delta_J \times 10^8$/cm^{-1}	-	58.580 ± 0.3
$\Phi_K \times 10^8$/cm^{-1}	-	8.039 ± 0.6
$\phi_J \times 10^{19}$/cm^{-1}	-	0.3458 ± 0.03
Δ_o/amuÅ^2	0.17 ± 0.02	0.4091 ± 0.02
$\varkappa$	-0.9863613	-0.9860273

(a) from reference [39].

(b) σ = 0.014cm^{-1}; 804 Transitions.

Correlation coefficients:

	B_x	B_y	B_z	Δ_J	Δ_{JK}	Δ_K	δ_J	Φ_K	ϕ_J	ν_o
B_x	1.00	-0.91	-0.06	-0.01	0.26	-0.12	0.89	-0.12	0.31	-0.13
B_y		1.00	0.10	0.34	-0.08	0.11	-0.92	0.10	-0.29	-0.11
B_z			1.00	0.03	0.21	0.92	-0.07	0.84	-0.09	-0.67
Δ_J				1.00	-0.03	0.03	-0.30	0.04	-0.16	-0.30
Δ_{JK}					1.00	-0.04	0.21	-0.09	0.26	-0.40
Δ_K						1.00	-0.11	0.98	-0.13	-0.46
δ_J							1.00	-0.11	0.51	0.00
Φ_K								1.00	-0.12	-0.37
ϕ_J									1.00	-0.01
ν_o										1.00

Table 4.4. Molecular constants of HCCCDO in the $\tilde{A}^1A''$ state

	Brand et al[a]	This work[b]
T_o/cm^{-1}	26206.49 ± 0.01	26206.505 ± 0.002
B_x/cm^{-1}	0.16201 ± 0.00004	0.1618998 ± 0.00001
B_y/cm^{-1}	0.14552 ± 0.00001	0.1455292 ± 0.00001
B_z/cm^{-1}	1.4921 ± 0.0002	1.4916548 ± 0.00008
$\Delta_J \times 10^8/cm^{-1}$	10.2 ± 0.4	10.631 ± 0.2
$\Delta_{JK} \times 10^6/cm^{-1}$	-3.87 ± 0.1	-3.2989 ± 0.02
$\Delta_K \times 10^4/cm^{-1}$	1.08 ± 0.1	1.01287 ± 0.008
$\delta_K \times 10^6/cm^{-1}$	-	2.1019 ± 0.6
$\Phi_K \times 10^8/cm^{-1}$	-	0.588 ± 0.1
$\phi_J \times 10^{12}/cm^{-1}$	-	1.0590 ± 0.6
Δ_o /amuÅ^2	0.49 ± 0.04	0.4117 ± 0.01
$\varkappa$	-0.9755083	-0.9756774

(a) from reference [39].

(b) σ = 0.014cm^{-1}; 912 Transitions.

Correlation coefficients:

	B_x	B_y	B_z	Δ_J	Δ_{JK}	Δ_K	δ_K	Φ_K	ϕ_J	ν_o
B_x	1.00	-0.65	-0.09	-0.02	0.30	-0.13	-0.20	-0.11	-0.79	-0.24
B_y		1.00	-0.09	0.29	0.12	-0.08	-0.07	-0.06	0.85	-0.16
B_z			1.00	-0.01	-0.13	0.93	0.12	0.85	-0.08	-0.51
Δ_J				1.00	-0.44	0.04	0.74	0.04	0.22	-0.17
Δ_{JK}					1.00	-0.34	-0.63	-0.34	-0.03	-0.29
Δ_K						1.00	0.13	0.98	-0.07	-0.31
δ_K							1.00	0.10	0.11	0.06
Φ_K								1.00	-0.06	-0.25
ϕ_J									1.00	0.04
ν_o										1.00

Table 4.5. Molecular constants of DCCCDO in the $\tilde{A}^1A''$ state

	Brand et al[a]	This work[c]
T_o /cm^{-1}	26235.51 ± 0.05	26235.461 ± 0.002
B_x /cm^{-1}	0.14994 ± 0.0002	0.1497407 ± 0.00001
B_y /cm^{-1}	0.13540 ± 0.00006	0.1353848 ± 0.00001
B_z /cm^{-1}	1.4649 ± 0.001	1.4641890 ± 0.00005
$\Delta_J \times 10^8$/cm^{-1}	[10.2][b]	4.690 ± 0.1
$\Delta_{JK} \times 10^6$/cm^{-1}	-2.0 ± 0.7	-3.3501 ± 0.04
$\Delta_K \times 10^4$/cm^{-1}	0.83 ± 0.2	1.26570 ± 0.004
$\delta_J \times 10^8$/cm^{-1}	-	32.088 ± 0.2
$\Phi_{JK} \times 10^{10}$/cm^{-1}	-	-1.288 ± 0.1
$\Phi_K \times 10^8$/cm^{-1}	-	0.343 ± 0.08
Δ_o /amuÅ^2	0.56 ± 0.2	0.4244 ± 0.01
κ	-0.9781271	-0.9783931

(a) from reference [39].

(b) constant fixed to value from another isotope.

(c) σ = 0.014 cm^{-1}, 900 transitions.

Correlation coefficients:

	B_x	B_y	B_z	Δ_J	Δ_{JK}	Δ_K	δ_J	Φ_{JK}	Φ_K	ν_o
B_x	1.00	-0.77	0.05	0.29	0.26	-0.06	0.89	0.24	-0.05	-0.24
B_y		1.00	0.02	0.34	0.21	-0.05	-0.90	0.19	-0.03	-0.18
B_z			1.00	0.09	0.16	0.89	0.04	0.15	0.84	-0.64
Δ_J				1.00	0.70	-0.13	-0.05	0.71	-0.09	-0.48
Δ_{JK}					1.00	-0.19	0.02	0.96	-0.16	-0.40
Δ_K						1.00	0.03	-0.15	0.98	-0.36
δ_J							1.00	0.03	0.02	-0.03
Φ_{JK}								1.00	-0.12	-0.31
Φ_K									1.00	-0.31
ν_o										1.00

number of transitions multiply assigned.

In the cases of HCCCDO and DCCCDO where the ground states were not well known the ground state constants were immediately refined by a weighted least squares fit to A", B", C", Δ_J'' , Δ_{JK}'' and Δ_K'' . The analysis then proceeded as above.

The final values for the molecular constants obtained are given in tables 4.2, 4.3, 4.4 and 4.5 to sufficient accuracy to allow reproduction of the data.

Finally least squares fits to both ground and excited states were carried out using the ratios of the standard deviations for the individual fits in order to determine the weightings of the ground state data over that of the excited state data. This is described as the correlated least squares formulation by Albritton [19]. These fits did not, however, significantly increase either the accuracy or the set of constants that could be solved for.

The observed and calculated spectra of the 0_o^o bands of HCCCHO and HCCCDO are shown in figures 4.1 and 4.5.

In this work we have avoided fixing the values of poorly determined constants to either the ground state values or values from another isotopically substituted molecule as this obviously introduces errors in the determination of correlated constants.

It should be noted that the correlation between B' and C' is always high unless a large number of high J low K transitions are included in the analysis. Since the assignment of these lines is uncertain, due to the overlapping near to the band origin, although (B'+ C')/2

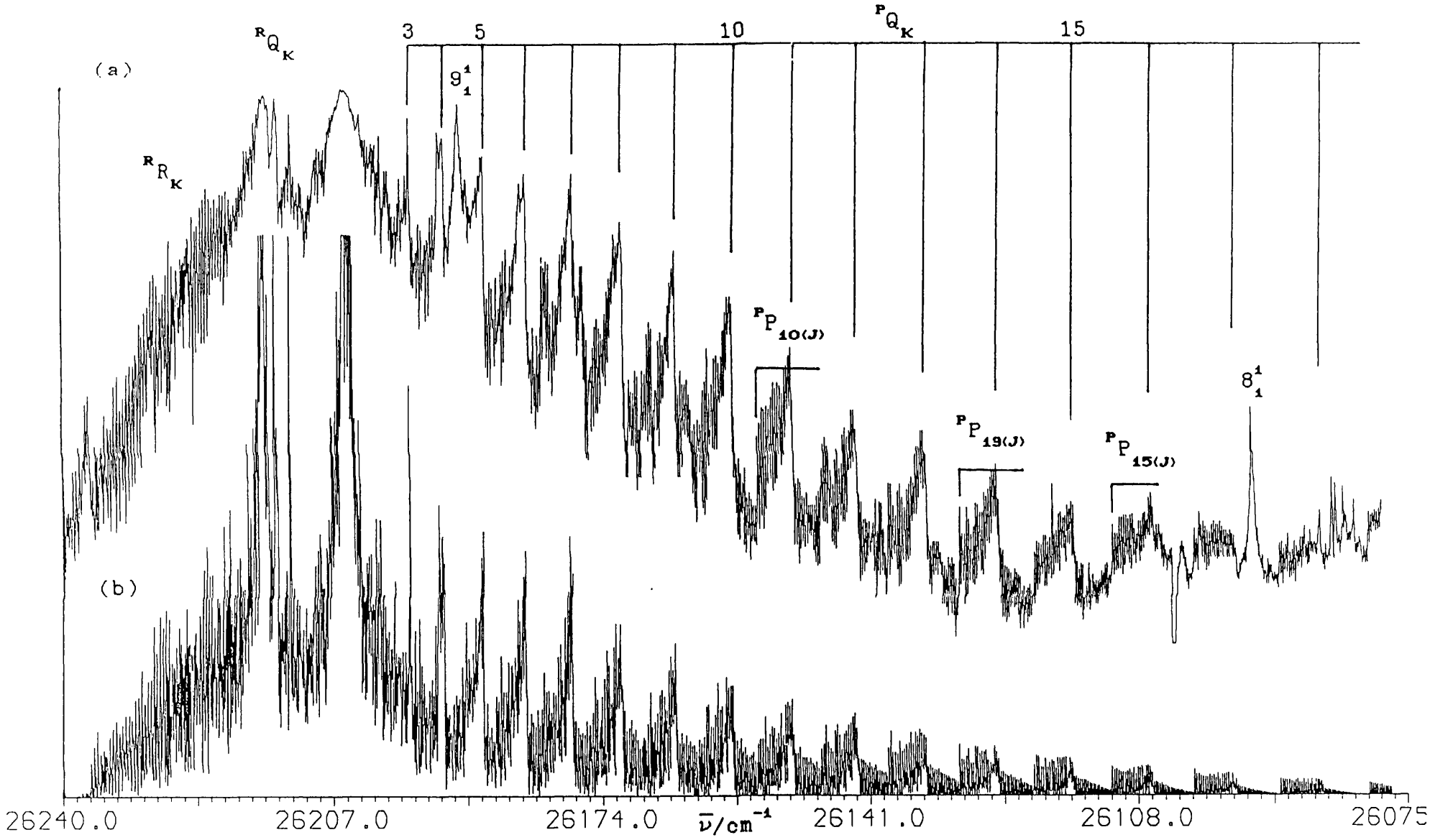

Figure 4.5. The 0_0^0 band of HCCCDO (a) observed and (b) calculated

is well determined, B' - C' and hence Δ_o is subject to error.

It is also important to note that the positions of broad features near the origin are dependent on the higher order centrifugal distortion constants and that this dependence can be of the same order of magnitude as that on B' - C'. In the light of this the treatment used by Brand et al [39] to find the asymmetry parameters of HCCCDO, DCCCHO and DCCCDO was ill conditioned in that it neglects the effects of the higher order centrifugal distortion constants. As a result of these two points the discrepancies between the values for the inertial defects obtained in this work and by that of Brand *et al* can easily be explained. The errors in the inertial defects were calculated from the propagation of errors equation [60]:

$$\sigma^2 = (\partial\Delta_o/\partial I_x)^2\sigma_{Ix}^2 + (\partial\Delta_o/\partial I_y)^2\sigma_{Iy}^2 + (\partial\Delta_o/\partial I_z)^2\sigma_{Iz}^2$$
$$+ 2r_{Ix,Iy}(\partial\Delta_o/\partial I_x)(\partial\Delta_o/\partial I_y)\sigma_{Ix}\sigma_{Iy}$$
$$+ 2r_{Iy,Iz}(\partial\Delta_o/\partial I_y)(\partial\Delta_o/\partial I_z)\sigma_{Iy}\sigma_{Iz}$$
$$+ 2r_{Iz,Ix}(\partial\Delta_o/\partial I_z)(\partial\Delta_o/\partial I_x)\sigma_{Iz}\sigma_{Ix}$$

where the correlation coefficient $r_{Ix,Iy} = r_{Bx,By}$.

Comparing the constants from this work with those obtained by Brand we see that for HCCCHO the accuracy and values of the band origin, the three rotational constants and the first three quartic distortion constants are relatively unchanged. We have, however, been able to fit for the other two quartic and two of the sextic constants.

For DCCCHO, HCCCDO and DCCCDO it can be seen that the fits are now to a similar level of accuracy as for HCCCHO.

Comparing the results for the various compounds we have the following general trends on ethynyl deuteration:

(i) increase of T_o by 29 cm^{-1}.

(ii) decrease of B_x and B_y by about 7% whereas B_z is only slightly lowered by about 2%. This is in good agreement with the corresponding trend seen in the ground state (see section III.1).

(iii) a small change in Δ_K whereas Δ_J is lowered by about 55% and Δ_{JK} by about 20%. This is similar to the effect seen in the ground state although the lowering of the constants in the excited state on ethynyl deuteration is in general greater. This is probably a result of the greater overall reduction in wavenumber of the fundamental frequencies in the excited state, in particular ν_8, ν_{11} and ν_{12} (see table 4.1).

On deuteration of the aldehyde group we see:

(i) increase of T_o by 43.6 cm^{-1}.

(i) decrease of B_z by about 20% whereas B_y is lowered by about 3% and B_x is only slightly reduced. These observations follow the corresponding trends in the ground state.

(ii) decrease of Δ_{JK} and Δ_K by about 50% whereas Δ_J is reduced by about 10%, again following the results obtained for the ground state.

Comparing the excited state molecular constants of tables 4.2, 4.3, 4.4 and 4.5 to the ground state constants of tables 3.1, 3.2, 3.3 and 3.4 we observe that on

excitation:

(i) B_x increases by about 1.3% whereas B_y decreases by 0.2% and B_z decreases by 15% suggesting that there is a small change in structure, with the largest change being away from the z axis.

(ii) Δ_J increases by about 80% for the ethynyl protonated compounds and decreases by about 10% for the ethynyl deuterated compounds.

(iii) Δ_{JK} increases by 30% and Δ_K decreases by 5% for the aldehydic protonated compounds whereas Δ_{JK} increases by 90% and Δ_K increases by 3% for the aldehydic deuterated compounds.

IV.2.4 FUNDAMENTALS, OVERTONES AND COMBINATION BANDS

IV.2.4.1 ν_1'

There is no firm evidence for the excited state ethynyl C-H stretching vibration ν_1' in any of the isotopically substituted species of propynal. From his normal coordinate analysis Williams [35] has calculated the frequencies and relative intensities of this fundamental for the normal and two singly deuterated compounds and his results are reproduced in table 4.6. The calculated intensities are on the same scale as appendices A1 and A2.

Table 4.6. Calculated frequencies and intensities of 1_0^1 [35]

	ν_1/cm^{-1}	intensity
HCCCHO	3326.0	0.00
DCCCHO	2545.0	0.01
HCCCDO	3325.9	0.02

IV.2.4.2 ν_2'

The aldehydic hydrogen stretch ν_2' gives rise to moderately strong fundamental bands in the molecules HCCCHO and DCCCHO and strong fundamentals in the aldehydic deuterated compounds. In HCCCHO the fundamental appears unperturbed but is too weak for a complete analysis of the J-structure. The K-structure has been analysed using equation 4.5 to give the band origin ν_o = 29116.0 cm^{-1} = 0_0^0 + 2953.1 cm^{-1}, $(A - \bar{B})'$ = 1.7923 cm^{-1} and D_K' = 3.94 × 10^{-4} cm^{-1} (σ = 0.07 cm^{-1}). The corresponding fundamental in DCCCHO has been similarly analysed to give ν_o = 0_0^0 + 2953.1 cm^{-1}, $(A - \bar{B})'$ = 1.7936 cm^{-1} and D_K' = 8.98 × 10^{-4} cm^{-1} (σ = 0.2 cm^{-1}).

The 2_0^1 band of HCCCDO is shown in figure 4.6. The band is overlapped by the band $4_0^1 6_0^1$ and the two levels are subject to a Coriolis interaction seen by an abrupt change in the ^PQ heads of 2_0^1 at K' = 12, as shown in figure 4.7. The ^PQ_K heads for K = 3 to 12 are exceptionally sharp whereas for K = 14 and 15 they are broad and there is no obvious head in the position expected for $^PQ_{13}$. The effect

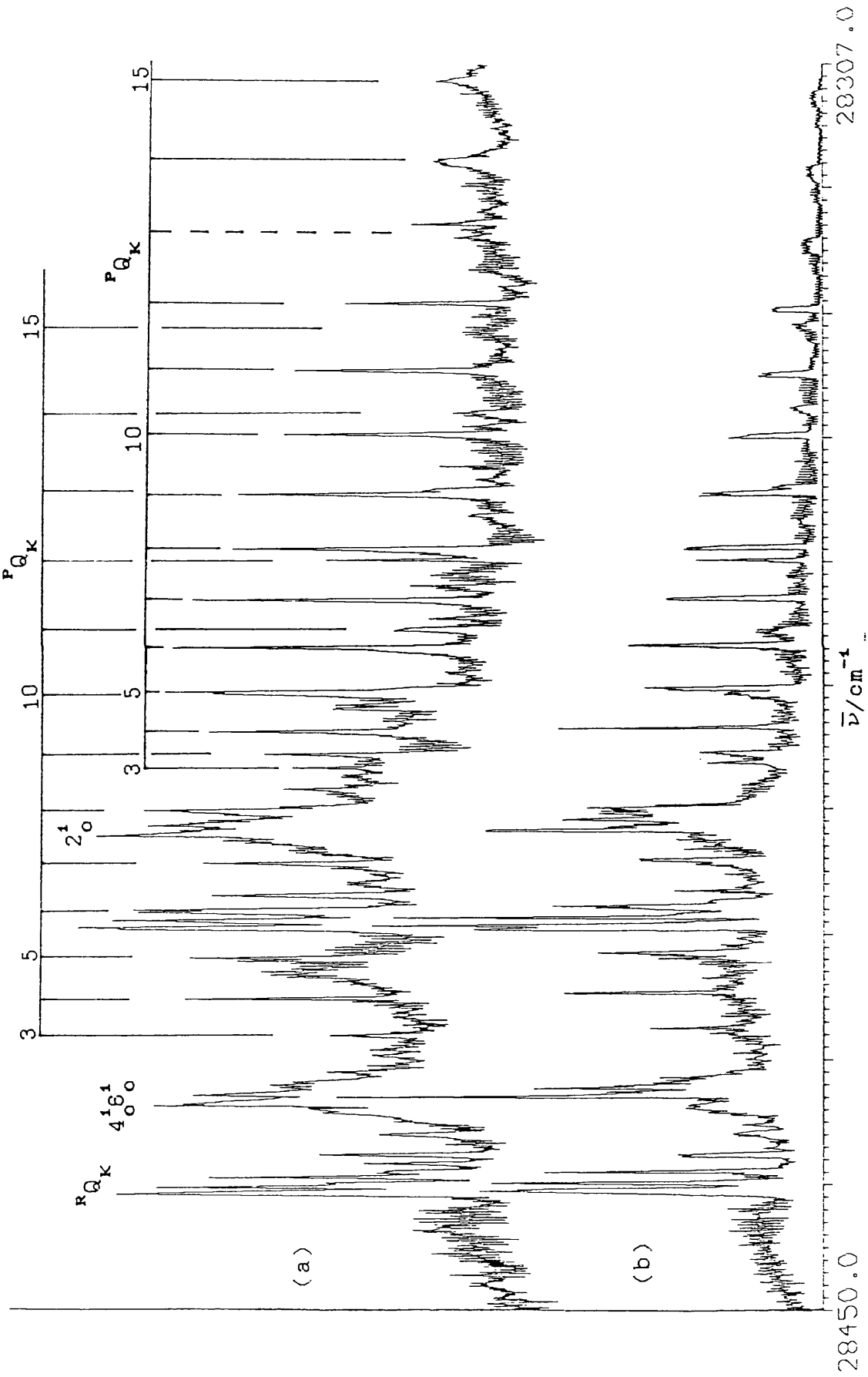

Figure 4.6. The bands 2_o^1 and $4_o^1 6_o^1$ of HCCCDO (a) observed and (b) calculated

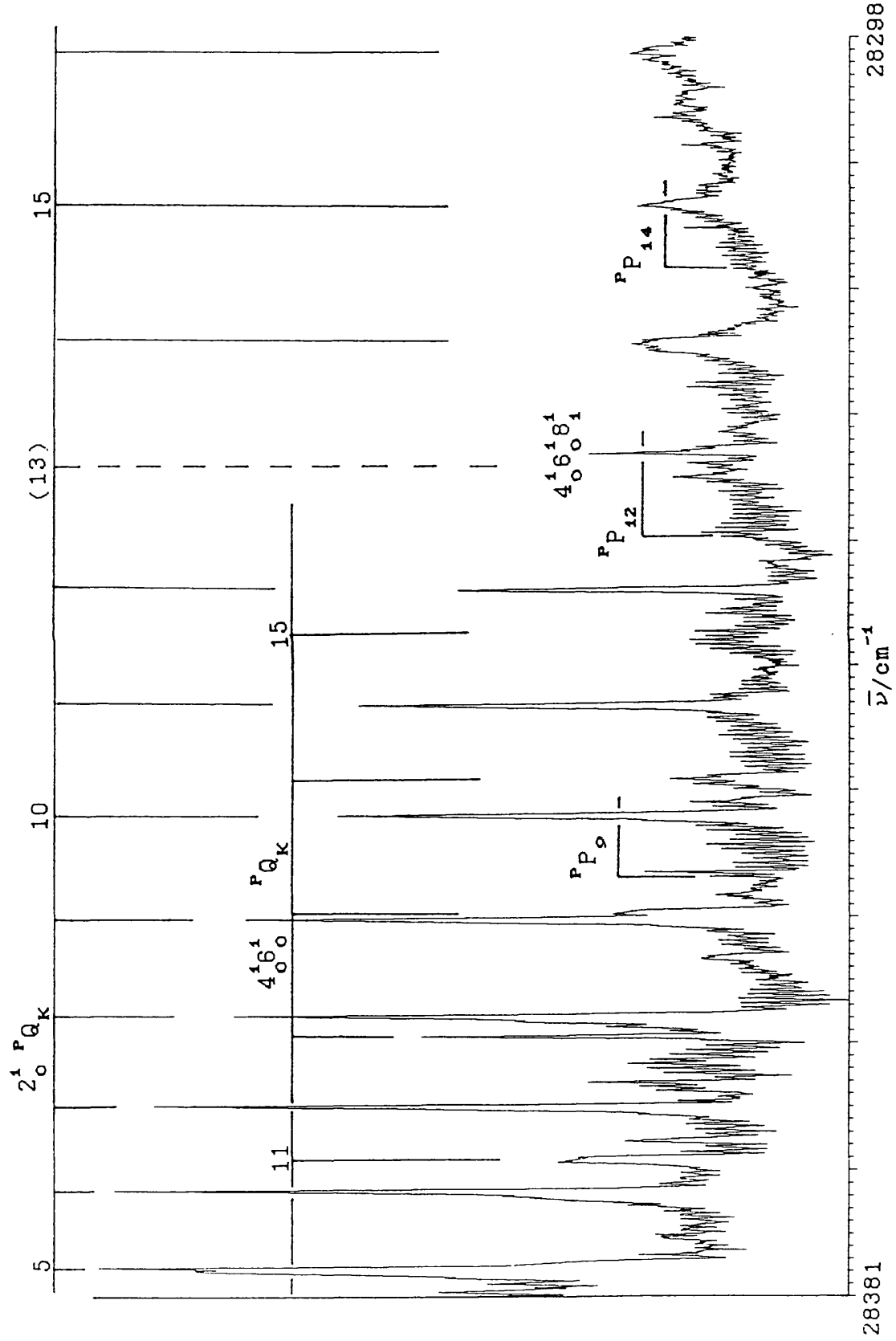

Figure 4.7. Perturbation in the 2_o^1 band of HCCCDO

Figure 4.8. Energy level diagram for the levels 2^1 and $4^1 6^1$ of HCCCDO

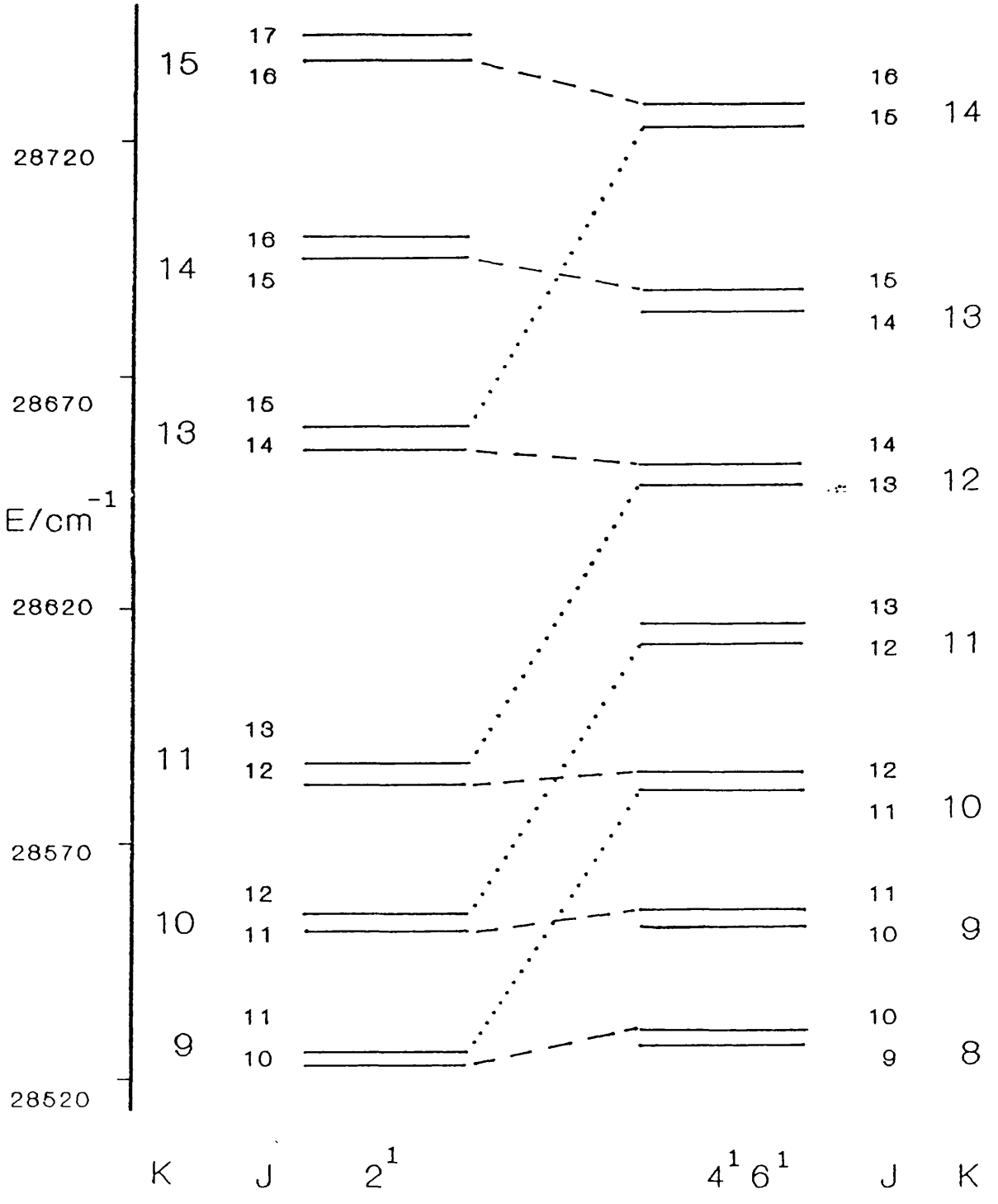

was originally attributed to a rotationally dependent predissociation [37] but this is unlikely since, as Watson noted [30], discrete rotational structure can still be seen above K' = 12 (see figure 4.7). Since the ground state rotational constants are known we can calculate the excited state energy levels of 2^1 and $4^1 6^1$ from the ^PQ heads of the two bands. Part of the resulting energy level diagram is shown in figure 4.8. The symmetries of the two levels are the same and therefore the selection rules for a Coriolis interaction are $\Delta J = 0$ and $\Delta K = \pm 1$ and the interaction term will be proportional to $[J(J+1) - K(K\pm1)]^{1/2}$. The allowed interactions are shown by the broken and dotted lines in the energy level diagram. From figure 4.8 we see that the J, K levels of 2^1 catch up with the J, K-1 levels of $4^1 6^1$ such that at K = 11 the J levels of 2^1 are lower than the J, K = 10 levels of $4^1 6^1$, and at K = 13 they are higher than the J, K = 12 levels of $4^1 6^1$. Extrapolating for the K = 12 levels of 2^1 we would expect the J levels to be very close to, but slightly higher than the J, K = 11 levels of $4^1 6^1$. Considering only the interactions indicated by the broken lines in the diagram we can now explain the appearance of the perturbation in the 2^1_0 band. For J ~ K the interaction will be small and thus the origins of the ^PQ heads will be relatively unperturbed. With increasing J the levels $K \leq 11$ will be increasingly pushed down such that the normal tendency of the heads to degrade to high frequency will be removed and the heads will appear sharp, as is observed. For $K \geq 12$ the J levels will be pushed up with increasing J which will enhance the normal degradation

and broaden the ^{P}Q heads. The effect will be largest for K = 12 and will decrease with increasing K. The opposite effect would then be expected for the $4^{1}6^{1}$ band and we do see that for this band the $^{P}Q_{12}$ head is much sharper than the $^{P}Q_{11}$ or the $^{P}Q_{13}$ heads (see figure 4.7). The corresponding effect of the interaction is also seen in the ^{R}Q heads of each band. The ^{P}P sub-bands of the band 2^{1}_{o} can not be followed for high J and the sub-bands of $4^{1}_{o}6^{1}_{o}$ are obscured and so a complete analysis of the interaction is not possible. The interaction has, however, been simulated as shown in figure 4.6. The simulated spectrum was obtained by using values for the band origins and $(A-\bar{B})'$ obtained from the first few ^{P}Q sub-band heads of each band and a value for $\bar{B}'$ obtained from the lower J,K ^{P}P lines of 2^{1}_{o}. It was assumed that $\bar{B}'$ was equal for the two bands. The best fit to the observed spectrum was obtained with the following constants: $\nu_{o}(2)$ = 28396.8 cm^{-1}, $(A-\bar{B})'_{2}$ = 1.36134 cm^{-1}, $\nu_{o}(4,6)$ = 28426.3 cm^{-1}, $(A-\bar{B})'_{4,6}$= 1.36451 cm^{-1}, $\bar{B}'_{2}$ = $\bar{B}'_{4,6}$= 0.1531 cm^{-1} and $|\zeta^{c}|$ = 0.075. The value obtained for the Coriolis constant is estimated to be accurate to ± 0.01.

The 2^{1}_{o} band of DCCCDO has been partially analysed from its K-structure and is seen to be perturbed for K' > 7. The ^{P}Q heads for K' = 2 to 7 give G_{o} = 2176.64 cm^{-1} and $(A - \bar{B})'$ = 1.292 cm^{-1} (σ = 0.04 cm^{-1}). The perturbation is clearly seen in the plot of $^{P}Q_{K+1}(2^{1}_{o}) - {}^{P}Q_{K+1}(0^{0}_{o})$ against K^{2} shown in figure 4.9 and is consistent with a $\Delta K = +1$ interaction with a level about 30 cm^{-1} lower than 2^{1}.

The only compound clearly containing the overtone 2^{2}_{o} is

Figure 4.9. Perturbation in the 2_o^1 band of DCCCDO

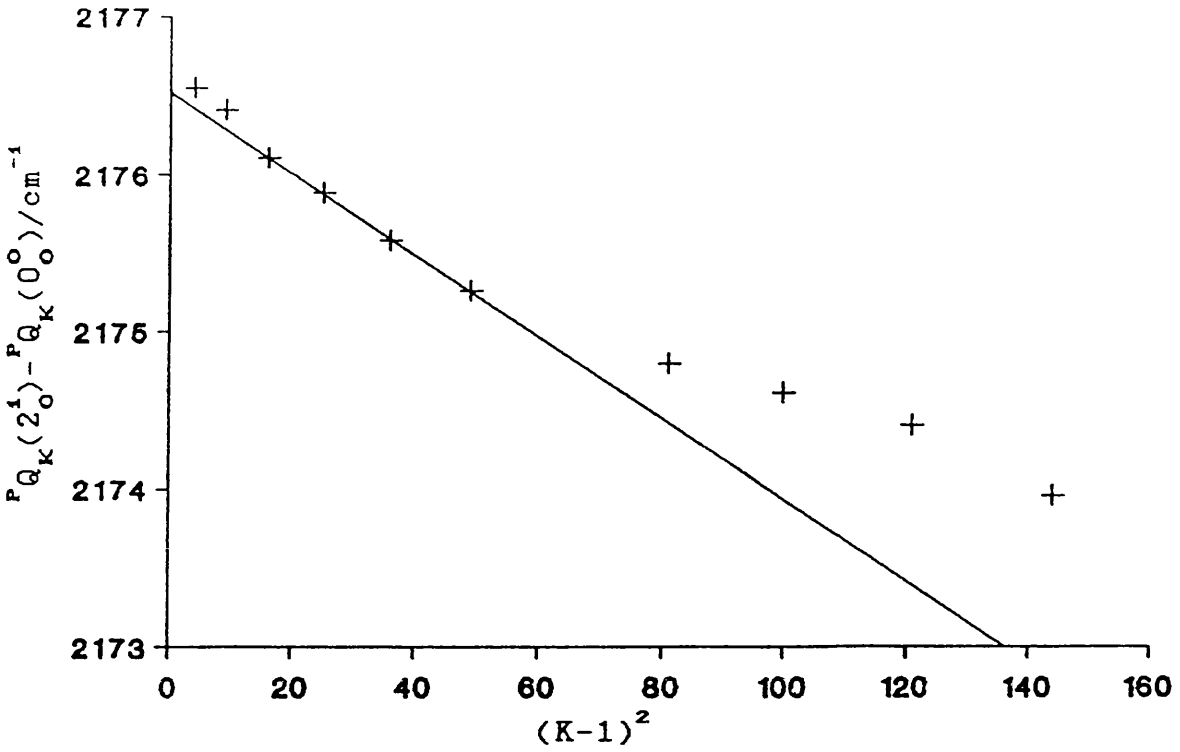

DCCCDO although the region where the band is expected in HCCCDO is complicated by other transitions. The rotational structure of the band in the spectrum of DCCCDO is very broad and there is no visible J-structure. The K-structure has been analysed to give G_o = 4316.1 cm^{-1} and $(A - \bar{B})'$ = 1.294 cm^{-1} (σ = 0.06 cm^{-1}).

The combination bands $2_o^1 4_o^1$ and $2_o^1 4_o^2$ are seen in the spectra of both HCCCDO and DCCCDO and in each case there is little or no J-structure. The band $2_o^1 4_o^1$ is also seen in the spectrum of the undeuterated compound. The $2_o^1 4_o^1$ band of DCCCDO is strongly perturbed for K' < 9 whereas the band $2_o^1 4_o^2$ appears to be well behaved and has been analysed to give G_o = 4646.3 cm^{-1} and $(A-\bar{B})'$ = 1.2958 cm^{-1} (σ = 0.09 cm^{-1}). The perturbation in the band $2_o^1 4_o^1$ is seen by a

Figure 4.10. Perturbation in the band $2^1_0 4^1_0$ of DCCCDO

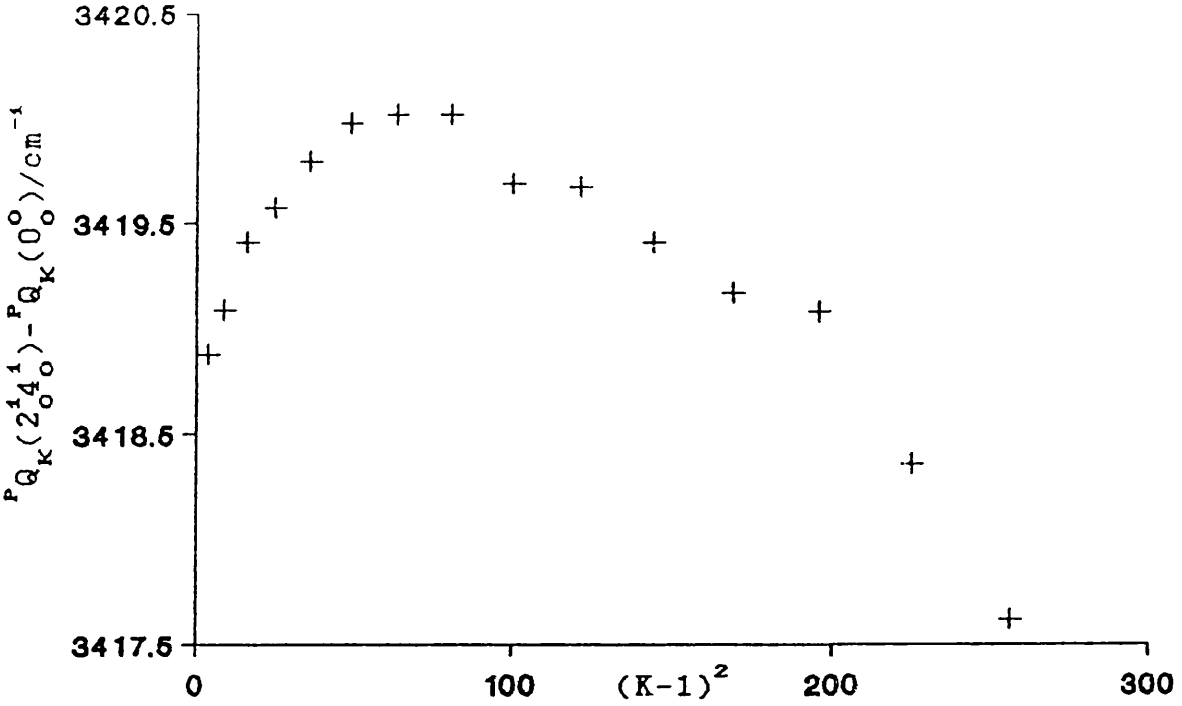

lowering of the ^PQ_K heads which decreases with increasing K as shown in the plot of $^PQ_K(2^1_0 4^1_0)$ - $^PQ_K(0^0_0)$ against $(K-1)^2$ in figure 4.10. The fact that the perturbation is largest at low K suggests that the perturbing level is only slightly higher in energy than the level $2^1 4^1$. The band $2^1_0 4^1_0$ in HCCCHO exhibits a similar perturbation although the ^PQ_K heads can not be followed beyond K = 12 in this case and do not approach an unperturbed nature.

The $2^1_0 4^2_0$ of HCCCDO is well behaved and analyses to give G_0 = 4678.9 cm^{-1}, $(A-\bar{B})'$ = 1.2989 cm^{-1} and D'_K = 1.647 cm^{-1}. The band $2^1_0 4^1_0$ however shows a small perturbation where the ^PQ_K heads are pushed down for K = 9 to 11 and pushed up for K = 13 to 15 with the other heads giving G_0 = 3443.8 cm^{-1}, $(A-\bar{B})'$ = 1.3057 cm^{-1} and D'_K = 6.902 × 10^{-5} cm^{-1}. By analogy

with the band 2_0^1 this perturbation is attributed to an interaction with the level $4^2 6^1$.

Brand and co-workers have followed the Fermi resonance between ν_2' and $\nu_4' + \nu_\sigma'$ in the spectrum of HCCCDO and have determined the unperturbed zero order frequencies and anharmonic coefficients to be ω_2^o = 2243.0, ω_4^o = 1275.0, ω_σ^o = 944.5, x_{22} = -39.0, x_{44} = -7.6, $x_{\sigma\sigma}$ = -2.6, x_{24} = -0.4, $x_{2\sigma}$ = -15.1 and $x_{4\sigma}$ = -1.3 (all in cm^{-1}) [38]. The values obtained for ν_4' agree well with those found in this work given in section IV.2.4.4.

IV.2.4.3 ν_3'

The ethynyl C≡C stretch forms medium intensity fundamentals observed in all four of the compounds analysed. The K-structure of the band 3_0^1 of HCCCHO exhibits a rotational perturbation between K' = 5 and 7. When the ^PQ heads are fitted to equation 4.5, as shown in figure 4.11, we see that ^PQ_K (K = 3, 4, 5, 9 and 10) lie on a fairly straight line which gives G_o = 1945.6 cm^{-1} and $(A - \bar{B})'$ = 1.755 cm^{-1}. $^PQ_\sigma$ is pushed down from this line whereas ^PQ_K (K = 7 and 8) are pushed up. This is consistent with a ΔK = -1 interaction with a level about 17 cm^{-1} higher than 3^1.

The fundamental in DCCCHO shows only weak J-structure and the K-structure analyses to give G_o = 1851.426 cm^{-1} and $(A - \bar{B})'$ = 1.6638 cm^{-1} (σ = 0.3 cm^{-1}). In HCCCDO the band is heavily overlapped and no analysis was attempted.

The fundamental band in DCCCDO exhibits a Coriolis

Figure 4.11. Perturbation in the band 3_o^1 of HCCCHO

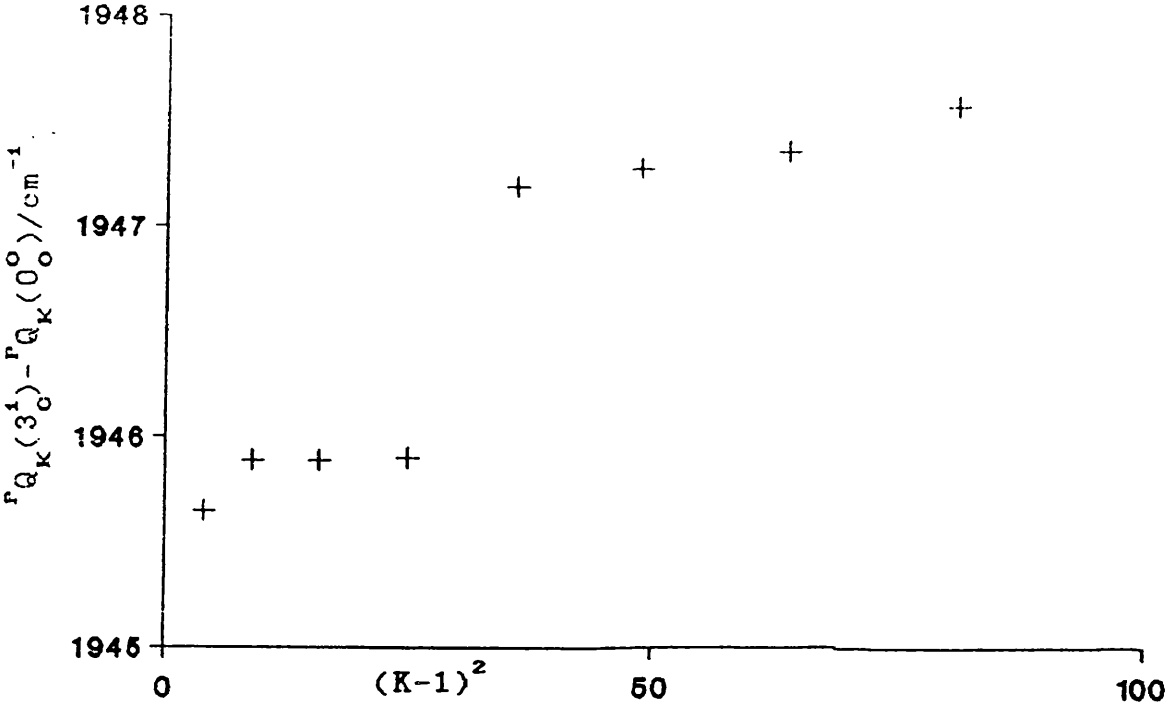

perturbation in the K-structure between K' = 7 and 8 with a maximum perturbation at K' = 8. The ^PQ heads either side of the perturbation analyse to give G_o = 1848.7 cm^{-1} and $(A - \bar{B})'$ = 1.345 cm^{-1}. The interaction is seen by a lowering of $^PQ_9$ and a raising of $^PQ_{10}$ and is consistent with a $\Delta K = -1$ interaction involving a level about 20 cm^{-1} above 3^1, for which the level 6^2 is one possibility although the ^PQ heads of this band can not be followed above K' = 6.

The only overtone of this vibration observed is the 3_o^2 band of HCCCDO and this assignment is only tentative as the band is rather weak and overlapped by other bands.

The combination bands $3_o^1 4_o^1$ are seen in all of the spectra but in each case they are either too weak or too overlapped for analysis. The band $3_o^1 4_o^2$ is seen in the

spectrum of HCCCDO and its K-structure analyses to give G_o = 4457.5 cm^{-1} and $(A-\bar{B})'$ = 1.2709 cm^{-1} (σ = 0.18 cm^{-1}).

IV.2.4.4 ν_4'

The principal progression forming mode is the carbonyl stretching frequency ν_4. The bands 4_o^n and their combination bands in both the normal compound and the molecule DCCCHO are all seriously overlapped and perturbed by Fermi and Coriolis resonances. In the aldehydic deuterated molecules, however, the bands are all single and in general are unperturbed. The rotational constants for the bands 4_o^1 and 4_o^3 of HCCCDO have been obtained by least squares fits as previously described and are given in tables 4.8 and 4.9. Similarly the constants for the bands 4_o^2 and 4_o^3 of DCCCDO are given in tables 4.10 and 4.11. The observed and calculated spectra of the 4_o^1 band of HCCCDO are compared in figure 4.12.

The 4_o^4 bands of the two molecules do not show any J structure and have been only partially analysed from the ^PQ heads. The results obtained are given below in table 4.7.

Table 4.7. The levels 4^4 of HCCCDO and DCCCDO

	HCCCDO	DCCCDO
G_o /cm^{-1}	4982.0	4955.9
$(A - \bar{B})'$/cm^{-1}	1.243	1.240
σ /cm^{-1}	0.3	0.1

Table 4.8. Molecular constants of the 4^1 level of HCCCDO

	This work[a]
ν_o/cm^{-1}	27474.095 ± 0.006
B_x/cm^{-1}	0.1681006 ± 0.0001
B_y/cm^{-1}	0.1381910 ± 0.0001
B_z/cm^{-1}	1.4615022 ± 0.0001
$\Delta_J \times 10^8/cm^{-1}$	18.928 ± 0.5
$\Delta_{JK} \times 10^6/cm^{-1}$	-8.532 ± 0.2
$\Delta_K \times 10^4/cm^{-1}$	0.92963 ± 0.004
$\Phi_{KJ} \times 10^8/cm^{-1}$	-1.230 ± 0.07
$\varkappa$	-0.95480

(a) σ = 0.034cm^{-1}, 496 transitions.

Correlation coefficients:

	B_x	B_y	B_z	Δ_J	Δ_{JK}	Δ_K	Φ_{KJ}	ν_o
B_x	1.00	-0.97	0.16	0.32	-0.22	0.20	-0.11	-0.21
B_y		1.00	-0.04	-0.31	0.38	-0.10	0.27	0.04
B_z			1.00	-0.41	0.77	0.95	0.80	-0.81
Δ_J				1.00	-0.61	-0.29	-0.50	0.13
Δ_{JK}					1.00	0.68	0.96	-0.60
Δ_K						1.00	0.79	-0.67
Φ_{KJ}							1.00	-0.58
ν_o								1.00

Table 4.9. Molecular constants of the 4^3 level of HCCCDO

	This work[a]
ν_o/cm^{-1}	29963.402 ± 0.007
B_x/cm^{-1}	0.1644025 ± 0.0002
B_y/cm^{-1}	0.1425993 ± 0.0002
B_z/cm^{-1}	1.4088887 ± 0.0002
$\Delta_J \times 10^8/cm^{-1}$	17.534 ± 1.0
$\Delta_{JK} \times 10^6/cm^{-1}$	-6.329 ± 0.6
$\Delta_K \times 10^4/cm^{-1}$	0.77077 ± 0.01
$\Phi_{KJ} \times 10^8/cm^{-1}$	-1.131 ± 0.3
$\varkappa$	-0.96556

(a) σ = 0.031cm^{-1}, 346 transitions.

Correlation coefficients:

	B_x	B_y	B_z	Δ_J	Δ_{JK}	Δ_K	Φ_{KJ}	ν_o
B_x	1.00	-0.98	-0.03	0.45	-0.41	0.04	-0.29	-0.02
B_y		1.00	0.12	-0.41	0.52	0.03	0.39	-0.11
B_z			1.00	-0.44	0.77	0.94	0.78	-0.80
Δ_J				1.00	-0.65	-0.40	-0.59	0.08
Δ_{JK}					1.00	0.70	0.96	-0.56
Δ_K						1.00	0.79	-0.65
Φ_{KJ}							1.00	-0.52
ν_o								1.00

Table 4.10. Molecular constants of the 4^2 level of DCCCDO

	This work[a]
ν_o/cm^{-1}	28742.245 ± 0.01
B_x/cm^{-1}	0.1604696 ± 0.001
B_y/cm^{-1}	0.1240822 ± 0.001
B_z/cm^{-1}	1.3893162 ± 0.0004
$\Delta_{JK}\times10^5/cm^{-1}$	-5.054 ± 0.5
$\Delta_K\times10^4/cm^{-1}$	0.12983 ± 0.02
$\delta_J\times10^5/cm^{-1}$	3.039 ± 0.2
$\varkappa$	-0.942481

(a) σ = 0.045cm^{-1}, 206 transitions.

Correlation coefficients:

	B_x	B_y	B_z	Δ_{JK}	Δ_K	δ_J	ν_o
B_x	1.00	-0.99	0.48	-0.80	0.64	0.10	-0.15
B_y		1.00	-0.49	0.83	-0.66	-0.05	0.12
B_z			1.00	-0.32	0.90	-0.11	-0.73
Δ_{JK}				1.00	-0.66	0.01	-0.20
Δ_K					1.00	-0.08	-0.44
δ_J						1.00	-0.20
ν_o							1.00

Table 4.11. Molecular constants of the 4^3 level of DCCCDO

	This work[a]
ν_o/cm^{-1}	29972.007 ± 0.01
B_x/cm^{-1}	0.1596250 ± 0.002
B_y/cm^{-1}	0.1248698 ± 0.002
B_z/cm^{-1}	1.3899361 ± 0.0004
$\Delta_{JK}\times10^6/cm^{-1}$	-3.785 ± 0.7
$\Delta_K\times10^4/cm^{-1}$	1.13159 ± 0.03
$\delta_J\times10^6/cm^{-1}$	2.324 ± 0.5
$\varkappa$	-0.945054

(a) σ = 0.036cm^{-1}, 131 transitions.

Correlation coefficients:

	B_x	B_y	B_z	Δ_{JK}	Δ_K	δ_J	ν_o
B_x	1.00	-0.99	0.57	-0.77	0.67	0.75	-0.35
B_y		1.00	-0.58	0.79	-0.68	-0.72	0.34
B_z			1.00	-0.55	0.92	0.36	-0.81
Δ_{JK}				1.00	-0.80	-0.43	0.16
Δ_K					1.00	0.39	-0.59
δ_J						1.00	-0.40
ν_o							1.00

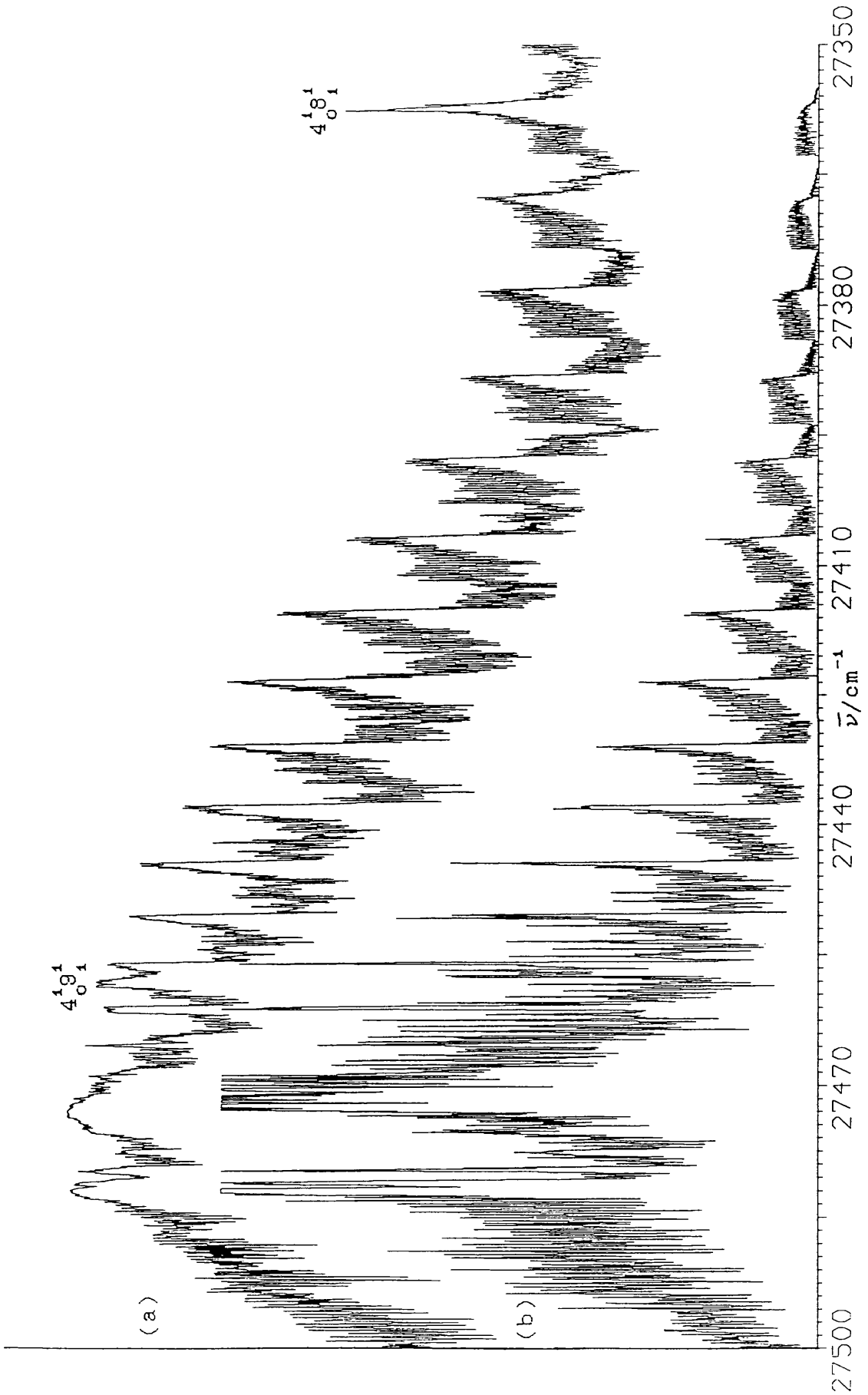

Figure 4.12. The 4_0^1 band of HCCCDO (a) observed and (b) calculated

From the band origins of the rotationally analysed bands we obtain the zero order frequencies and the x_{44} anharmonic coefficients given in table 4.12.

Table 4.12. ν_4' of HCCCDO and DCCCDO

	HCCCDO	DCCCDO
ω_4^o/cm^{-1}	1275.236	1269.145
x_{44}/cm^{-1}	-7.6455	-7.8767

The 4_o^1 band of DCCCDO and the 4_o^2 band of HCCCDO are both subject to rotational perturbations which are seen as a doubling of the ^PQ sub-band heads. The effect is more easily seen in HCCCDO and is shown in figure 4.13. In this band the at first weak low frequency ^PQ satellite appears for K' = 7 and gradually takes over the intensity until the other higher frequency component disappears after K' = 10. Using the relative intensities of the two perturbed bands we calculate the unperturbed levels and the matrix elements of the perturbation function W which appear to be linear in K (W = 0.185 × K) and zero at K = 0, as would be expected for a Coriolis interaction about the a axis. However this treatment does not extrapolate beyond K' = 10 or below K' = 7 when the predicted levels of the 4^2 state are used in the calculation. These levels can be interpolated from the other well behaved members of the 4^n progression. It therefore seems likely that there is at least one

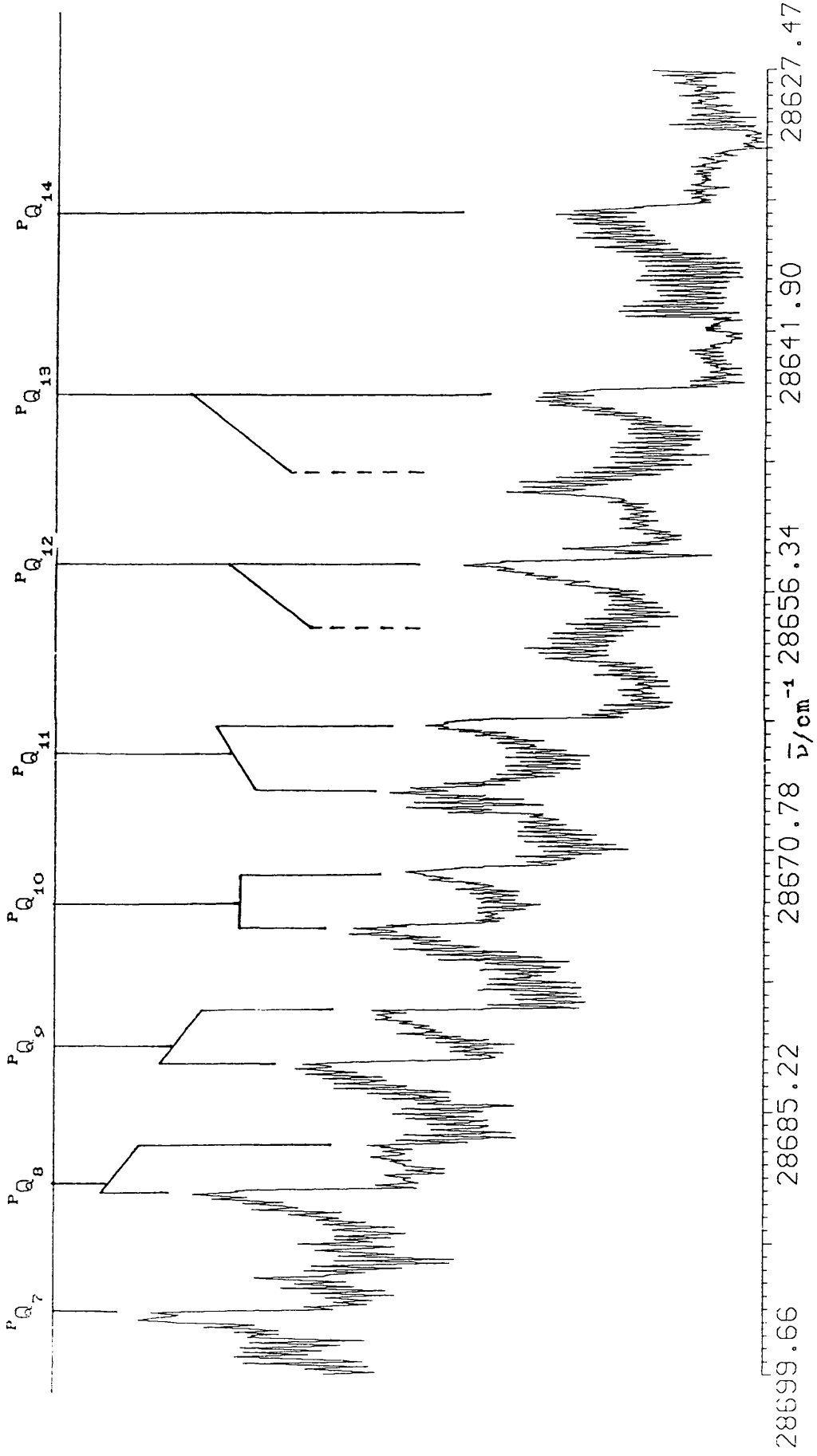

Figure 4.13. Perturbation in the 4_0^2 band of HCCCDO

additional level involved. A possible interpretation is a three level interaction involving 4^2, a level about 5 cm^{-1} below it with $(A-\bar{B})' \approx 1.35$ cm^{-1} and probably of A" symmetry, and an additional level very close to 4^2 with $(A-\bar{B})$ considerably less than 4^2. A possible candidate for the first perturbing state is $2^1 12^1$ which is calculated to lie about 5 cm^{-1} above 4^2 but would be pushed down by Fermi resonance with $4^1 6^1 12^1$ and would be expected to have a value of $(A-\bar{B})$ close to that predicted for the unknown state. If this is the case then we have $|\zeta^a| \sim 0.10$. More information may be obtained by an analysis of the ^RQ sub bands and also of the spectrum of the band $4_0^2 9_1^0$ although this band is rather overlapped by other systems.

The similar perturbation in the 4_0^1 band of DCCCDO is more localised and is only seen for K' = 7 and 8 and is therefore more difficult to analyse. However as this band is relatively low in energy (1260 cm^{-1} above the electronic origin) there are only a small number of candidates for the perturbing state. The most likely levels and their harmonic energies above the electronic origin are $5^1 10^1$ (1214 cm^{-1}), $5^1 8^1$ (1295 cm^{-1}), $6^1 11^1$ (1219 cm^{-1}) and $6^1 12^1$ (1250 cm^{-1}) of which the latter is clearly the most attractive. The $^PP_{K(J)}$ sub-branches of the 4_0^1 band have been analysed for K = 11 to 15 to give the following constants: $\nu_0(4^1)$ = 27495.324 cm^{-1}, $(A-\bar{B})'$ = 1.30204 cm^{-1}, $\bar{B}'$ = 0.14245 cm^{-1}, D_K' = 1.4385×10^{-4} cm^{-1}, D_{JK} = -3.385×10^{-6} cm^{-1} and D_J = 6.05×10^{-8} cm^{-1} (σ = 0.01 cm^{-1}).

As noted by Watson the expected position of the 4_0^1 band of HCCCHO lies between two strong C-type bands which are

separated by about 12 cm^{-1}. The rotational analyses of these bands is made complicated by severe overlapping of the sub-bands. Watson assigned these to a Fermi diad of which 4_0^1 is the lower, and $5_0^1 9_0^1$ the higher frequency component. Huber and co-workers [61] have detected a third band close to $5_0^1 9_0^1$ in the fluorescence excitation spectrum, recorded at a vibrational temperature of ~ 60 K and a rotational temperature of 1.5 K, thereby subjecting the previous assignment to some doubt. Huber's low temperature fluorescence spectrum is reproduced in figure 4.14 and the room temperature absorption spectrum is shown in figure 4.15.

In order to analyse the bands, labelled 1,2 and 3 in order of increasing frequency by Huber, we have used data obtained from figures 4.14 and 4.15.

From the large 1-2 and 1-3 separations we make the initial assumption that at low K band 1 is relatively unperturbed by Coriolis forces. A fit of the transitions to the excited state rotational constants B_x, B_y and B_z and the band origin ν_o confirms this prediction giving a standard deviation of 0.030 cm^{-1}. The constants obtained are given below in table 4.13.

Bands 2 and 3 have similarly been analysed to obtain the rotational constants given in tables 4.14 and 4.15. The calculated spectrum is compared to that observed by Huber in figure 4.14. In this figure all three bands were calculated as C-type bands but it should be noted that at this low rotational temperature there is very little difference between B-type and C-type bands.

Figure 4.14. Fluorescence excitation spectrum of bands 1, 2 and 3 of HCCCHO (lower plot) from reference [61] and the calculated absorption spectrum (upper plot)

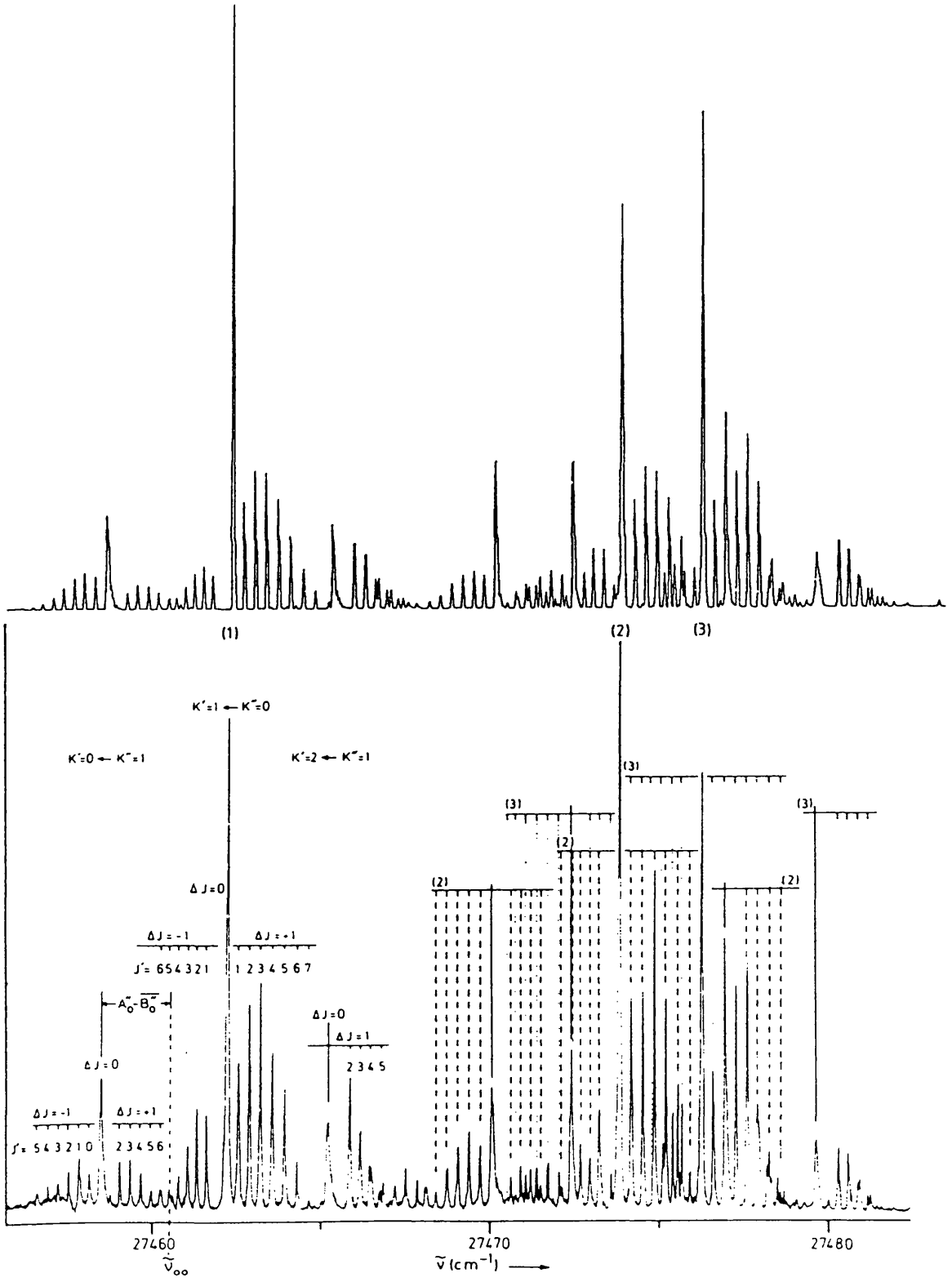

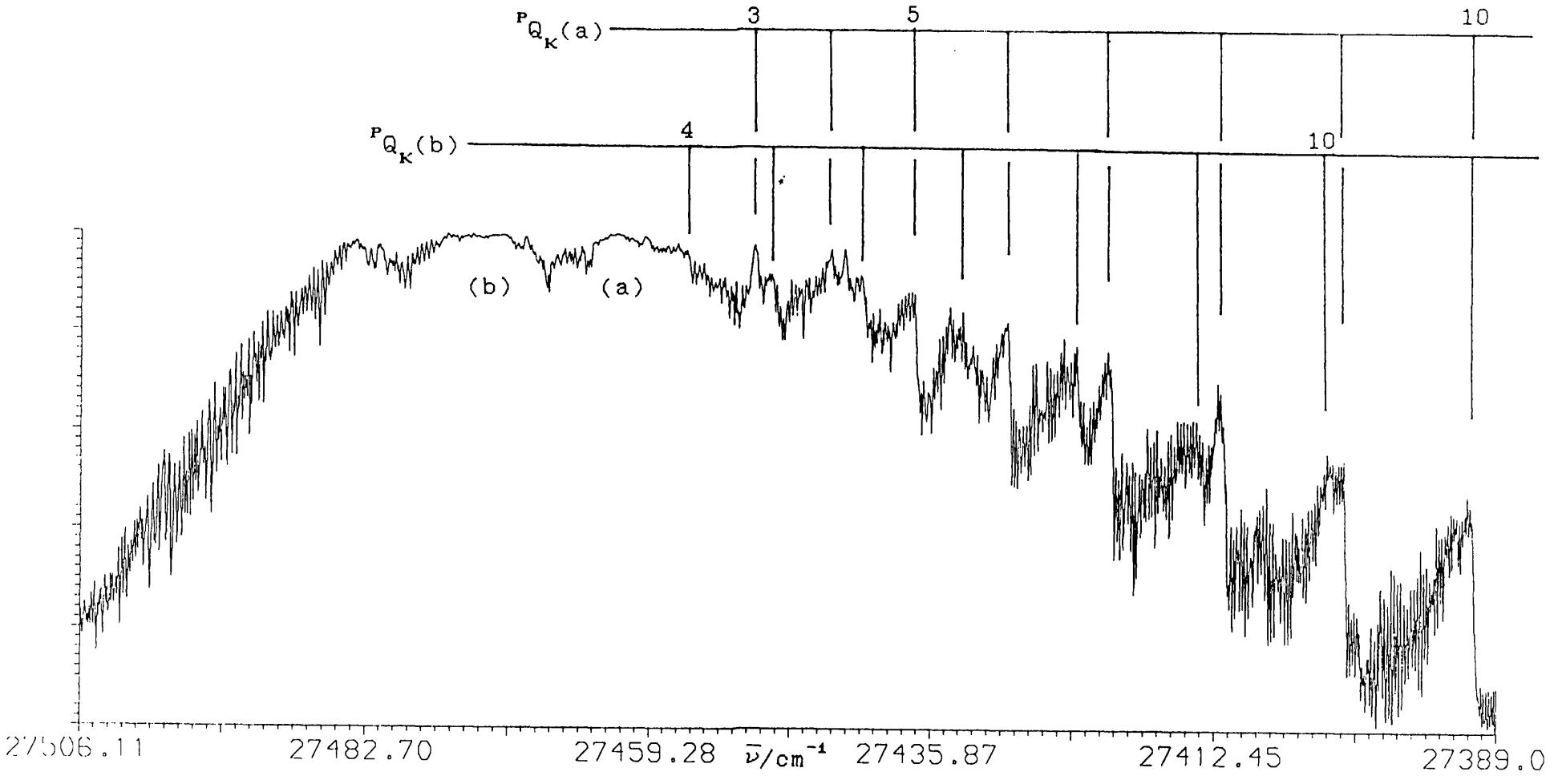

Figure 4.15. Absorption spectrum of HCCCHO in the 4_o^1 region

Table 4.13. Rotational constants of band 1 of HCCCHO

B_x/cm^{-1}	0.1631455 ± 0.0006
B_y/cm^{-1}	0.1538016 ± 0.001
B_z/cm^{-1}	1.8647097 ± 0.003
ν_o/cm^{-1}	27460.481 ± 0.009
σ/cm^{-1}	0.03

Correlation coefficients

	B_x	B_y	B_z	ν_o
B_x	1.00	-0.58	0.02	-0.24
B_y		1.00	-0.01	-0.39
B_z			1.00	-0.48
ν_o				1.00

Table 4.14. Rotational constants of band 2 of HCCCHO

B_x/cm^{-1}	0.1652505 ± 0.0009
B_y/cm^{-1}	0.1476009 ± 0.001
B_z/cm^{-1}	1.8867669 ± 0.004
ν_o/cm^{-1}	27472.103 ± 0.01
σ/cm^{-1}	0.033

Correlation coefficients

	B_x	B_y	B_z	ν_o
B_x	1.00	-0.49	0.04	-0.31
B_y		1.00	-0.06	-0.42
B_z			1.00	-0.51
ν_o				1.00

Table 4.15. Rotational constants of band 3 of HCCCHO

B_x/cm^{-1}	0.1608028 ± 0.001
B_y/cm^{-1}	0.1507015 ± 0.002
B_z/cm^{-1}	1.9726381 ± 0.007
ν_o/cm^{-1}	27474.430 ± 0.02
σ/cm^{-1}	0.05

Correlation coefficients

	B_x	B_y	B_z	ν_o
B_x	1.00	-0.44	0.20	-0.41
B_y		1.00	-0.18	-0.23
B_z			1.00	-0.65
ν_o				1.00

Any Coriolis interaction about either the b- or c-axes between bands 2 and 3 would be expected to be large for low K and have a maximum at K'(2) = 1, K'(3) = 0. However as the transitions to these levels are apparently well behaved we conclude that any such coupling is negligible. Any Coriolis interaction about the a-axis between these two bands would be reflected in the values for $(A-\bar{B})'$ obtained for the two states. The results of tables 4.14 and 4.15 give $(A-\bar{B})'_2$ = 1.73034 cm^{-1} and $(A-\bar{B})'_3$ = 1.81689 cm^{-1} which are not unusual and indeed if we assume that the difference between the two values is entirely due to an interaction we obtain $|\zeta^{a}_{2,3}| \sim 1\times10^{-3}$. However, any such interaction would become more important at higher values of K'.

In the room temperature ultraviolet absorption spectrum we see only two obvious bands which we have labelled (a) and (b) in figure 4.15. These bands are both of C-type and are centred on approximately 27462.2 cm^{-1} and 27474.6 cm^{-1} respectively. The ^{P}Q heads of the lower (a) band are relatively easy to pick out and have been analysed to give ν_o = 27462.6 cm^{-1} and $(A-\bar{B})'$ = 1.7119 cm^{-1} (σ = 0.1 cm^{-1}). This corresponds well with the results obtained for band 1 observed by Huber when we consider that his estimated accuracy of calibration is ± 2 cm^{-1}. Similarly the $^{P}Q_K$ heads of band (b) have been analysed for K = 5, 6, 8, 9 and 12 to give ν_o = 27474.4 cm^{-1} and $(A-\bar{B})'$ = 1.7127 cm^{-1} (σ = 0.2 cm^{-1}) corresponding to band 2 in the fluorescence excitation spectrum. The larger discrepancy between the values for $(A-\bar{B})'$ obtained from the two spectra (0.02cm^{-1} compared to 0.006 cm^{-1} for band 1) is not unexpected considering the relatively few ^{P}Q heads used in the analysis. Since both both bands 1 and 2 are of type C the upper levels of the two transitions can only be coupled by a $\Delta K = \pm 1$ interaction proportional to $[J(J+1)-K(K\pm1)]^{1/2}$. From the constants so far obtained we see that the K+1 levels of 1 catch up with the K levels of 2 at K=2 and overtake them for K > 3 and thus we would expect to see a maximum perturbation in the $^{P}P_4$ and $^{P}P_5$ sub-bands of 1 and in the $^{P}P_3$ and $^{P}P_4$ sub-bands of 2. Similarly if we assume a similar type of 1-3 interaction we would expect the maximum effect to be in the $^{P}P_6$ sub-band of 1.

Since the ground state is known the $^{P}P_{K(J)}$ sub-bands of band 1 can be used to calculate the energy levels for a

series of J' values for each K' value from K' = 4 to 13. These series have been fitted to the equations

$$E'(J',K') = C_o(K') + C_1(K')J'(J'+1) - D'_J J'^2(J'+1)^2 \quad (4.9)$$

where $C_o(K') = \nu_o + (A-\bar{B})'K'^2 - D'_K K'^4$ and $C_1(K') = \bar{B}' - D'_{JK}K'^2$. The values of $C_o(K')$ have been plotted against K' to give $\nu_o = (27462.58 \pm 0.09)cm^{-1}$, $(A-\bar{B})' = (1.71223 \pm 0.004)cm^{-1}$ and $D'_K = (2.63 \pm 0.4)\times10^{-4}cm^{-1}$. The D'_J values obtained vary from 2×10^{-8} to $8\times10^{-8}cm^{-1}$. The plot of $C_1(K')$ against K'^2 is shown in figure 4.16.

Figure 4.16. Plot of $\bar{B}' - D'_{JK}K'^2$ against K'^2 for band 1

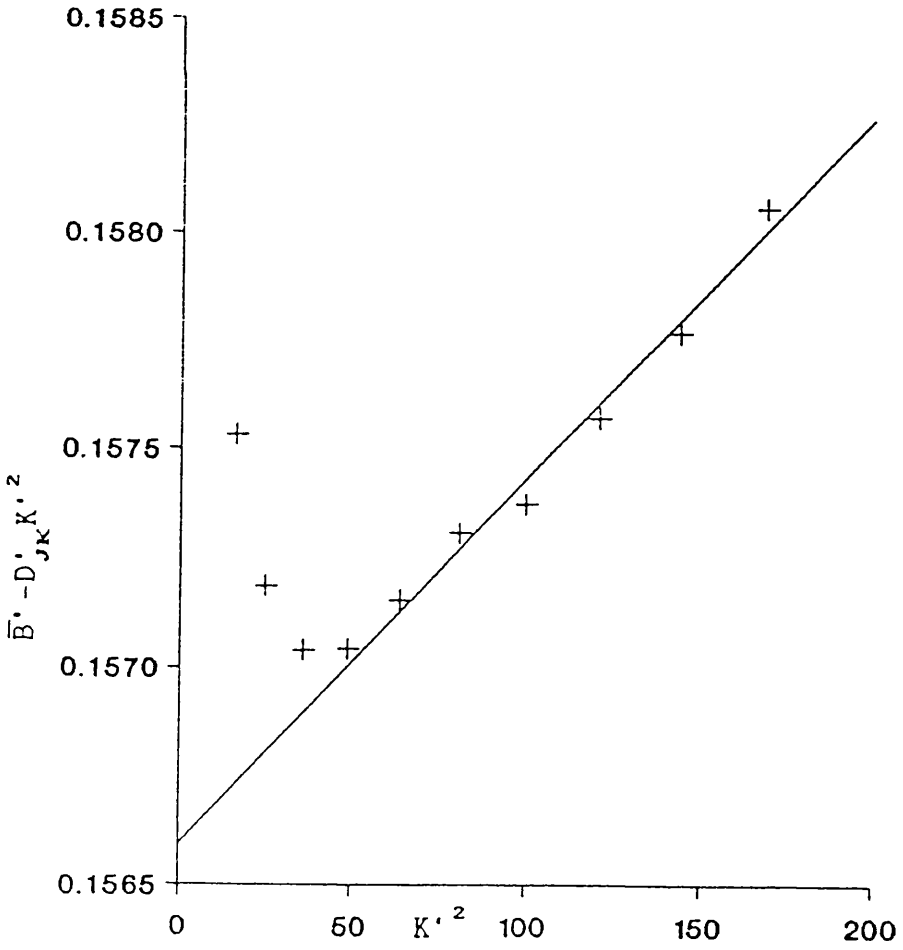

From figure 4.16 we see that for K' = 4 and 5 there is a significant deviation from the behaviour of the other K' levels. For K' > 7 we obtain $\bar{B}'$ = (0.15660 ± 0.0001) cm^{-1} and D'_{JK} = (-8.338 ± 0.06)×$10^{-6}cm^{-1}$. As expected the interaction between bands 1 and 2 is reflected in a raising of the effective $\bar{B}'$ value for K' = 4 and to a lesser extent for K' = 5. The smaller deviation of the K' = 5 levels suggests that any similar 1-3 interaction is much smaller.

From the apparent lack of 1-3 and 2-3 interactions about the c-axis we tentatively suggest that band 3 is due to a transition to a level of a'' symmetry giving rise to a B-type band. This suggestion is also attractive since it would explain both the absence of the band from the absorption spectrum, as such a band would be very much weaker than the C-type bands, and also the apparent lack of a Fermi interaction between bands 2 and 3. If this proposal is true then it follows that Watson's original assignment of band 1 to 4^1_0 and band 2 to $5^1_0 9^1_0$ is probably correct. The only vibration giving rise to B-type bands in the spectrum of HCCCHO is ν'_{10} and a possible assignment for band 3 is $10^2_0 11^1_0$ which is calculated to be at 27476.8 cm^{-1} in the harmonic approximation.

The 4^2_0 and 4^3_0 bands of HCCCHO have been partially analysed to give $G_0(4^2)$ = 2582.3cm^{-1}, $(A-\bar{B})'$ = 1.6829 cm^{-1} (σ = 0.09 cm^{-1}) and $G_0(4^3)$ = 3845.8cm^{-1}, $(A-\bar{B})'$ = 1.6577 cm^{-1} (σ = 0.03cm^{-1}).

The Fermi resonance between ν'_4 and $\nu'_5 + \nu'_9$ has been followed throughout the spectrum as shown below. Using the fact that the sum of the perturbed levels equals the sum of

the unperturbed levels we have fitted the vibrational levels 9^1, 9^2, 9^3, 5^1, 5^2, $4^1 + 5^19^1$, $4^19^1 + 5^19^2$, $4^19^2 + 5^19^3$, $4^15^1 + 5^29^1$, $4^2 + 4^15^19^1$, 5^29^2, $4^29^1 + 4^15^19^2 + 5^29^3$, $4^25^1 + 4^15^29^1 + 5^39^2$ and $4^3 + 4^25^19^1 + 4^15^29^2 + 5^39^3$ to the equation $E(i,j,k) = i\omega_4^o + iix_{44} + j\omega_5^o + jjx_{55} + k\omega_9^o + kkx_{99} + ijx_{45} + ikx_{49} + jkx_{59}$ by a least squares method, to obtain the constants given in table 4.16. The observed and calculated levels are also reproduced in table 4.16.

From table 4.16 we see that this treatment works fairly well except for the level 4^3 where the observed level is higher than the calculated level, however additional resonances cannot be ruled out at this high vibrational energy.

The three level interactions were calculated by splitting the overall effect into three separate two level interactions.

The 4_o^n series of DCCCHO is also subject to Fermi resonances with the $5_o^n9_o^n$ series. However, these interactions are made more complicated by the additional resonances of ν_5' and $\nu_6' + \nu_9'$.

IV.2.4.5 ν_5'

The aldehydic hydrogen bend produces strong fundamentals in the molecules HCCCHO and DCCCHO and weaker bands in the other two molecules. The 5_o^1 band in HCCCHO has been partially analysed to give G_o = 1119.5 cm^{-1}, $(A - \bar{B})'$ = 1.7097 cm^{-1} and D_K' = 2.668 cm^{-1}. All the other

Table 4.16. Fermi resonance of ν_4' and $\nu_5' + \nu_9'$ of HCCCHO

level	observed	calculated	
		perturbed	unperturbed
9^1	189.400	-	189.106
9^2	379.559	-	378.781
9^3	568.325	-	569.027
5^1	1119.537	-	1119.283
4^1	1299.639	1299.308	1304.493
$5^1 9^1$	1311.471	1311.139	1305.954
$5^1 9^2$	1485.200	1485.739	1493.195
$4^1 9^1$	1502.859	1503.393	1495.936
$5^1 9^3$	1676.759	1676.430	1681.006
$4^1 9^2$	1692.859	1692.525	1687.949
5^2	2232.859	-	2232.859
$4^1 5^1$	2406.940	2407.067	2416.257
$5^2 9^1$	2426.159	2426.286	2417.096
4^2	2582.310	2581.494	2584.058
$5^2 9^2$	2595.950	2595.135	2601.902
$4^1 5^1 9^1$	2617.859	2617.044	2605.266
$4^2 9^1$	2765.659	2765.673	2777.839
$5^2 9^3$	2784.959	2784.973	2787.278
$4^1 5^1 9^2$	2809.259	2809.273	2794.845
$4^2 5^1$	3676.661	3676.647	3688.304
$5^3 9^2$	3698.859	3698.845	3704.902
$4^1 5^2 9^1$	3726.659	3726.645	3708.889
4^3	3845.770		3838.696
$4^2 5^1 9^1$	3862.659		3879.651
$5^3 9^3$	3887.959		3887.844
$4^1 5^2 9^2$	3917.159		3896.033

ω_4^o = 1316.956, ω_5^o = 1122.137, ω_9^o = 188.821,

x_{44}= -12.464, x_{55}= -2.854, x_{99}= 0.285,

x_{45}= -7.519, x_{59}= -2.435, x_{49}= 2.338 all in cm^{-1}.

fundamental bands are either too overlapped or too weak for an analysis. The only overtone observed is the band 5_0^2 in the parent compound although there is also some evidence for the band 5_0^3.

For the normal compound we also see several combination bands involving ν_5'. The bands $4_0^1 5_0^1$ and $4_0^2 5_0^1$ have been analysed to give values for G_0, $(A-\bar{B})'$ and D_K' which are 2406.9 cm^{-1}, 1.6804 cm^{-1} and 1.5723×10^{-4} cm^{-1}; and 3676.7 cm^{-1}, 1.6064 cm^{-1} and -1.0472×10^{-3} cm^{-1} respectively. The negative effective value for D_K' obtained for the level $4^2 5^1$ implies that it is strongly perturbed. The combination bands of ν_4' and ν_5' of both HCCCDO and DCCCDO are too weak for analysis.

The band $4_0^1 5_0^1 9_0^1$ of HCCCHO has also been analysed to give G_0 = 2596.0 cm^{-1} and $(A-\bar{B})'$ = 1.6950cm^{-1}.

IV.2.4.6 ν_6'

The C-C stretching frequency ν_6 gives relatively strong fundamental bands in all four molecules although in HCCCHO and DCCCHO the bands are complicated by overlapping and resonances. The 6_0^1 bands of HCCCDO and DCCCDO have been subject to rotational analyses and the results are given in tables 4.17 and 4.18. The ^PQ and ^RQ heads of the fundamental band for HCCCDO are exceptionally sharp as shown in figure 4.17 and this is due to the relatively small change in $\bar{B}$ on excitation.

The 6_0^1 band of HCCCHO is shown in figure 4.18 and has

Table 4.17. Molecular constants of the 6^1 level of HCCCDO

	This work[a]
ν_o/cm^{-1}	27148.908 ± 0.005
B_x/cm^{-1}	0.1605502 ± 0.0002
B_y/cm^{-1}	0.1455671 ± 0.0002
B_z/cm^{-1}	1.5352903 ± 0.0001
$\Delta_J \times 10^8/cm^{-1}$	3.354 ± 1.0
$\Delta_{JK} \times 10^6/cm^{-1}$	-1.850 ± 0.2
$\Delta_K \times 10^4/cm^{-1}$	1.41169 ± 0.007
$\varkappa$	-0.978435

(a) σ = 0.043cm^{-1}, 332 transitions.

Correlation coefficients:

	B_x	B_y	B_z	Δ_J	Δ_{JK}	Δ_K	ν_o
B_x	1.00	-0.97	0.10	0.30	-0.28	0.16	-0.16
B_y		1.00	-0.14	-0.12	0.34	-0.23	0.05
B_z			1.00	-0.16	0.24	0.85	-0.57
Δ_J				1.00	-0.29	-0.09	-0.33
Δ_{JK}					1.00	-0.21	-0.29
Δ_K						1.00	-0.31
ν_o							1.00

Table 4.18. Molecular constants of the 6^1 level of DCCCDO

	This work[a]
ν_o/cm^{-1}	27166.978 ± 0.01
B_x/cm^{-1}	0.1568926 ± 0.0004
B_y/cm^{-1}	0.1293110 ± 0.0004
B_z/cm^{-1}	1.5386589 ± 0.0006
$\Delta_J \times 10^6/cm^{-1}$	1.235 ± 0.1
$\Delta_K \times 10^4/cm^{-1}$	2.71682 ± 0.05
$\varkappa$	-0.960859

(a) σ = 0.050cm^{-1}, 116 transitions.

Correlation coefficients:

	B_x	B_y	B_z	Δ_J	Δ_K	ν_o
B_x	1.00	-0.88	0.19	0.64	0.13	-0.32
B_y		1.00	-0.34	-0.22	-0.28	0.23
B_z			1.00	-0.10	0.96	-0.78
Δ_J				1.00	-0.13	-0.27
Δ_K					1.00	-0.67
ν_o						1.00

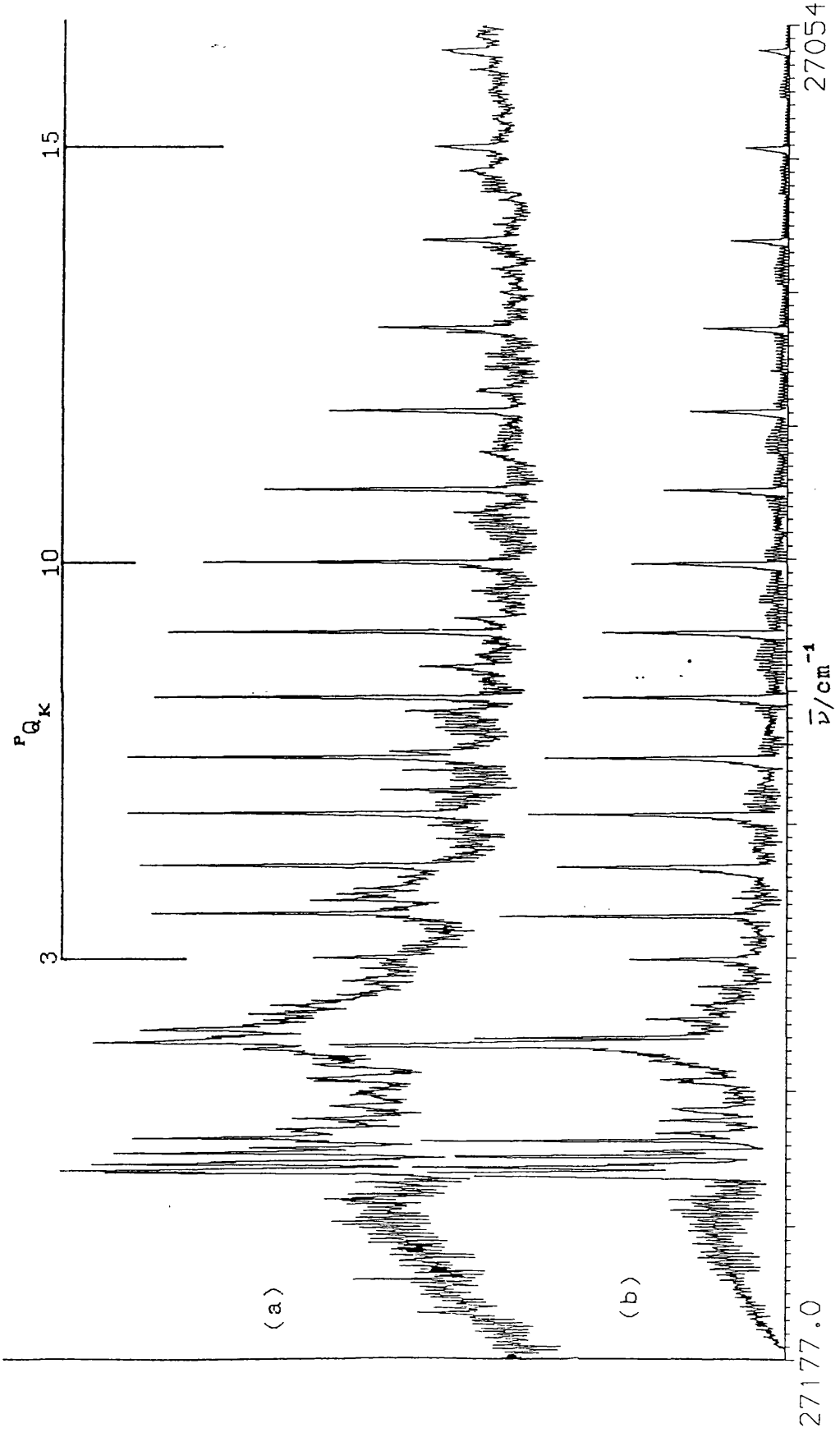

Figure 4.17. The 6_0^1 band of HCCCDO (a) observed and (b) calculated

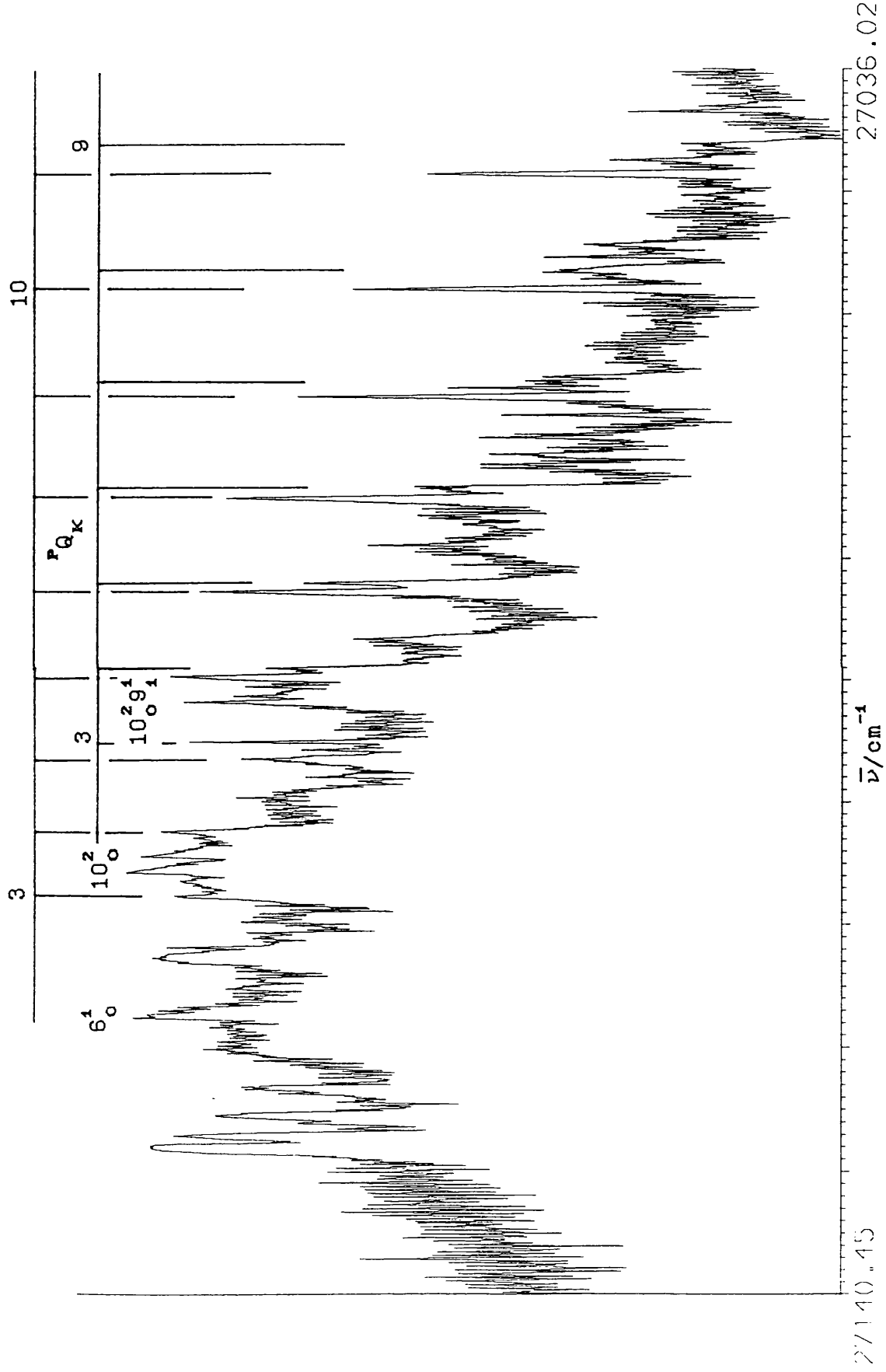

Figure 4.18. The bands 6^{1}_{o} and 10^{2}_{o} of HCCCHO

been partially analysed to give G_o = 956.9cm^{-1} and $(A-\bar{B})'$ = 1.773cm^{-1}. The 6^1 level is in resonance with the 10^2 level and if we assume that the intensity is entirely due to the fundamental [30] we obtain the unperturbed frequencies and the perturbation matrix element $W(6^1,10^2)$. This resonance can also be followed for the various combination bands involving ν_6' and $2\nu_{10}'$ and the results of this analysis are given in table 4.19. The unperturbed levels were calculated from the relative intensities of the observed bands and the relevant zero order frequencies and anharmonicity coefficients obtained are: ω_6^o = 957.369, x_{66} = -6.245, x_{69} = 2.359, x_{68} = -5.054, x_{610} = -4.986, x_{56} = 3.452, ω_{10}^o = 449.541, x_{1010} = 12.382, x_{910} = 0.031, x_{810} = -1.268 and x_{510} = -0.199 (all in cm^{-1}).

Table 4.19. Fermi resonance between ν_6' and $2\nu_{10}'$ of HCCCHO

level	observed	calculated	|W|
10^2	943.574	948.610	6.165
6^1	956.157	951.124	
$10^2 9^1$	1133.025	1137.778	6.575
$6^1 9^1$	1147.025	1142.589	
$10^2 8^1$	1446.759	1453.209	6.450
$6^1 8^1$	1459.659	1453.213	
$6^1 10^2$	1886.359	1889.758	3.400
6^2	1893.159	1889.762	
$5^1 10^2$	2063.859	2068.291	9.189
$5^1 6^1$	2075.859	2073.859	
$5^2 10^2$	3179.159	3182.265	5.315
$5^2 6^1$	3199.459	3190.887	

From the ^{P}Q heads of the bands 6^{1}_{0} and 10^{2}_{0} we can calculate the J ~ K energy levels for the two excited vibronic states and some of these are reported in table 4.20. Any Coriolis interaction between the two states would be largest between the J, K levels of 6^{1} and the J, K+1 levels of 10^{2} and from table 4.20 we would expect a maximum interaction for K = 4 and 5. Thus we would predict that an interaction would be seen in the $^{P}P_{J(5)}$ and $^{P}P_{J(6)}$ sub-bands of 6^{1}_{0} and the $^{P}P_{J(6)}$ and $^{P}P_{J(7)}$ sub-bands of 10^{2}_{0}. Unfortunately this region of the spectrum is complicated by the band $10^{2}_{0}9^{1}_{1}$ although there does seem to be some disruption of the $^{P}P_{7}$ structure of 10^{2}_{0} and the $^{P}Q_{7}$ head is slightly shifted up in energy when compared to the other

Table 4.20. The calculated energy levels of the vibronic levels 6^{1} and 10^{2} of HCCCHO

J	K	$E(J,K)6^{1}$	$E(J,K+1)10^{2}$
4	2	27130.2	27124.4
5	3	27140.8	27137.1
6	4	27155.0	27153.3
7	5	27172.8	27173.8
8	6	27194.6	27196.5
9	7	27220.2	27223.6
10	8	27249.4	27254.1
11	9	27282.3	27287.8
12	10	27318.7	27324.6
13	11	27358.7	26367.1
14	12	27402.1	27409.1

heads. Similarly the $^{P}Q_{\sigma}$ head of 6^{1}_{o} is shifted down in energy.

The 6^{2}_{o} band is seen in the spectrum of DCCCDO as a weak band for which only the lower K $^{P}Q_{K}$ heads are visible. These heads analyse to give G_{o} = 1867.1cm^{-1} and $(A-\bar{B})'$ = 1.385cm^{-1} (σ = 0.03 cm^{-1}). The same band in the spectrum of HCCCDO has been also been analysed giving G_{o} = 1878.2cm^{-1}, $(A-\bar{B})'$ = 1.444cm^{-1} and D'_{K} = 6.104×10^{-4}cm^{-1}.

The combination bands $4^{1}_{o}6^{1}_{o}$ and $5^{1}_{o}6^{1}_{o}$ are seen in the spectrum of HCCCHO and the first of these appears to be strongly perturbed when the ^{P}Q heads are fitted to equation 4.5. The perturbation is seen by a lowering of the $^{P}Q_{K}$ heads for K > 9.

IV.2.4.7 ν'_{7}

The ν'_{7} fundamental is not observed in the compounds HCCCHO and HCCCDO and gives only weak bands in DCCCHO and DCCCDO. Kelly and co-workers [62] have determined the 7^{1}_{o} band of HCCCHO in a Neon matrix to be at 0^{o}_{o} + 656 cm^{-1} and since the average gas-matrix shift of the other fundamentals was less than 0.2% this is probably close to the gas phase value. There is no evidence of any overtone bands in any of the spectra.

IV.2.4.8 ν_8'

The ν_8' vibration gives rise to weak fundamental bands in all of the compounds and the overtone 8_0^2 is seen as a weak band in all but the doubly deuterated molecule. The 8_0^1 band of HCCCHO has been analysed to give G_0 = 507.1 cm^{-1} and $(A - \bar{B})'$ = 1.810 cm^{-1}. Similar analysis of the fundamental in HCCCDO gives G_0 = 500.075 cm^{-1} and $(A - \bar{B})'$ = 1.384 cm^{-1} (σ = 0.08 cm^{-1}).

IV.2.4.9 ν_9'

The bands 9_0^1 and 9_0^2 are seen as medium and weak bands respectively in all four of the molecules and in all cases are overlapped by other similarly intense bands. The HCCCDO fundamental has been analysed from its K-structure to give G_0 = 187.4 cm^{-1} and $(A - \bar{B})'$ = 1.317 cm^{-1} (σ = 0.04 cm^{-1}). The 9_0^1 band of DCCCHO analyses to give G_0 = 181.5cm^{-1} and $(A-\bar{B})' \sim (A-\bar{B})_0'$.

IV.2.4.10 ν_{10}'

The out of plane fundamental ν_{10}' gives medium strength A-type or A/B-hybrid bands in all of the molecules studied. All of the 10_0^1 bands have been partially analysed and the results are tabulated in table 4.21. The observed and calculated spectra of the 10_0^1 bands of HCCCHO and DCCCDO

are shown in figures 4.2 and 4.4 respectively. The band in HCCCHO is primarily a B-type band whereas that of DCCCDO is an A/B-hybrid band. The best fit to the observed spectrum of the fundamental in the doubly deuterated molecule was achieved by simulating the band as a 55% A-type and 45% B-type mixture.

Table 4.21. The levels 10^1

molecule	$G_o(10)/cm^{-1}$	$(A-\bar{B})'_{10}/cm^{-1}$	$(A-\bar{B})'_{10}-(A-\bar{B})'_o/cm^{-1}$
HCCCHO	461.9	1.697	-0.036
DCCCHO	458.7	1.665	-0.034
HCCCDO	411.2	1.308	-0.030
DCCCDO	401.2	1.278	-0.044

The overtones 10^2_o are seen as weak bands in all but the normal compound where the intensity is enhanced by resonance with 6^1_o. These bands are shown in figure 4.18.

The combination bands $4^1_o10^1_o$ and $4^1_o10^2_o$ of HCCCHO are sufficiently strong for partial analysis and the results give $G_o(4^110^1) = 1754.8cm^{-1}$, $(A-\bar{B})' = 1.6664cm^{-1}$ (σ = 0.1 cm^{-1}) and $G_o(4^210^1) = 3028.2cm^{-1}$, $(A-\bar{B})' = 1.6402cm^{-1}$ (σ = 0.1cm^{-1}).

IV.2.4.11 ν'_{11}

The ν'_{11} fundamental is seen only in the normal compound where it is extremely weak and the overtones 11^2_o in the molecules DCCCHO and DCCCDO are tentative assignments to weak bands.

IV.2.4.12 ν'_{12}

The band 12^1_o is seen as a medium A-type band in all the compounds and the overtone 12^2_o is observed as weak bands in all but the doubly deuterated molecule. The fundamental bands have been analysed from their ^QQ_K heads for all the compounds and the results are given in table 4.22. The 12^1_o band of HCCCHO is shown together with the calculated band in figure 4.3 (page 57).

Table 4.22. The levels 12^1

constant/cm^{-1}	HCCCHO	DCCCHO	HCCCDO	DCCCDO
$G_o(12)$	345.7	347.0	321.8	320.1
$(A-\bar{B})'_{12}$	1.7199	1.6727	1.3435	1.3248
$(A-\bar{B})'_{12}-(A-\bar{B})'_o$	-0.014	-0.027	+0.006	+0.003
$D'_K \times 10^4$	3.03	4.05	-	1.24
σ	0.1	0.04	0.1	0.01

The combination band $4_0^1 12_0^1$ of DCCCHO has been partially analysed from its ${}^{Q}Q_K$ structure giving G_o = 1649.16cm^{-1}, $(A-\bar{B})'$ = 1.6775cm^{-1} and D_K' = 3.26×10^{-4}cm^{-1} (σ = 0.2cm^{-1}) for the level $4^1 12^1$. The same band in HCCCDO analyses to give G_o = 1587.88 cm^{-1}, $(A-\bar{B})'$ = 1.3117cm^{-1} and D_K' = 1.082cm^{-1} (σ = 0.1cm^{-1}).

IV.2.5 HOT BANDS

Several hot bands are observed in the ultraviolet spectrum of propynal, the strongest in all four of the isotopically substituted species studied being the band 9_1^0, as would be expected since ν_9'' is the lowest frequency vibration in the ground state. Watson [30] has analysed the bands 9_1^0 and 12_1^1 for the normal and singly deuterated compounds to obtain $(A - \bar{B})_9''$, $(A - \bar{B})_{12}''$ and $\zeta_{9,12}^{a''}$. In this work the corresponding result for DCCCDO has been calculated from the bands 9_1^0 and 12_1^0 and the complete set of results are summarised in table 4.23. The analysis is based on the assumption that the observed values for $(A - \bar{B})_9''$ and $(A - \bar{B})_{12}''$ lie symmetrically about the unperturbed value which is close to the vibrationless value $(A - \bar{B})_o''$.

Analysis of the band 9_2^0 for DCCCDO gives G_o = 385.2 cm^{-1} and $(A - \bar{B})''$ = 1.349 cm^{-1}. Assuming that the unperturbed value of $(A - \bar{B})''$ = 1.570 cm^{-1} the observed value is in good agreement with the equation

$$(A-\bar{B})''_{obs}(2\nu_9) - (A-\bar{B})''(2\nu_9) = 2\{(A-\bar{B})''_{obs}(\nu_9) - (A-\bar{B})''(\nu_9)\}.$$

Similarly the 9_2^0 band of DCCCHO has been analysed to

Table 4.23. Coriolis coupling of ν_9'' and ν_{12}''

	HCCCHO	DCCCHO	HCCCDO	DCCCDO[a]
ν_9'' /cm^{-1}	205.3	195.6	201.5	192.2
ν_{12}''/cm^{-1}	260.6	248.5	249.9	237.7
$(A - \bar{B})''_{9,12}$/cm^{-1}	2.122	2.090	1.570	1.570
$\lvert\zeta^{a}''_{9,12}\rvert$	0.639	0.634	0.675	0.661

From reference [30] except a: this work.

give G_0 = 392.2 cm^{-1} and $(A-\bar{B})''$ = 1.805 cm^{-1}.

For HCCCHO we see the three hot bands 9_2^0, $9_1^0 12_1^0$ and 12_2^0 and these have been analysed to give values for G_0 and $(A - \bar{B})''$ which are 410.9 and 1.862; 470.2 and 2.188; 520.0 and 2.425 cm^{-1} respectively. We see from this that the levels $2\nu_9''$ and $2\nu_{12}''$ are approximately equally placed either side of the level $\nu_9''\nu_{12}''$ as are the corresponding values of $(A - \bar{B})''$. These observations can be discussed in terms of Coriolis interactions between $2\nu_9''$ and $\nu_9''\nu_{12}''$ and between $\nu_9''\nu_{12}''$ and $2\nu_{12}''$ having a net result of leaving the intermediate level close to its unperturbed character.

The 10_1^0 hot band of DCCCDO analyses to give G_0 = 840.0 cm^{-1} and $(A - \bar{B})''_{10}$ = 1.525 cm^{-1}. From infrared results of ν_6'' and his ultraviolet study Watson has calculated the Coriolis coupling constants $\lvert\zeta^{a}''_{6,10}\rvert$ for HCCCHO and DCCCHO to be 0.25 in both cases. Using the assumption that the unperturbed value of $(A - \bar{B})''_{10} = (A - \bar{B})''_0$ we obtain the similar result $\lvert\zeta^{a}''_{6,10}\rvert$ = 0.26 for DCCCDO.

The 4_1^0 hot bands are relatively unperturbed for HCCCHO and DCCCHO whereas they are doubled by Fermi resonance for

HCCCDO and DCCCDO. A partial analysis of the K-structure of the hot band for HCCCHO gave G_o = 1697.3 cm^{-1} and $(A - \bar{B})''_1$ = 2.093 cm^{-1}.

From the ^RQ_K heads of the bands $10^2_0 9^0_1$ and 9^0_1 of DCCCHO we obtain G_o = 949.32cm^{-1} and $(A-\bar{B})'$ = 1.7469cm^{-1} for the level 10^2. This level is pushed up from its expected position by Fermi resonance with the level 6^1.

IV.2.6 SEQUENCES AND CROSS SEQUENCES

All of the strong C-type bands and indeed most of the weaker ones are followed by the sequence bands $X^y_z 9^n_n$ where n has values from 1 up to 3 for the strongest bands. The sequence bands 8^1_1 are also seen in the spectra of all of the compounds and can be seen in combination with the bands 4^n_o and some of the other strong bands. Similarly for DCCCHO and DCCCDO we see the sequence bands 7^1_1 and $4^n_o 7^1_1$. In addition we see the cross sequence $7^1_o 8^0_1$ in DCCCHO and the two bands $7^1_o 8^0_1$ and $7^0_1 8^1_o$ in DCCCDO.

The $6^1_o 9^1_1$ band of HCCCDO has been studied by plotting the differences $^PQ_K(6^1_o 9^1_1)$ - $^PQ_K(9^0_1)$ against $(K-1)^2$ to give $G_o(6^1 9^1)$ = 1130.70cm^{-1} and $(A-\bar{B})'$ = 1.3755cm^{-1} (σ = 0.1 cm^{-1}). Similarly we can use the differences $^PQ_K(9^1_2)$ - $^PQ_K(9^0_2)$ of DCCCDO to obtain $G_o(9^1)$ = 180.1 cm^{-1} and $(A-\bar{B})'$ = 1.3040cm^{-1} (σ = 0.08cm^{-1}).

All the sequence bands v^1_1 are seen for the out of plane vibrations in each of the four compounds studied with 12^1_1 about 10 times as intense as 10^1_1 or 11^1_1 in each case. The

band 12_2^2 is also seen in the spectra of all but the doubly deuterated compound and the band 12_3^3 is seen in the spectrum of HCCCDO.

In addition to the sequences mentioned above we also see a number of cross sequences of the type $i_0^1 k_1^0$ which implies some mixing of the normal coordinates on excitation. In particular the band $11_0^1 12_1^0$ is seen in all the spectra and the band $11_1^0 12_0^1$ is seen in all but the spectrum of DCCCHO implying that the excited state vibrations are mixtures of the two ground state coordinates [38].

From the band 11_1^1 in HCCCHO we can use Watson's infrared analysis of ν_{11}'' to analyse the excited state fundamental. ν_{11}'' is coupled by Coriolis forces to ν_7'' and we obtain the effective value for $(A - \bar{B})''_{eff} = 2.542$ from second order perturbation theory by

$$(A - \bar{B})''_{eff} = (A - \bar{B})''_{11} + \left\{\left(\frac{\nu}{\nu_7}\right)^{\frac{1}{2}} + \left(\frac{\nu_7}{\nu_{11}}\right)^{\frac{1}{2}}\right\}^2 A^2 \zeta^2_{7,11}/(\nu_{11} - \nu_7).$$

Analysis of the ^PQ sub-bands of 11_1^1 then gives $G_o = 385.3$ cm^{-1} and $(A - \bar{B})' = 1.982$ cm^{-1} for the level 11^1.

The level 11^1 is therefore close to the level 12^1 which has $G_o = 345.7$ cm^{-1} and we might expect there to be a Coriolis interaction between the two. However since the symmetries of the two levels are the same the only allowed interaction is about the c axis and would not give a simple K^2 dependence. Such an interaction could only therefore be investigated from the J-structure which is however weak.

A similar investigation of the 11_1^1 band of DCCCHO gives $G_o = 288.1$ cm^{-1} and $(A - \bar{B})' = 1.866$ cm^{-1} for the level

11^1. For HCCCDO the corresponding analysis gives $G_o(11)$ = 372.5 cm^{-1} and $(A - \bar{B})'_{11}$= 1.450 cm^{-1}.

The 12^2_1 band of DCCCHO has been analysed from its ^QQ_K sub-bands giving G_o = 692.46 cm^{-1}, $(A-\bar{B})'$ = 1.6585 cm^{-1} and D'_K = $2.321\times10^{-4}cm^{-1}$ for the 12^2 level (σ = 0.07cm^{-1}). From these results and those previously obtained for 12^1_o we obtain $\alpha_{12}^{(A-\bar{B})}$ = 0.014 cm^{-1}, ω^o_{12}= 347.838 cm^{-1} and $x_{12,12}$ = -0.804 cm^{-1}, assuming that the levels are relatively unperturbed. The same band in HCCCDO gives G_o = 642.16cm^{-1} and $(A-\bar{B})'$ = 1.3577cm^{-1} for the level 12^2. For this compound we also see the band 12^2_2 and using the differences $^QQ_{(K-1)}(12^2_1) - {}^QQ_{(K-1)}(12^o_1) - {}^PQ_K(12^2_2) + {}^PQ_K(0^o_o)$ we obtain $G_o(12_2)$ = 499.14cm^{-1} and $(A-\bar{B})''$ = 1.7910cm^{-1} (σ = 0.2cm^{-1}). The 12^2_1 band of HCCCHO has also been analysed in this way and the level 12^2 is seen to be perturbed by a lowering of the ^QQ heads for K < 6 with the heads for K > 5 giving $G_o(12^2)$ = 692.6 cm^{-1} and $(A-\bar{B})'$ = 1.7149 cm^{-1} (σ = 0.05 cm^{-1}).

The $10^1_o12^1_1$ band of HCCCDO has been analysed from the differences $^QQ_K(10^1_o12^1_1) - {}^QQ_K(12^o_1)$ to give $G_o(10^112^1)$ = 739.32cm^{-1} and $(A-\bar{B})'$ = 1.3116cm^{-1}.

We have used the $6^1_o12^1_1$ band of HCCCHO to obtain information about the level 6^112^1 by fitting the differences $^PQ_K(6^1_o12^1_1) - {}^QQ_K(12^o_1)$ to the equation $G_o(6^112^1) + (A-\bar{B})'(K-1)^2 - (A-\bar{B})'_oK^2$. The results of this fit were G_o = 1305.5 cm^{-1} and $(A-\bar{B})'$ = 1.7901cm^{-1}.

IV.3 THE $\tilde{a}^3A'' \longleftarrow \tilde{X}^1A'$ TRANSITION

The vibrational analyses of the $T_1 \longleftarrow S_0$ transitions of HCCCHO and DCCCHO have been reported by Moule and co-workers [42,43] from studies of both the emission and the absorption spectra. Their work has resulted in the assignment of the excited state fundamentals ν'_4 to ν'_{12} for the two compounds and these are reproduced in table 4.24.

During the course of this work it has been possible to obtain spectra of the origin bands and some of the more intense vibrational bands of the first triplet absorption spectrum of HCCCDO and DCCCDO. The origin band for the compound HCCCDO is shown in figure 4.19. The excited state fundamentals measured in this work are reported in table 4.24.

As noted by King and Moule [43] the origin bands show a complex rotational structure (see figure 4.19) and are difficult to analyse. However a series of peaks can be seen extending to lower frequencies from the strong central maximum, which are assigned to unresolved heads caused by $\Delta K = 0$ transitions. A fit of these heads to $T_o + \Delta(A-\bar{B})K^2$ gives first estimates of the electronic origins and the change in $(A-\bar{B})$ on excitation. The results obtained for HCCCHO and DCCCHO from reference [43] are compared to the results for HCCCDO and DCCCDO from this work in table 4.25. We have also been able to complete a similar analysis of the band 9^1_0 in the spectrum of HCCCDO giving ν_o = 24357.91 cm^{-1} and $(A-\bar{B})'_{9}-(A-\bar{B})''_{0}$ = -0.2637 cm^{-1}.

From table 4.25 we see that ethynyl deuteration

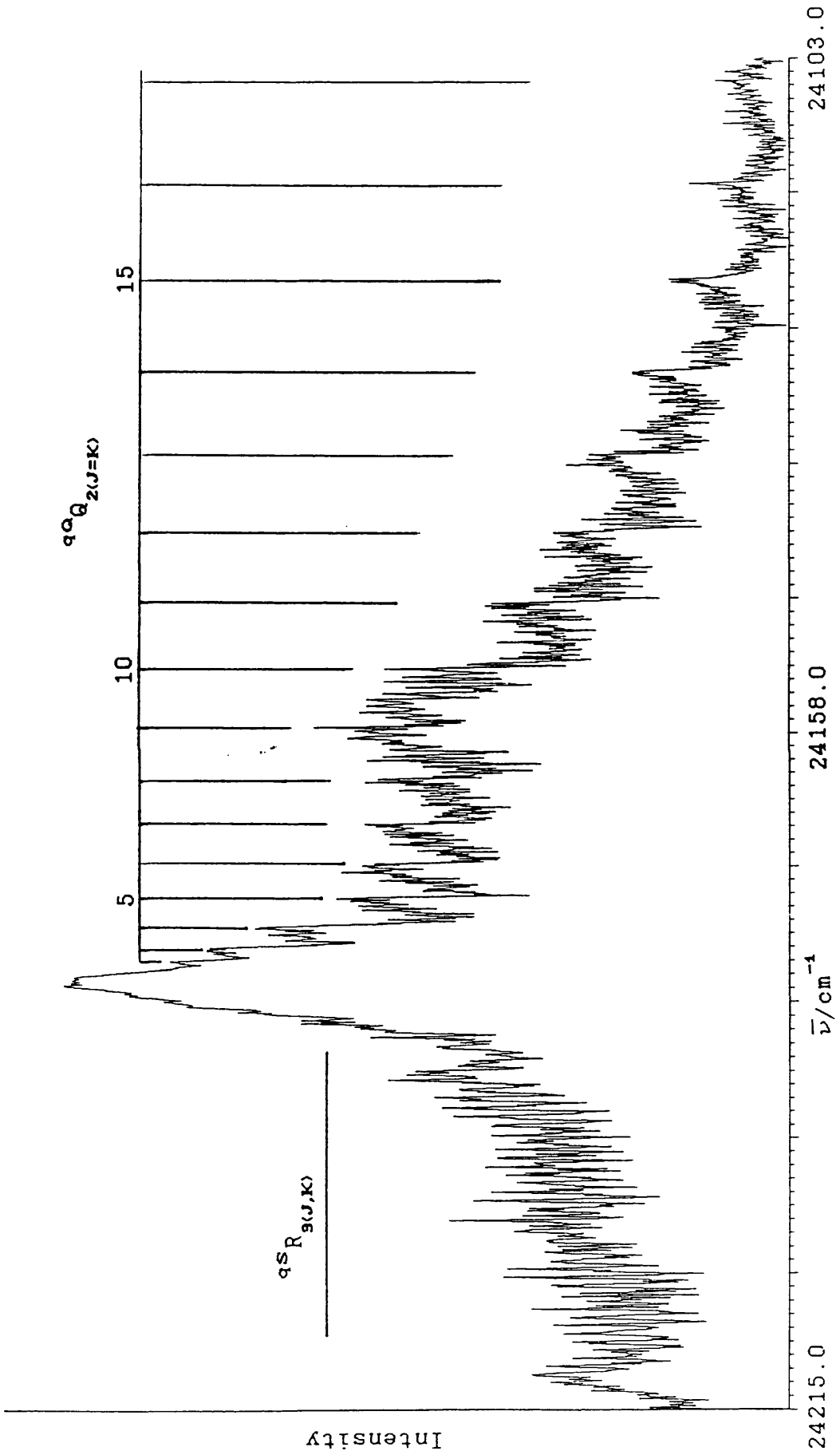

Figure 4.18. The 0_o^o band of the $T_1 \longleftarrow S_o$ transition of HCCCDO

Table 4.24. Fundamental frequencies of propynal in the $\tilde{a}^3A''$ state

mode/cm^{-1}		HCCCHO	DCCCHO	HCCCDO	DCCCDO
ν_1	a'	3330[a]	2538[a]		
ν_2	a'	2951[a]	2951[a]		
ν_3	a'	1952[a]	1872[a]		
ν_4	a'	1323.3	1316.9	–	1291.9[b]
ν_5	a'	1118.4	1116.1	–	–
ν_6	a'	987.6	986.5	–	954[b]
ν_7	a'	664.9	537.3	–	530.4[b]
ν_8	a'	518.0	515.1	–	–
ν_9	a'	181.9	174.4	178.6[b]	172.5[b]
ν_{10}	a''	384.7	383.6	300.5[b]	–
ν_{11}	a''	422.0	315.1	411[c]	–
ν_{12}	a''	340.0	336.0	376.7[b]	372.3[b]

From reference [42] except: (a) calculated from reference [44]; (b) this work; (c) [46].

increases T_o by about 24.3cm^{-1} and aldehydic deuteration leads to an increase in T_o of about 52.5cm^{-1}. These results compare to the increases of 29.0 and 43.6cm^{-1} observed in the S_1 state. We also see a small decrease in $(A-\bar{B})$ (~1%) on ethynyl deuteration whereas aldehydic deuteration leads to a larger decrease in $(A-\bar{B})$ of about 22.5%.

Comparing the changes in $(A-\bar{B})$ on deuteration with those for the S_1 and S_o states we see that on ethynyl deuteration there is a decrease of about 1% compared to

Table 4.25. Partial analyses of the $T_1 \leftarrow S_0$ origin bands

constant/cm^{-1}	HCCCHO[a]	DCCCHO[a]	HCCCDO[b]	DCCCDO[b]
T_0	24126.86	24151.12	24179.31	24203.75
$(A-\bar{B})'_0-(A-\bar{B})''_0$	-0.4090	-0.4039	-0.2573	-0.2574
$(A-\bar{B})'_0$	1.7049	1.6794	1.3165	1.3047

(a) from reference [43] (b) this work.

about 1.5% for the S_1 state and about 1% for the S_0 state, whereas on aldehydic deuteration there is a decrease of about 22.6% compared to 22.6% and 25.3% for the two singlet states.

If we compare the changes of $(A-\bar{B})$ on excitation to the T_1 state from the S_0 level to those on excitation to the S_1 state we see for HCCCHO and HCCCDO a decrease of about 19.3% compared to 18% and for DCCCHO and DCCCDO a decrease of about 16.4% compared to 15%.

Ramsay and co-workers [41] have published a complete rotational analysis of the origin band of the spectrum of HCCCHO and their results are reproduced in table 4.26. These workers have also studied the Stark effect on the rotational structure of this band and have determined the dipole moment of the $\tilde{a}^3A''$ state of HCCCHO (μ'_a) to be 0.5±0.1D [63].

We see from Ramsay's results that on excitation to the T_1 state B_x increases by 2.5% (compared to 1.3% for S_1), B_y increases by 0.7% (compared to a decrease of 0.2%), B_z decreases by 18.3% (15% in S_1), Δ_J increases by 57% (80% in

Table 4.26. Molecular constants of HCCCHO in the $\tilde{a}^3A''$ state

	$\tilde{a}^3A''$ [41]
B_x/cm^{-1}	0.16497 ± 0.00005
B_y/cm^{-1}	0.15122 ± 0.00005
B_z/cm^{-1}	1.8550 ± 0.0002
$\Delta_J \times 10^8/cm^{-1}$	10.0 ± 0.9
$\Delta_{JK} \times 10^6/cm^{-1}$	-7.9 ± 0.2
$\Delta_K \times 10^4/cm^{-1}$	2.84 ± 0.02
$\delta_J \times 10^8/cm^{-1}$	1.8 ± 1.1
$\delta_K \times 10^6/cm^{-1}$	5.0 ± 3.0
a_o/cm^{-1}	0.0099 ± 0.0005
a/cm^{-1}	0.0084 ± 0.0005
α/cm^{-1}	-0.033 ± 0.010
b/cm^{-1}	0.0004 ± 0.0002
β/cm^{-1}	-0.04 ± 0.04
$\varkappa$	-0.9839
$\Delta/amuÅ^2$	0.20
T_o/cm^{-1}	24127.10

S_1), Δ_{JK} increases by 60% (30% in S_1) and Δ_K decreases by 5.3% (5% in S_1).

Lin and Moule [44] have completed a structural calculation for propynal in the T_1 state from the Franck-Condon principle and conclude that the molecule is nonplanar as a result of the aldehydic hydrogen position. The calculated changes in structure on excitation to the T_1 state are $\Delta r(C_1 = O) = +0.095Å$, $\Delta r(C_1 - C_2) = -0.041Å$, $\Delta r(C_2 \equiv C_3) = +0.014Å$, $\Delta r(C_3 - H_2) = +0.005Å$ and $\Delta r(C_1 - H_1) = +0.006Å$ for the bond lengths and $\Delta\theta(C_2C_1O) = -5°31'$, $\Delta\theta(C_1C_2C_3) = +13'$, $\Delta\theta(C_2C_1H_1) = +6°44'$ and $\Delta\theta(C_2C_3H_2) = +1°1'$.

CHAPTER V ENERGY DECAY OF THE EXCITED ELECTRONIC STATES

The various processes for the decay of the excited electronic states of propynal described in section IV.1 are summarised in figure 5.1.

Figure 5.1. Energy level diagram for the decay of the S_1 and T_1 states

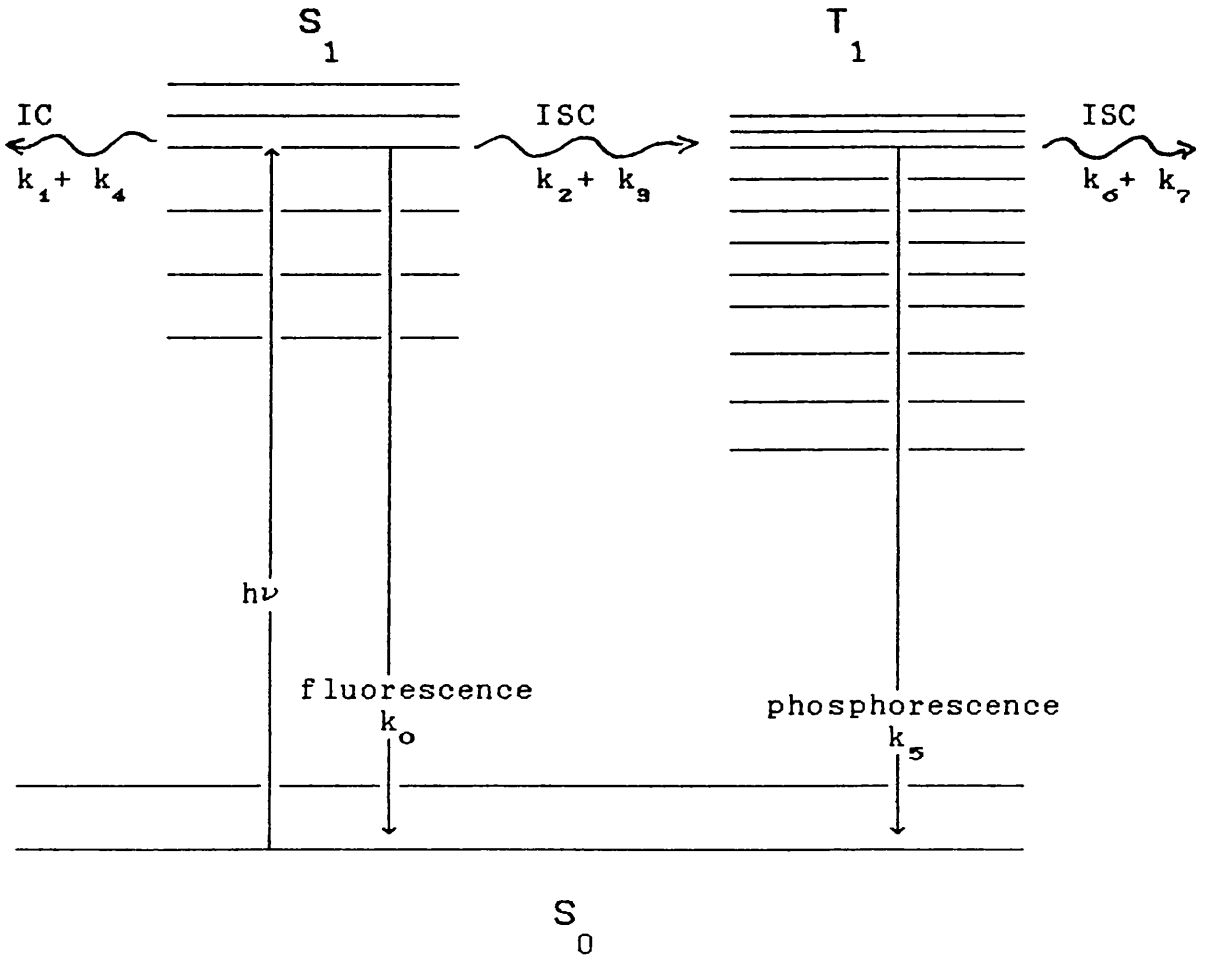

V.1 ENERGY DECAY FROM THE S_1 ELECTRONIC STATE

Thayer and Yardley have measured the lifetime of the vibrationless level of the S_1 state [53] at a pressure of 0.02 torr to be 5.5×10^{-7}s from the fluorescence decay and have extrapolated the zero-pressure lifetime to be 9.78×10^{-7}s. These workers have also studied the effect of collisions on the lifetime of the S_1 state with a number of collision partners.

Subsequently the same workers managed to derive values for each of the rate constants shown in figure 5.1 [52] from Stern-Volmer plots, quantum yields and integrated absorption coefficients in the pressure range of 0.05 to 1.0 torr. Their results for the decay of the S_1 state are $k_0 = (0.12 \pm 0.03)\mu s^{-1}$, $0 \leq k_1 = 0.35 \leq 0.83\ \mu s^{-1}$, $0.12 \leq k_2 = 0.69 < 0.99\ \mu s^{-1}$, $0.0022 \leq k_3 = 0.0094 \leq 0.015\ \mu s^{-1}mtorr^{-1}$ and $0 \leq k_4 = 0.0047 \leq 0.013\ \mu s^{-1}mtorr^{-1}$. These results suggest that both collision-free internal conversion and intersystem crossing occur from the S_1 state and that the dominant collision-induced process is intersystem crossing. Thayer *et al* [54] have also been able to perform similar experiments on some excited vibrational levels of the S_1 state.

Huber and co-workers have performed several studies on the S_1 decay from the vibrationless levels and some of the excited vibronic levels of both HCCCHO and HCCCDO [64,61,65,66]. Their results give a similar lifetime for the vibrationless level of HCCCHO to that found by Thayer and they conclude that the dominant decay process is

internal conversion which is independent of the rotational level. The lifetime of the vibrationless level of HCCCDO is roughly an order of magnitude larger and it is suggested that in this case fluorescence is dominant.

Huber's results for excited vibrational levels suggest that internal conversion is mode dependent and that ν_{10} is the main promoting mode.

As previously mentioned vibronic bands in the $S_1 \leftarrow S_0$ absorption spectrum become noticeably diffuse when higher levels are excited [30] and this broadening of the rotational structure is interpreted as a predissociation [3] caused by a mixing of the eigenfunctions with those of a dissociated state. The 4_0^n progression shows the onset of this diffuseness after the level 4^2 which is about 2600 cm^{-1} above the zero point of the excited state. In figures 5.2 enlarged sections of these bands for n = 0 to 4 are shown for the compound HCCCDO. In these figures the ^PP sub-band structure between $^PQ_7$ and $^PQ_9$ is shown (lower portion) together with the calculated spectrum (upper portion). The frequency scale is $1cm^{-1}$/cm in each case.

The linewidths (full width at half maximum) of the rotational transitions of the stronger bands have been estimated by comparison to calculated spectra for each of the four compounds. These linewidths range from about 0.10 cm^{-1} to about 0.40 cm^{-1} and have been plotted against excess vibrational energy in figure 5.3. The linewidths (fwhm) are related to the lifetimes of the states (τ) by the equation fwhm = $\hbar(1/\tau)$ and hence the observed lifetimes range from 5.31×10^{-11}s to 1.33×10^{-11}s.

Figure 5.2. Linebroadening in the 4_o^n progression of HCCCDO

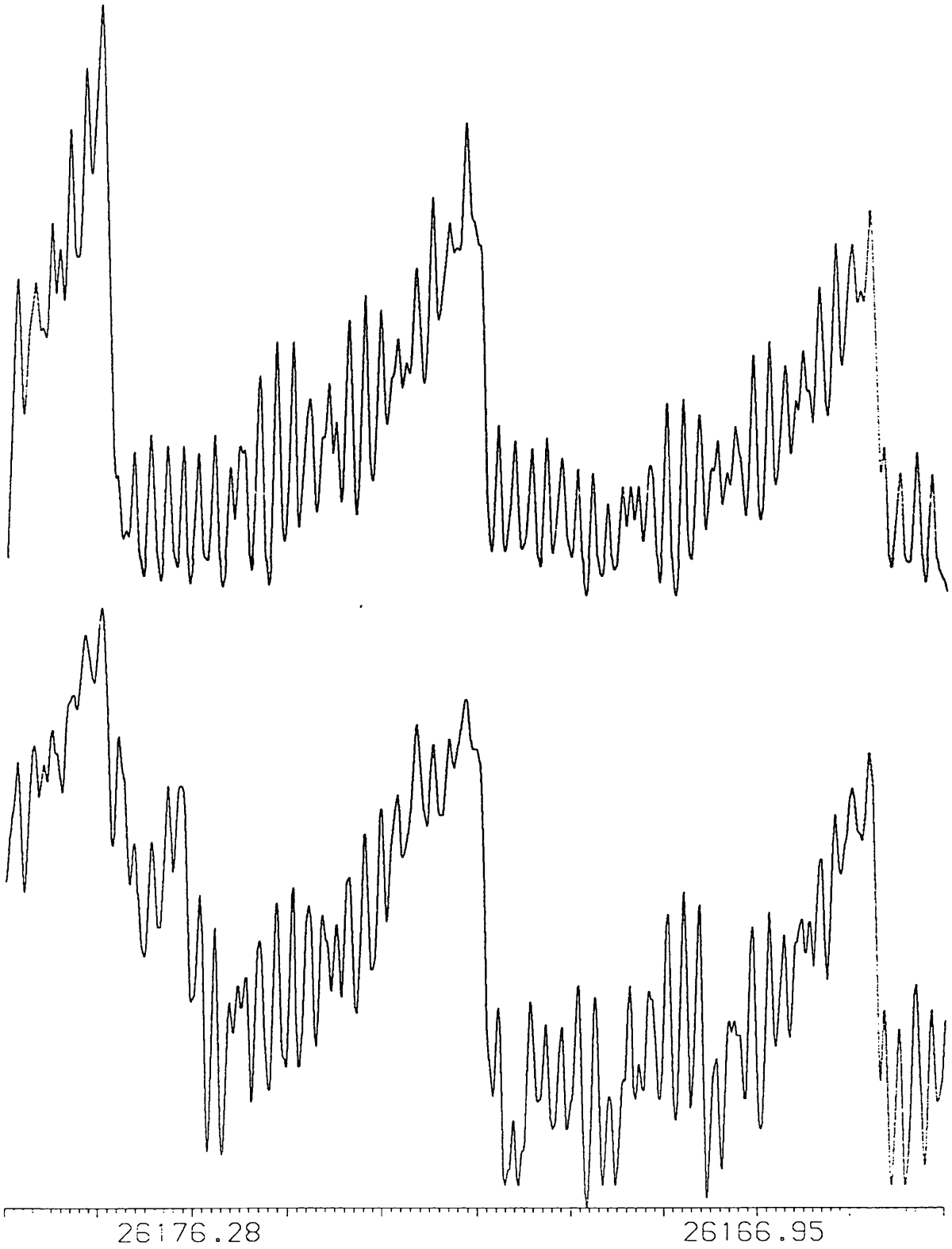

5.2a. $^PQ_7$ to $^PQ_9$ of the 0_o^o band of HCCCDO

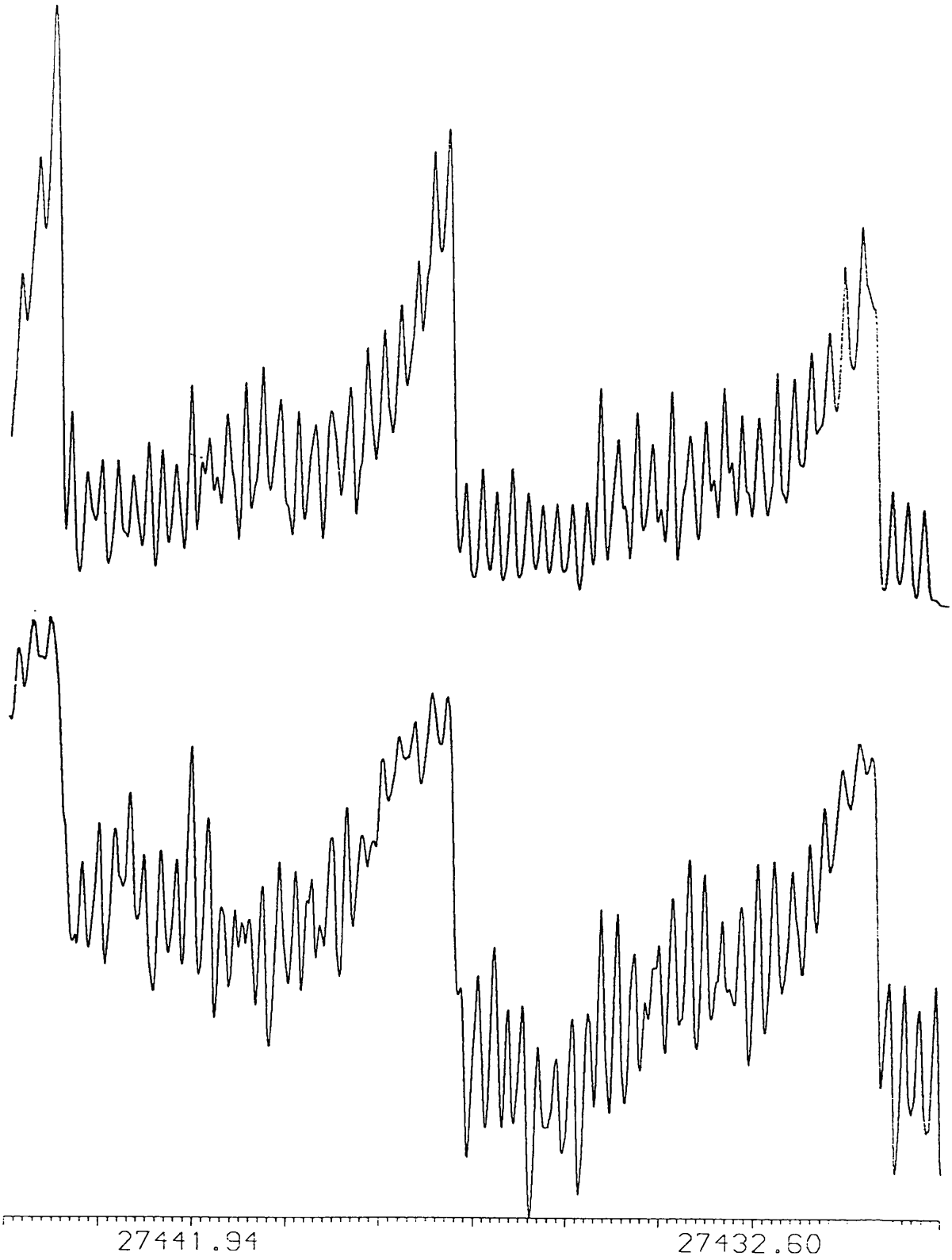

5.2b. $^{P}Q_{7}$ to $^{P}Q_{9}$ of the 4_{0}^{1} band of HCCCDO

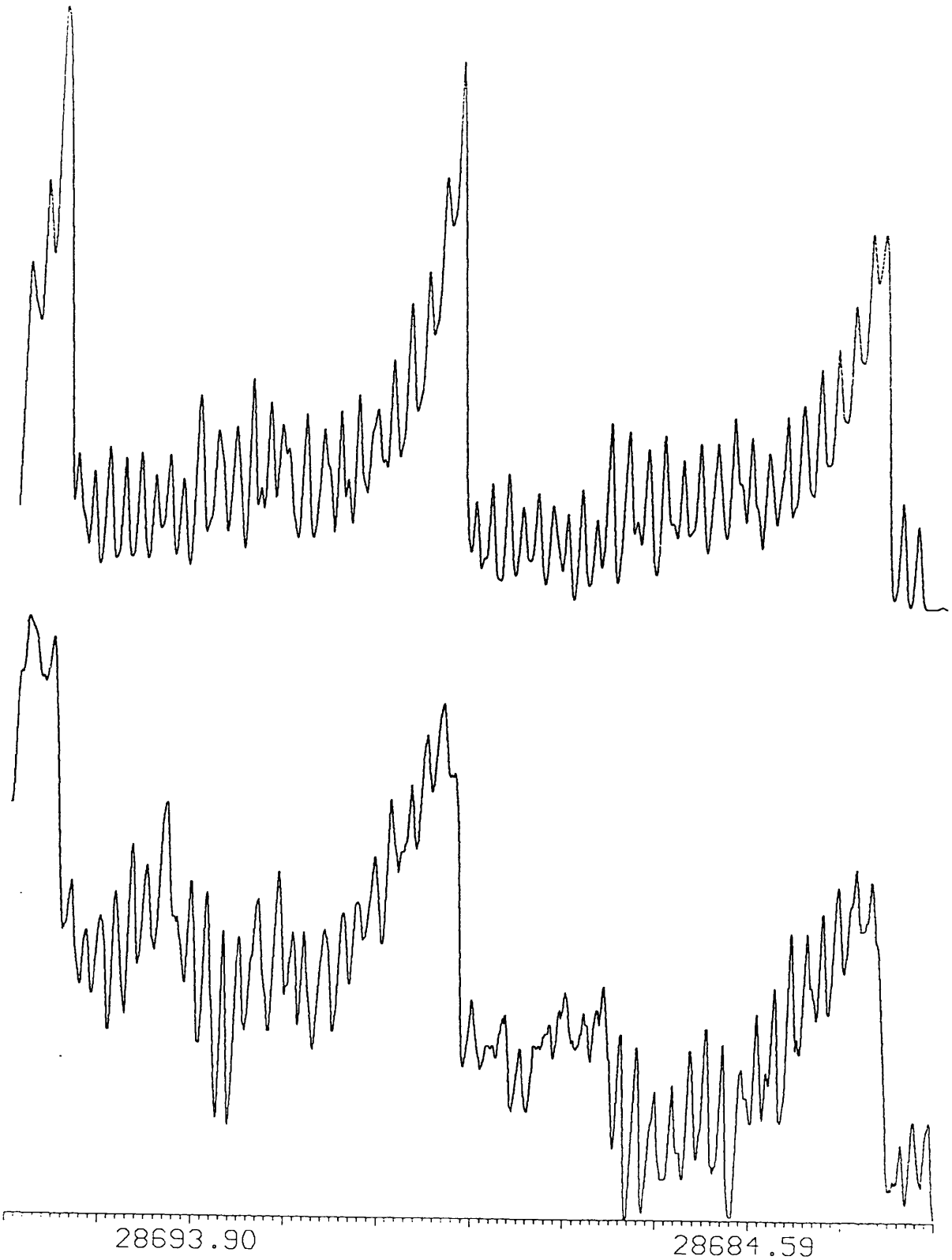

5.2c. $^{P}Q_{7}$ to $^{P}Q_{9}$ of the 4_{o}^{2} band of HCCCDO

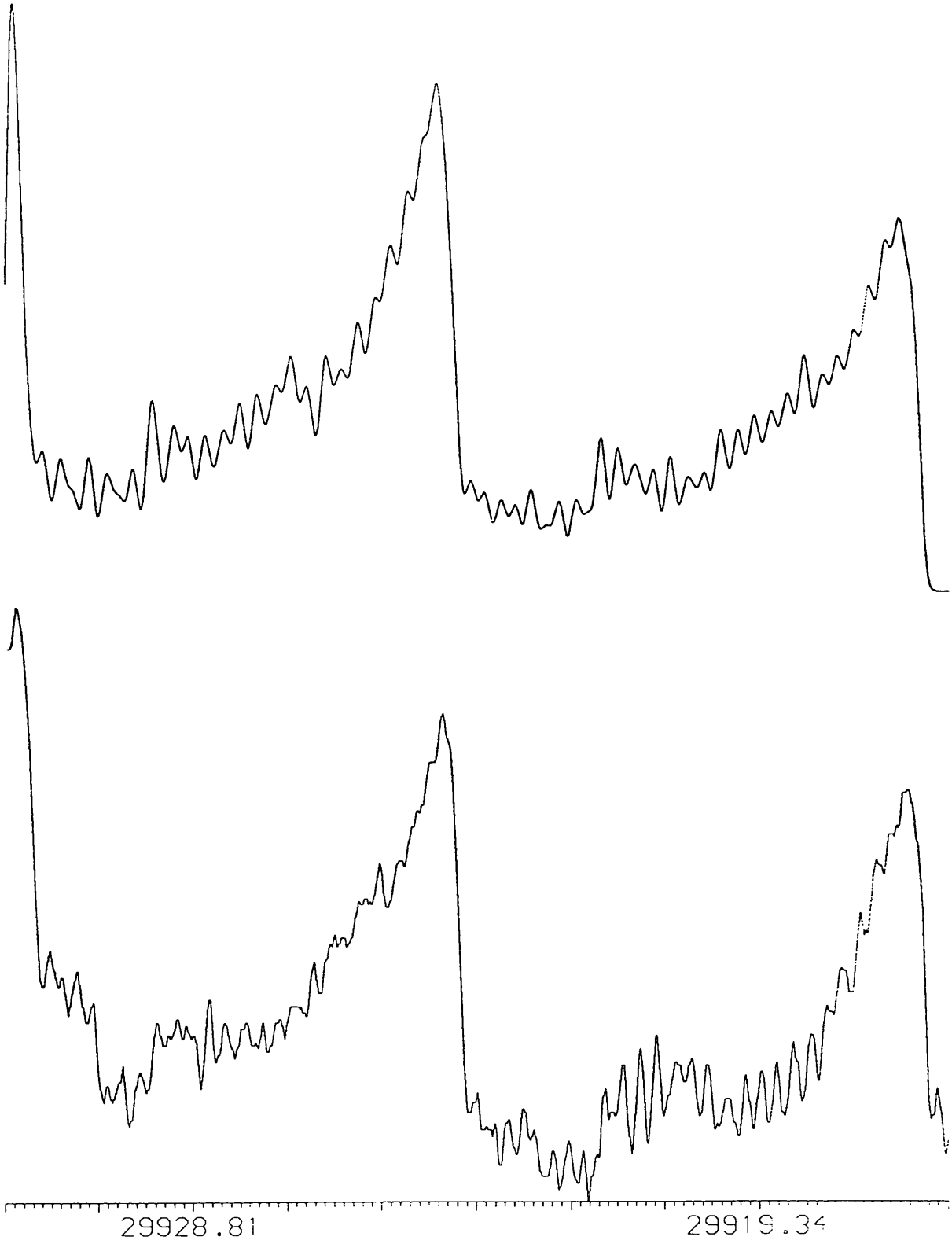

5.2d. $^{P}Q_{7}$ to $^{P}Q_{9}$ of the 4_{0}^{3} band of HCCCDO

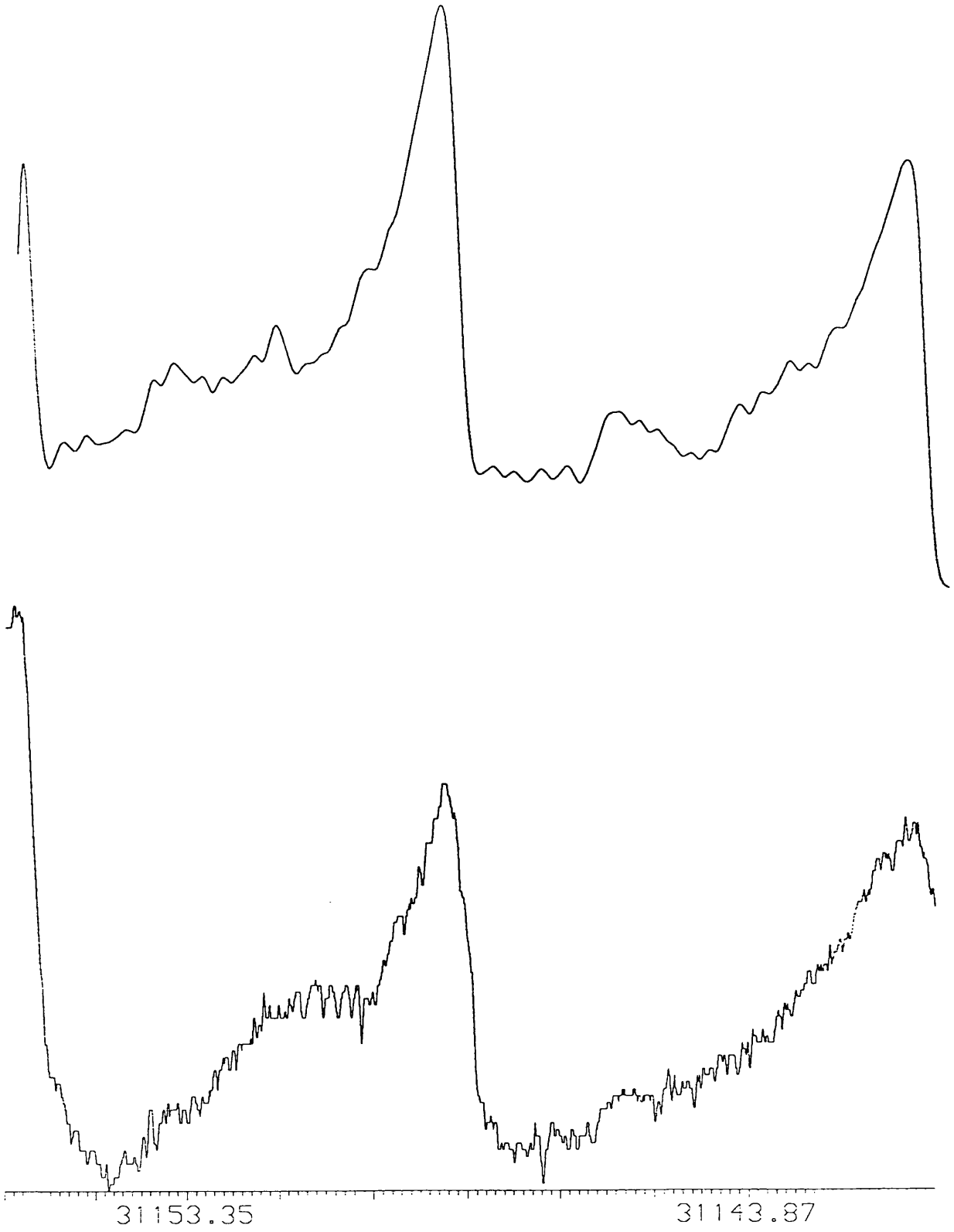

5.2e. $^{P}Q_{7}$ to $^{P}Q_{9}$ of the 4_{0}^{4} band of HCCCDO

From the plots shown in figure 5.3 we see that for each compound the broadening of the rotational structure sets in at an excess vibrational energy of about 3000cm^{-1} and thereafter increases with E_{vib}.

Huber and co-workers [67] have studied the fluorescence and phosphorescence excitation spectra of HCCCHO up to an excess vibrational energy of 6000 cm^{-1} and have determined the relative quantum yield of the photodissociation ϕ_{diss} over this energy range using the assumption that the quantum yield of CO production $\phi_{CO} \approx 2\phi_{diss}$. Their results are plotted in figure 5.4 as quantum yields of fluorescence ϕ_F, phosphorescence ϕ_P and photodissociation against excess vibrational energy.

From Huber's results we see a clear drop in ϕ_P above an excess vibrational energy of about 3000 cm^{-1} and a corresponding increase in in ϕ_{diss}. They conclude that this is due to the onset of a radiationless deactivation pathway which is photochemical in nature. It can clearly be seen that the onset of the effects observed by Huber corresponds well with the onset of linebroadening observed in this work.

The sharp decrease in ϕ_F after the electronic origin band is interpreted as due to a non-radiative channel which is below the onset of photodissociation and is probably caused by internal conversion or intersystem crossing. The later channel is more likely as the strong decrease in fluorescence does not appear to lead to a drop in the phosphorescence.

In a subsequent experiment Huber and Kumar [68] found

Figure 5.3. Plot of linewidth against excess vibrational energy of the S_1 state.

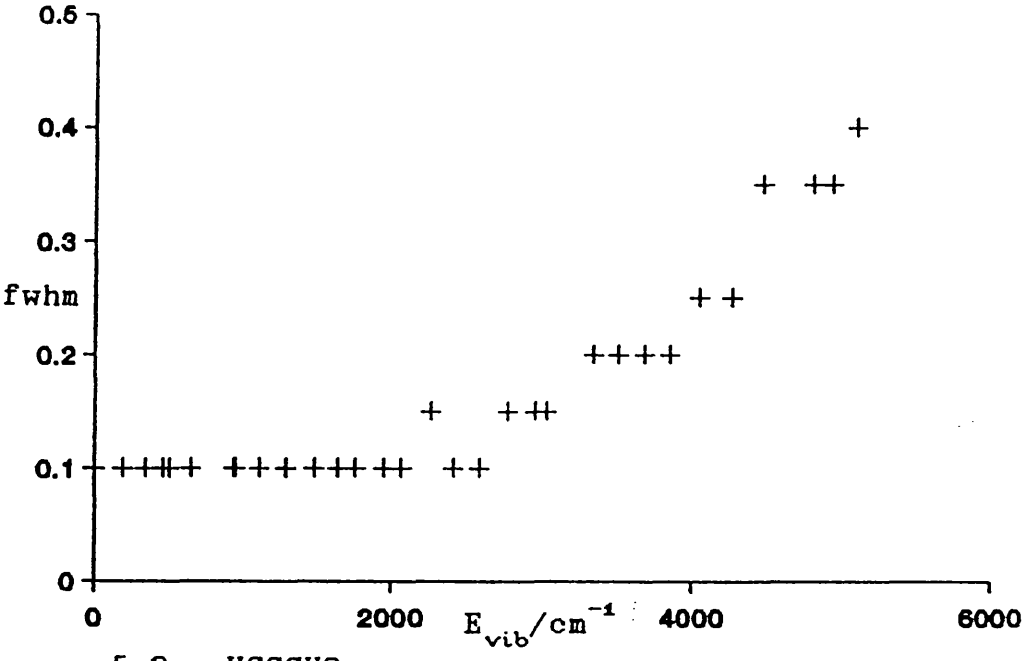

5.3a. HCCCHO

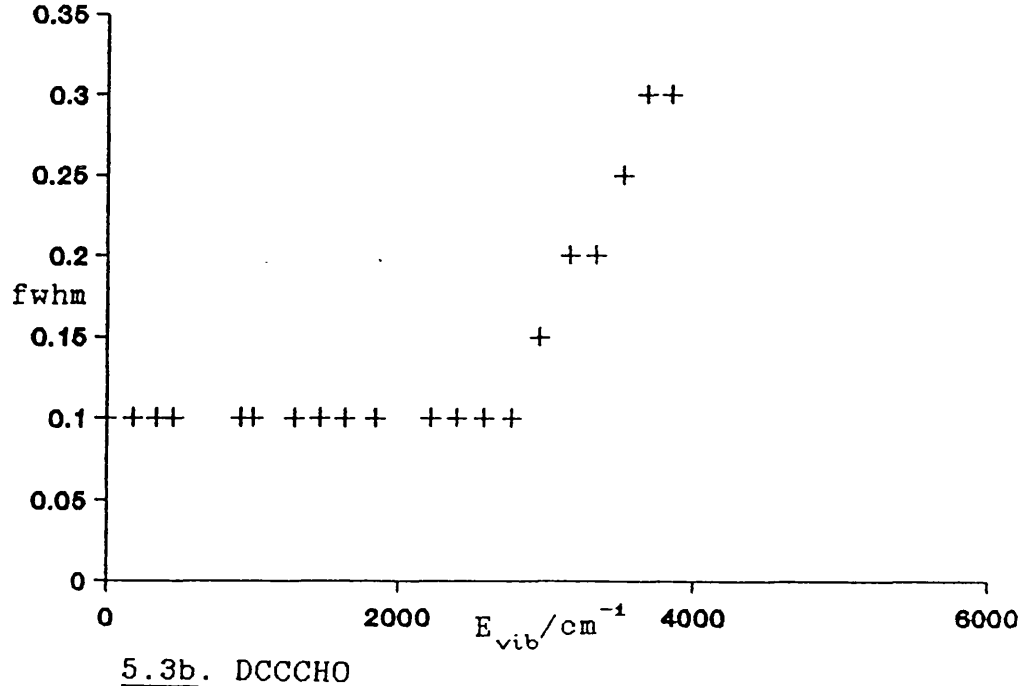

5.3b. DCCCHO

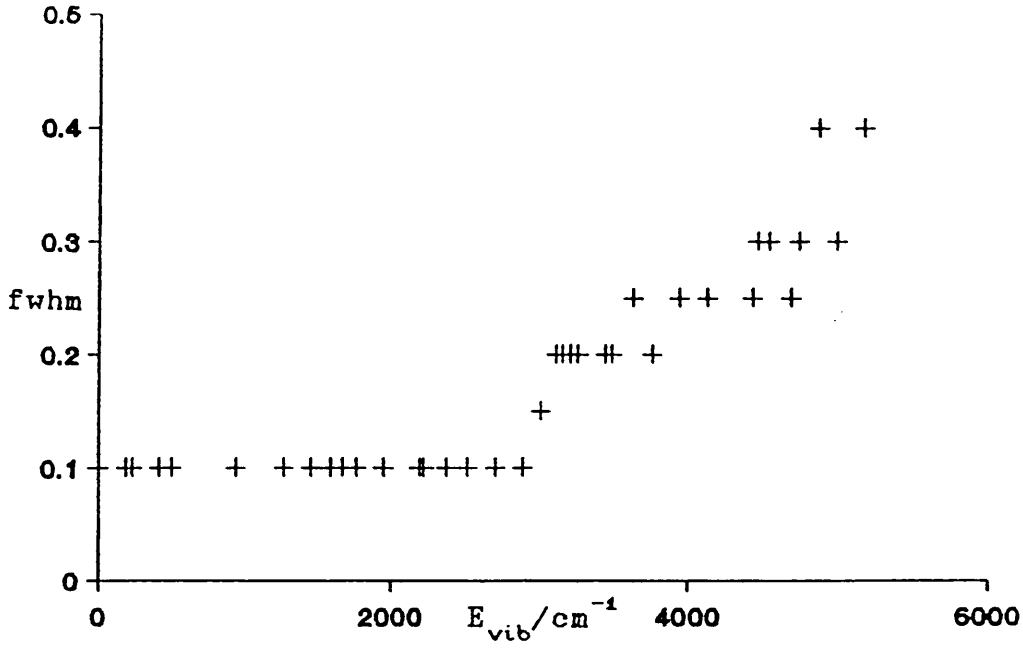

5.3c. HCCCDO

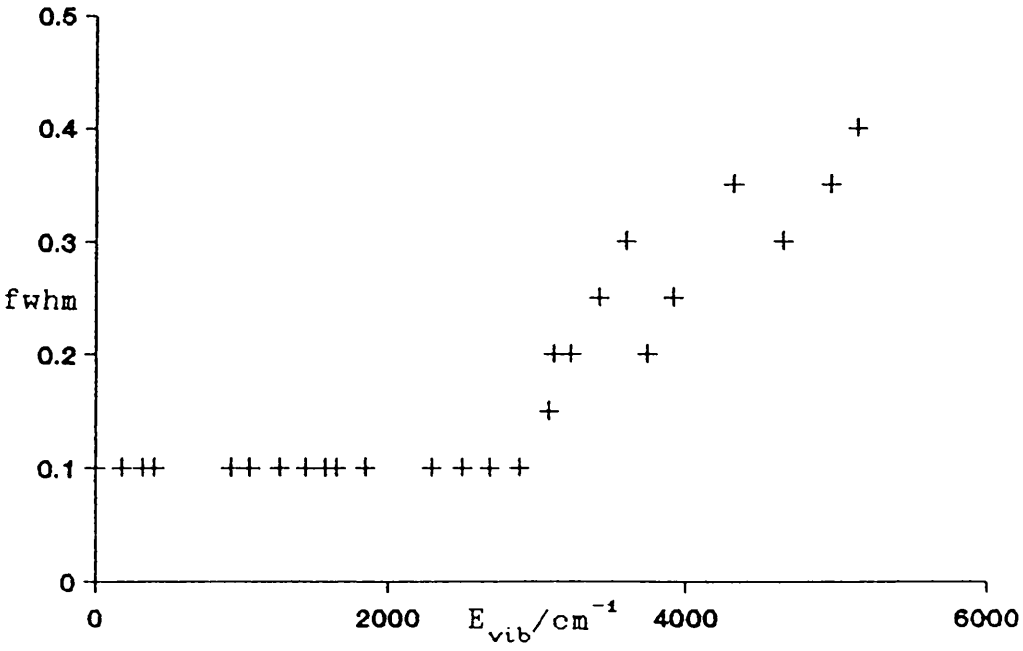

5.3d. DCCCDO

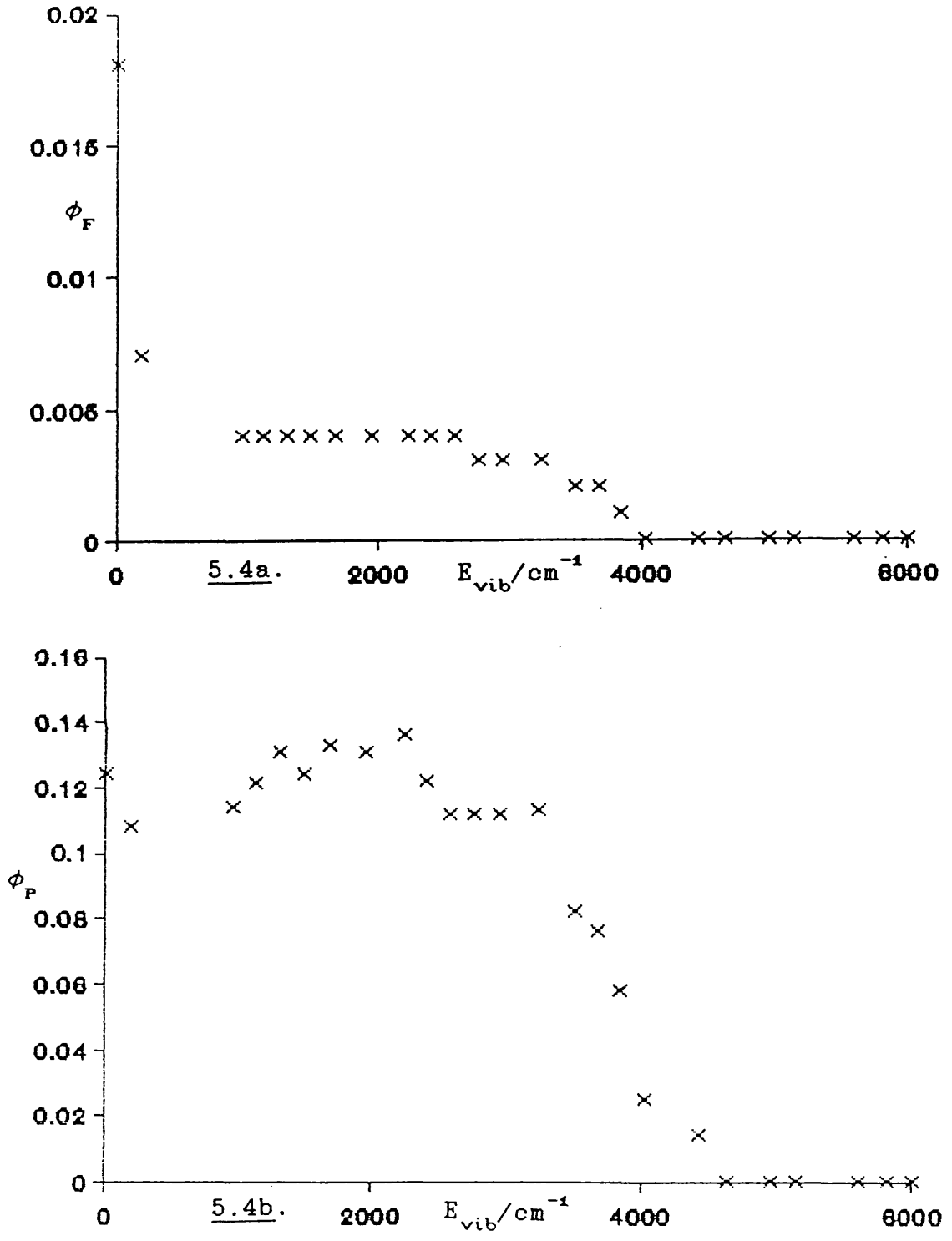

Figure 5.4. Plot of quantum yield of fluorescence, phosphorescence and photodissociation against excess vibrational energy [67]

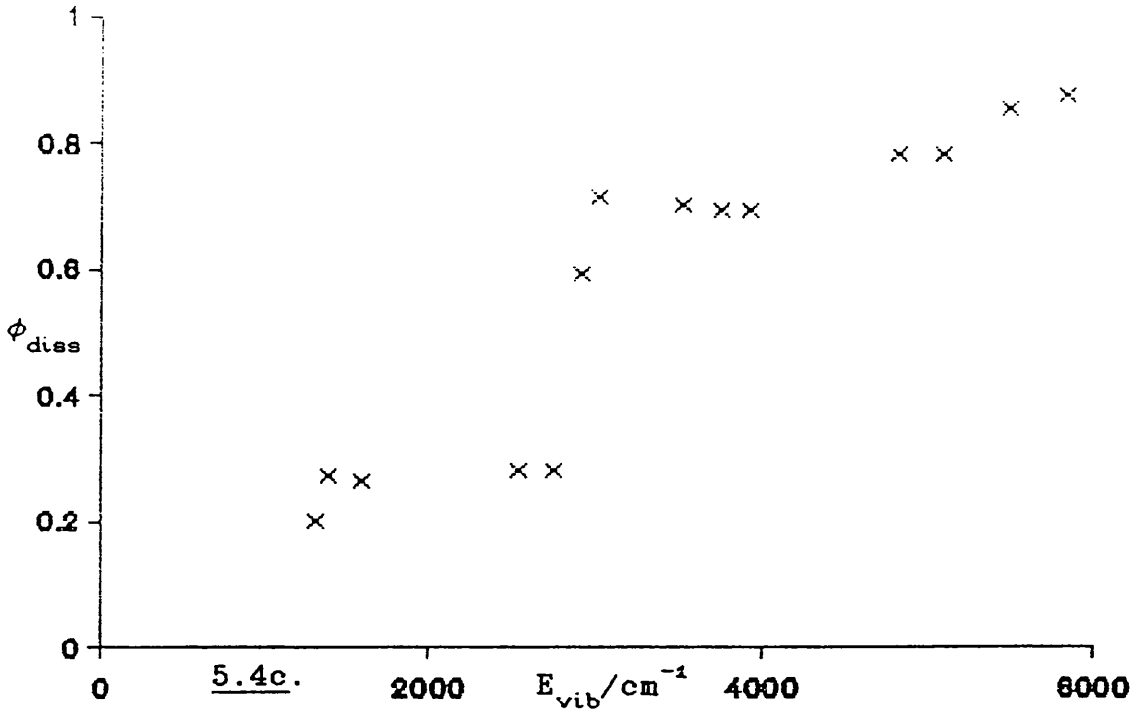

that excitation to some vibronic bands with an excess energy higher than 3000cm^{-1} resulted in a reduced photodecomposition although the phosphorescence intensity was almost zero. These workers concluded, therefore, that there is an additional non-radiative channel above 3000 cm^{-1} and they suggest that this channel is due to internal conversion. This work also suggested that there is a vibronic dependence of the photodecomposition with the level 2^1 being particularly effective in leading to predissociation. However, this result was partly based on the report by Brand *et al* [37] that the 2^1_0 band exhibited a rotationally dependent predissociation in its sub-band

structure. Watson later suggested that this was not the case [30] and in this work we have been able to simulate the observed irregularities in the band by introducing a Coriolis perturbation (see section IV.2.4.2). Huber's work also neglected the fact that this irregular band is in the spectrum of HCCCDO and no similar observations are seen in the 2_0^1 band of HCCCHO, on which his experiments were performed.

In this work we do appear to see some variation of the linebroadening with vibrational level although when we compare the results for the four species there is no obvious correlation suggesting that any particular level promotes predissociation more effectively than the others.

Although there are some inconsistencies between the work of Thayer and Yardley and that of Huber we can make the observation that for low pressures the vibrationless level of the S_1 state of HCCCHO has a lifetime of about 1μs and decays primarily by internal conversion. The excited vibrational levels up to an excess energy of about 3000cm^{-1} have lifetimes of the same order of magnitude and decay primarily by the same route although some levels are seen to promote internal conversion more effectively. Internal conversion demonstrates no simple dependence on rotational level. Intersystem crossing which is negligible for the vibrationless level increases with vibrational energy but is still small at 3000cm^{-1}. At higher pressures (greater than about 6 torr) intersystem crossing becomes dominant and is dependent on the vibrational mode.

For HCCCDO and DCCCDO internal conversion is

inefficient and these compounds probably decay primarily by fluorescence. The lifetimes of the vibrationless levels of the S_1 state of these molecules is of the order of 10μs.

For all four species of propynal the is a sudden decrease in lifetime after an excess energy of about 3000cm^{-1} and this is due to predissociation leading to photodissociation.

V.2 ENERGY DECAY FROM THE T_1 ELECTRONIC STATE

Brühlmann and co-workers have measured the phosphorescence lifetimes of both HCCCHO and HCCCDO between 0.04 and 1.0 torr and their results give the zero pressure lifetimes of the T_1 states to be 3.2×10^{-4}s and 5.9×10^{-4}s respectively [46]. Thayer and Yardley obtained the similar result of 3.83×10^{-4}s [53] for HCCCHO. The increase on deuteration has been attributed to a decrease in the $T_1 \rightarrow S_0$ intersystem crossing with $k_\sigma^H/k_\sigma^D = 2.4$. These workers further conclude that ν_4 and ν_{10} are the dominant accepting modes for the ISC process [46,47].

Thayer and Yardley have determined the rate constants for the T_1 decay of HCCCHO to be $0.0003 \leq k_5 = 0.0008 \leq 0.0018\ \mu s^{-1}$, $0.0016 \leq k_\sigma = 0.0026 \leq 0.0032\ \mu s^{-1}$ and $k_7 = (0.135 \pm 0.009)\times10^{-2} ms^{-1} mtorr^{-1}$ [52].

V.3 COUPLING OF THE S_1 AND T_1 ELECTRONIC STATES

The coupling between the S_1 and T_1 electronic states has been studied by a number of workers. Brand *et al* [57] initially produced evidence for this coupling by observing a shift and/or broadening of 18 rotational lines in the origin band of the absorption spectrum of the $S_1 \leftarrow S_0$ transition of HCCCHO when a Zeeman field was employed. Their results suggest that the vibrational symmetry of the perturbing triplet level is a'' and that the interaction occurs for $\Delta K = 0, \pm 1$, which is consistent with a second order interaction of individual rotational levels of S_1 with individual rotational levels of an excited vibrational state of T_1 by vibronic spin-orbit coupling (type I as described in section I.2.6). They tentatively proposed the vibrational state to be $6^1 7^1 10^1$ and concluded that the zero field perturbations are less than $0.05 cm^{-1}$.

Subsequently, in the course of investigations into the fluorescence decay of single rovibronic levels of the S_1 states of HCCCHO and HCCCDO Huber and co-workers [61,69] observed quantum beat structure in the decay of some levels. They interpreted this behaviour as due to a weak coupling to rotational levels in T_1. They calculated the state density of T_1 to be about 1-10 states/cm^{-1} in the region of the lower vibrational states of S_1. They also concluded that the effect is due to vibronic spin-orbit coupling and observed coupling matrix elements to be in the range $0.2 \leq \nu_{sl}/MHz \leq 8.0$.

Huber and co-workers also studied the Zeeman splittings

in the quantum beat decays of specific rotational levels in the 6^1 vibrational level [70,71,72] allowing the calculation of Landé factors and spin-orbit coupling strengths of individual hyperfine components of the triplet levels involved. In some cases they were able to assign the interacting rotational levels of the triplet state.

From the preliminary results of an anticrossing experiment Pique *et al* [73] suggested that the strength of the S_1- T_1 coupling does not decrease with increasing energy.

CHAPTER VI DISCUSSION

From the results presented in section IV.2.4 we see that there is a vast amount of information available concerning the excited vibrational levels of the first singlet excited electronic state (S_1) of propynal and its deuterated compounds. For many of these levels we have been able to fit the frequencies of the fundamentals and overtone bands to equation 1.5 to obtain the ω_i^c and x_{ii} constants. Similarly from the combination bands we have obtained many of the anharmonicity coefficients of the form x_{ik}. These results are given in appendix 3. As far as possible all levels involving $\nu_i + \nu_k$ have been used to obtain ω_i^o, ω_k^o, x_{ii}, x_{kk} and x_{ik} by a least squares refinement. In a small number of cases the effects of Fermi resonances have not yet been fully explored and hence some of the constants will contain contributions from these resonances.

Brand *et al* have used the fundamental frequencies of the S_1 excited states of HCCCHO, DCCCHO and HCCCDO to obtain estimates of the excited state bond lengths by means of both Badger's and Clark's rules [38]. However this analysis is very approximate and our results do not add anything to the accuracy of the determination of the structure of the excited state. Brand's results give $C_1 = O = 1.325$ Å, $C_2 \equiv C_3 = 1.238$ Å and $C_1 - H_1 = 1.091$ Å.

These workers have also calculated the Teller-Redlich

product [3] for the electronic ground states and for the a" fundamentals of the S_1 states. We have extended the calculation for the excited state to the doubly deuterated compound and to the a' fundamentals using the calculated values of ν_i' [35] and the results are given below. Strictly speaking the zero-order frequencies should be used in this calculation.

Product rule for a" fundamentals:

	calculated	observed
HCCCHO/HCCCDO	1.2397	1.2546
HCCCHO/DCCCHO	1.3318	1.3301
HCCCDO/DCCCDO	1.3348	1.3362
DCCCHO/DCCCDO	1.2425	1.2603
HCCCHO/DCCCDO	1.6548	1.6764

Product rule for a' fundamentals:

	calculated	observed
HCCCHO/HCCCDO	1.9243	1.9366
HCCCHO/DCCCHO	1.8405	1.8563

The results of the partial rotational analyses of many of the bands and of the more complete analyses of a smaller number of the bands have allowed us to calculate many of the constants $\alpha^{(\bar{A}-\bar{B})}$. These results are detailed in appendix 4. The constants were calculated by using the analyses of the lowest frequency vibrations but will in some cases be modified by the effects of Coriolis interactions.

There are a large number of rotational interactions observable in the fine-structure of the vibrational bands of the $S_1 \longleftarrow S_0$ transition and a few of these have been analysed here. There are many bands which have been noted to show perturbations which have yet to be analysed. There are also many whose rotational structures analyse to give anomalous $(A-\bar{B})$ values which therefore indicate rotational interactions.

In this work it has only been possible to perform detailed rotational analyses on the origin bands of the electronic transition for each of the isotopically substituted species of propynal, and transitions to a few of the vibrationally excited bands. In order to extend the analysis, spectra at considerably larger pressures and/or path lengths will need to be recorded and here one is obviously limited by experimental considerations and pressure induced line broadening. From our extensive analyses of the origin bands it is clear that the room temperature spectrum can not give an accurate determination of the asymmetry of the molecule because of the overlapping of rotational lines at low K. This information will only be obtained from low temperature studies similar to those carried out by Huber and co-workers [61,64]. It would also be desirable to obtain the millimetre wave spectra of the molecules HCCCDO and DCCCDO in order to improve the analyses for these two compounds.

The predissociation observed in the $S_1 \longleftarrow S_0$ transition has been followed in this work and no obvious vibrational or rotational dependency was found. However the

higher resolution experiments and more accurate measurements of lifetimes which Huber has performed on some of the lower energy vibronic levels [69] could be helpful in confirming these observations if extended to the higher levels.

APPENDIX 1

Additions to the vibrational analyses of HCCCHO, DCCCHO and HCCCDO in the electronic spectrum.

A1.1 HCCCHO

Frequency/cm^{-1}	Assignment	Intensity	Band type	Separation From 0_0^0
24622.8	$4_1^0 9_2^3$	0.0005	C	-1540.1
24640.2	$4_1^0 8_1^2$	0.001	C	-1522.7
24776.2	5_1^0	0.0005	C	-1386.7
25204.3	$6_1^0 9_1^1$	0.01	C	-958.6
26210.8	$9_2^2 12_1^1$	0.1	C	47.9
26363.7	$10_0^1 12_1^0$	0.2	C	200.8
26553.3	11_0^1	0.1	A	390.4
27174.6	$5_0^1 8_1^1$	0.2	C	1011.7
27474.5	$10_0^2 11_0^1$	-	B	1311.6
27835.8	$6_0^1 9_1^0 10_0^2$	0.3	C	1672.9
29166.7	$4_0^1 6_0^2 9_1^0$	0.3	C	3003.8
29748.3	$4_0^1 6_0^2 9_0^2$	0.5	C	3585.4
30094.6	$4_0^3 12_1^1$	1.0	C	3931.7
30189.3	$4_0^3 8_0^1$	1.0	C	4026.4
30212.3	$4_0^2 5_0^1 9_0^2$	1.2	C	4049.4
30427.6	$2_0^1 4_0^1$	3.0	C	4264.7
30515.6	$2_0^1 4_0^1 12_1^1$	0.5	C	4352.7
30626.0	$2_0^1 4_0^1 9_0^1$	0.5	C	4463.1
30959.0	$4_0^3 6_0^1$	1.0	C	4796.1
31047.3	$4_0^4 9_1^0$	0.1	C	4884.4

A1.1 continued

31090.2	$4_o^3 5_o^1$	0.5	C	4927.3
31252.8	4_o^4	1.0	C	5089.9
31275.8	$4_o^3 5_o^1 9_o^1$	1.0	C	5112.9
31303.0	$4_o^2 5_o^2 9_o^2$	0.5	C	5140.1

A1.2 DCCCHO

Frequency/cm^{-1}	Assignment	Intensity	Band type	Separation From 0_o^o
26876.4	$11_o^2 12_1^1$	0.20	C	684.5
26942.9	$10_o^1 11_o^1$	0.3	C	751.0
27051.0	$10_o^1 11_o^1 12_1^1$	0.3	C	859.1
27072.5	$9_o^1 12_o^2$	0.5	C	880.6
27346.6	$9_o^1 8_o^2$	0.3	C	1154.7
27592.2	$4_o^1 12_1^1$	1.0	C	1400.4
27666.4	$4_o^1 9_o^1$	2.0	C	1474.7
27836.8	$4_o^1 12_o^1$	0.5	A	1645.0
28041.8	3_o^1	1.0	C	1850.0
28410.0	$4_o^1 6_o^1$	3.0	C	2218.2
28589.6	$4_o^1 5_o^1$	4.0	C	2397.8
28770.9	4_o^2	8.0	C	2579.1
28874.0	$4_o^2 12_1^1$	1.0	C	2682.2
28954.6	$4_o^2 9_o^1$	2.0	C	2762.8
29145.2	2_o^1	0.5	C	2953.4
29347.7	$3_o^1 4_o^1$	1.0	C	3155.9
29526.1	$4_o^1 5_o^1 6_o^1$	0.5	C	3334.3
29707.8	$4_o^2 6_o^1$	2.0	C	3516.0
29871.0	$4_o^2 5_o^1$	2.0	C	3679.2
30035.6	4_o^3	2.0	C	3843.8

A1.3 HCCCDO

Frequency/cm^{-1}	Assignment	Intensity	Band type	Separation From 0_0^0
25740.6	$10_1^0 11_0^1$	0.04	C	-465.9
26331.8	$11_0^1 12_1^0$	0.1	C	125.3
26367.4	$10_0^1 12_1^0$	0.3	C	160.9
26666.2	$10_0^1 11_1^2$	0.3	C	459.7
26796.1	$9_1^0 10_0^1 11_0^1$	0.05	C	589.6
27003.1	$8_0^2 9_1^0$	0.1	C	796.6
27008.2	$4_0^1 10_1^0 11_0^1$	0.1	C	801.7
27053.1	$10_0^1 11_0^1 12_1^1$	0.1	C	846.6
28042.0	$3_0^1 8_1^1$	0.5	C	1835.5
28325.4	$4_0^1 10_0^1 11_0^1 12_1^1$	0.2	C	2118.9
28550.7	$2_0^1 12_2^2$	0.3	C	2344.2
28810.4	$4_0^2 8_1^1 9_0^1$	0.5	C	2603.9
29713.2	$4_0^2 9_0^1 10_0^1 11_0^1$	1.5	C	3506.7
30036.0	$4_0^3 12_1^1$	0.2	C	3829.5
30088.1	3_0^2	0.2	C	3881.6
30268.8	$2_0^1 6_0^2$	0.1	C	4062.3
30471.5	$4_0^2 6_0^1 10_0^1 11_0^1$	0.5	C	4265.0
30633.2	$4_0^2 6_0^2$	1.5	C	4426.7
30645.5	$4_0^1 2_0^1 6_0^1 12_1^1$	2.0	C	4439.0
32106.3	$4_0^3 2_0^1$	3.0	C	5899.8
32402.5	4_0^5	2.0	C	6196.0
33317.4	$4_0^4 2_0^1$	0.5	C	7110.9
33611.4	4_0^6	0.5	C	7404.9

APPENDIX 2

Vibrational analysis of DCCCDO.

Frequency/cm^{-1}	Assignment	Intensity	Band type	Separation From 0_0^0
24546.6	4_1^0	0.005	C	-1688.9
25365.3	6_1^0	0.001	C	-870.2
25782.2	$9_1^1 10_1^1$	0.6	C	-453.3
25794.8	10_1^1	0.9	C	-440.7
25974.3	11_1^1	1.4	C	-261.2
25998.4	12_1^0	0.8	A	-237.1
26002.4	9_4^3	0.6	C	-233.1
26013.1	$11_1^0 12_0^1$	0.6	C	-222.4
26016.5	9_3^2	0.9	C	-219.0
26029.9	9_2^1	1.6	C	-205.6
26042.7	9_1^0	2.0	C	-192.8
26110.4	8_1^1	1.2	C	-125.1
26155.0	$7_0^1 8_1^0$	1.8	C	-80.5
26209.8	9_2^2	2.1	C	-25.7
26210.0	$7_1^0 8_0^1$	1.5	C	-25.5
26223.0	9_1^1	2.7	C	-12.5
26235.5	0_0^0	10.0	C	0.0
26254.9	7_1^1	1.9	C	19.4
26283.2	$11_0^1 12_1^0$	1.1	C	47.7
26303.2	$9_1^1 12_1^1$	1.0	C	67.7
26317.1	12_1^1	4.7	C	81.6
26375.7	9_3^4	0.9	C	140.2

A2 continued.

26389.7	9_2^3	1.3	C	154.2
26403.1	9_1^2	3.4	C	167.6
26415.7	9_0^1	6.0	C	180.2
26436.0	$7_1^1 9_0^1$	1.2	C	200.5
26454.1	$9_3^4 12_1^1$	0.1	C	218.6
26469.6	$9_2^3 12_1^1$	0.4	C	234.1
26484.4	$9_1^2 12_1^1$	1.2	C	248.9
26498.4	$9_0^1 12_1^1$	1.4	C	262.9
26555.6	12_0^1	0.9	A	320.1
26568.8	9_2^4	0.2	C	333.3
26582.6	9_1^3	0.3	C	347.1
26595.7	9_0^2	0.4	C	360.2
26636.7	10_0^1	1.1	AB	401.2
26690.7	$8_0^1 9_2^2$	0.2	C	455.2
26705.1	$8_0^1 9_1^1$	0.4	C	469.6
26717.4	8_0^1	1.4	C	481.9
26728.6	$10_0^1 12_1^1$	0.6	AB	493.1
26762.2	7_0^1	0.4	C	526.7
26812.6	11_0^2	0.7	C	577.1
26851.6	$11_0^1 12_0^1$	0.7	C	616.1
26884.7	$8_0^1 9_1^2$	0.1	C	649.2
26897.7	$8_0^1 9_0^1$	0.4	C	662.2
26906.7	$9_1^1 10_0^1 11_0^1$	0.1	C	671.2
26935.6	$10_0^1 11_0^1$	0.4	C	700.1
26943.4	$7_0^1 9_0^1$	0.2	C	707.9
26961.8	$10_0^1 12_0^1$	0.5	C	726.3
26973.4	$6_0^1 9_1^0$	0.5	C	737.9
27025.6	$9_0^1 11_0^1 12_0^1$	0.5	C	790.1

A2 continued.

27048.2	5_0^1	1.1	C	812.7
27051.5	10_0^2	0.6	C	816.0
27116.0	$9_0^1 10_0^1 11_0^1$	0.5	C	880.5
27165.7	6_0^1	5.2	C	930.2
27237.6	$4_0^1 11_1^1$	2.0	C	1002.1
27274.4	$4_0^1 11_1^0 12_0^1$	1.2	C	1038.9
27291.1	$4_0^1 9_2^1$	2.0	C	1055.6
27304.2	$4_0^1 9_1^0$	3.7	C	1068.7
27324.2	$4_0^1 7_1^1 9_1^0$	0.5	C	1088.7
27347.2	$6_0^1 9_0^1$	1.2	C	1111.7
27373.1	$4_0^1 8_1^1$	1.0	C	1137.6
27416.6	$4_0^1 7_0^1 8_1^0$	1.0	C	1181.1
27482.9	$4_0^1 9_1^1$	3.0	C	1247.4
27495.9	4_0^1	11.4	C	1260.4
27514.6	$4_0^1 7_1^1$	1.1	C	1279.1
27546.7	$4_0^1 11_0^1 12_1^0$	1.8	C	1311.2
27576.7	$4_0^1 12_1^1$	5.1	C	1341.2
27649.0	$4_0^1 9_2^3$	1.0	C	1413.5
27661.5	$4_0^1 9_1^2$	3.0	C	1426.0
27674.0	$4_0^1 9_0^1$	7.8	C	1438.5
27692.4	$4_0^1 7_1^1 9_0^1$	0.9	C	1456.9
27756.8	$4_0^1 9_0^1 12_1^1$	1.4	C	1521.3
27808.6	$4_0^1 12_0^1$	1.4	A	1573.1
27840.5	$4_0^1 9_0^2$	0.8	C	1605.0
27883.6	$4_0^1 10_0^1$	2.8	AB	1648.1
27974.7	$4_0^1 8_0^1$	0.8	C	1739.2
28021.4	$4_0^1 7_0^1$	0.5	C	1785.9
28063.3	$4_0^1 9_1^1 11_0^2$	0.5	C	1827.8

A2 continued.

28076.1	$4_0^1 11_0^2$	1.0	C	1840.6
28083.4	3_0^1	1.5	C	1847.9
28101.6	6_0^2	0.5	C	1866.1
28139.8	$4_0^1 8_0^1 9_0^1$	1.0	C	1904.3
28165.5	$3_0^1 12_1^1$	0.8	C	1930.0
28189.5	$4_0^1 10_0^1 11_0^1$	1.0	C	1954.0
28214.2	$4_0^1 10_0^1 12_0^1$	1.0	C	1978.7
28219.1	$2_0^1 9_1^0$	0.5	C	1983.6
28231.2	$4_0^1 6_0^1 9_1^0$	1.0	C	1995.7
28279.8	$4_0^1 10_0^2$	0.8	C	2044.3
28295.1	$4_0^1 5_0^1$	1.0	C	2059.6
28411.0	2_0^1	4.2	C	2175.5
28425.4	$4_0^1 6_0^1$	2.0	C	2189.9
28457.5	$2_0^1 11_0^1 12_1^0$	1.0	C	2222.0
28493.2	$2_0^1 12_1^1$	0.4	C	2257.7
28533.9	$4_0^2 9_2^1$	2.0	C	2298.4
28547.6	$4_0^2 9_1^0$	1.0	C	2312.1
28579.3	$2_0^1 9_1^2$	1.0	C	2343.8
28591.5	$2_0^1 9_0^1$	1.5	C	2356.0
28608.4	$4_0^2 8_1^1$	0.5	C	2372.9
28663.4	$4_0^2 7_0^1 8_1^0$	0.5	C	2427.9
28738.9	4_0^2	8.2	C	2503.4
28759.0	$4_0^2 7_1^1$	1.0	C	2523.5
28792.6	$4_0^2 11_0^1 12_1^0$	1.5	C	2557.1
28820.5	$4_0^2 12_1^1$	1.9	C	2585.0
28905.4	$4_0^2 9_1^2$	5.0	C	2669.9
28919.3	$4_0^2 9_0^1$	7.1	C	2683.8
28938.2	$4_0^2 7_1^1 9_0^1$	0.7	C	2702.7

A2 continued.

28999.7	$4_0^2 9_0^1 12_1^1$	1.0	C	2764.2
29120.0	$4_0^2 10_0^1$	0.9	AB	2884.5
29319.5	$4_0^2 11_0^2$	2.0	C	3084.0
29349.4	$3_0^1 4_0^1$	1.0	C	3113.9
29444.0	$4_0^2 7_0^1 9_0^1$	0.8	C	3208.5
29450.7	$2_0^1 4_0^1 9_2^1$	0.8	C	3215.2
29461.0	$2_0^1 4_0^1 9_1^0$	4.0	C	3225.5
29654.2	$2_0^1 4_0^1$	8.0	C	3418.7
29713.5	$2_0^1 4_0^1 12_1^1$	4.0	C	3478.0
29779.2	$4_0^3 9_1^0$	7.0	C	3543.7
29832.2	$2_0^1 4_0^1 9_0^1$	4.0	C	3596.7
29892.0	$4_0^3 7_0^1 8_1^0$	1.0	C	3656.5
29959.0	$4_0^3 9_1^1$	1.2	C	3723.5
29972.7	4_0^3	5.9	C	3737.2
29989.7	$4_0^3 7_1^1$	0.5	C	3754.2
30046.9	$4_0^3 12_1^1$	2.0	C	3811.4
30150.0	$4_0^3 9_0^1$	3.8	C	3914.5
30171.6	$4_0^3 7_1^1 9_0^1$	0.2	C	3936.1
30549.0	2_0^2	2.0	C	4313.5
30880.0	$2_0^1 4_0^2$	3.5	C	4644.5
31058.8	$2_0^1 4_0^2 9_0^1$	1.0	C	4823.3
31190.4	4_0^4	3.7	C	4954.9
31369.2	$4_0^4 9_0^1$	1.2	C	5133.7

APPENDIX 3

Zero-order vibrational frequencies and anharmonicity coefficients of the S_1 state determined from the ultraviolet absorption spectrum (all in cm^{-1}).

A3.1 HCCCHO

$\omega_2^o + x_{22} = 2949.082$, $\omega_3^o + x_{33} = 1945.643$, $\omega_4^o = 1316.956$,[a]

$\omega_5^o = 1122.138$, $\omega_6^o = 957.369$, $\omega_8^o = 506.147$, $\omega_9^o = 188.821$,[a]

$\omega_{10}^o = 449.541$, $\omega_{11}^o + x_{11} = 385.300$, $\omega_{12}^o = 346.849$,

$x_{24} = 7.307$, $x_{29} = 6.736$, $x_{212} = 5.102$,

$x_{34} = -10.027$, $x_{35} = -7.798$, $x_{39} = -3.690$,

$x_{44} = -12.464$,[a] $x_{45} = -7.519$, $x_{46} = -6.610$, $x_{48} = -2.522$,

$x_{49} = 2.338$, $x_{410} = -9.094$, $x_{411} = 7.596$, $x_{412} = 1.219$,

$x_{55} = -2.854$, $x_{56} = 3.452$, $x_{58} = -0.762$, $x_{59} = -2.435$,

$x_{510} = 0.199$, $x_{511} = 1.142$, $x_{512} = 0.652$,

$x_{66} = -6.245$, $x_{68} = -5.054$, $x_{69} = 2.359$, $x_{610} = -4.986$,

$x_{612} = 2.987$,

$x_{88} = 0.992$, $x_{89} = 1.280$, $x_{810} = -1.268$, $x_{812} = -0.335$

$x_{99} = 0.285$,[a] $x_{910} = 0.031$, $x_{911} = 4.993$, $x_{912} = 0.948$,

$x_{1010} = 12.382$, $x_{1011} = -7.493$, $x_{1012} = 1.681$

$x_{1212} = -0.513$.

[a]Ground state values $\omega_4^o = 1708$, $x_{44} = -11$, $\omega_9^o = 209.5$, $x_{99} = -1.5$ [74].

A3.2 DCCCHO

$\omega_2^o + x_{22} = 2953.088$, $\omega_3^o + x_{33} = 1851.426$,

$\omega_4^o = 1300.780$, $\omega_5^o + x_{55} = 1111.409$, $\omega_6^o + x_{66} = 928.289$,

$\omega_7^o + x_{77} = 528.988$, $\omega_8^o = 486.382$, $\omega_9^o = 182.227$,

$\omega_{10}^o = 441.400$, $\omega_{11}^o = 292.942$, $\omega_{12}^o = 346.717$,

$x_{34} = 6.044$,

$x_{44} = -6.202$, $x_{45} = -5.161$, $x_{46} = 3.509$, $x_{48} = 6.716$,

$x_{49} = 1.175$, $x_{411} = 8.093$, $x_{412} = 4.750$,

$x_{56} = 1.796$, $x_{57} = 4.709$, $x_{58} = 3.005$, $x_{59} = -2.471$,

$x_{512} = 5.823$,

$x_{69} = 7.084$,

$x_{78} = -3.960$, $x_{79} = 1.745$

$x_{88} = 0.712$, $x_{89} = -1.183$,

$x_{99} = -0.039$, $x_{912} = 2.837$,

$x_{1010} = 15.416$, $x_{1011} = 3.553$, $x_{1012} = 4.024$,

$x_{1111} = -0.206$, $x_{1112} = 2.613$,

$x_{1212} = -0.181$.

A3.3 HCCCDO

$\omega_2^o = 2243.0^a$, $\omega_3^o = 1951.678$, $\omega_4^o = 1274.403$,

$\omega_5^o + x_{55} = 823.595$, $\omega_6^o = 945.682$, $\omega_8^o = 498.371$,

$\omega_9^o = 187.805$, $\omega_{10}^o = 401.708$, $\omega_{11}^o = 366.422$,

$\omega_{12}^o = 323.177$,

$x_{22} = -39.0^a$, $x_{24} = -0.4^a$, $x_{26} = -15.1^a$,

$x_{33} = -5.440$, $x_{38} = -1.365$,

$x_{44} = -7.253$, $x_{46} = -7.6^a$, $x_{48} = -4.335$, $x_{49} = -0.915$,

$x_{410} = -2.695$, $x_{411} = 3.249$, $x_{412} = -1.705$,

$x_{66} = -3.279$,

$x_{88} = 1.421$, $x_{89} = -0.500$, $x_{812} = -1.285$,

$x_{99} = -0.166$, $x_{910} = 0.402$, $x_{911} = 0.256$, $x_{912} = -1.693$,

$x_{1010} = 7.720$, $x_{1011} = -7.505$, $x_{1012} = 8.940$,

$x_{1111} = 5.984$, $x_{1112} = -5.811$,

$x_{1212} = -0.956$.

a: From reference [38].

A3.4 DCCCDO

$\omega_2^o = 2196.215$, $\omega_3^o + x_{33} = 1848.700$, $\omega_4^o = 1266.689$,

$\omega_5^o + x_{55} = 812.739$, $\omega_6^o = 929.486$, $\omega_7^o + x_{77} = 527.110$,

$\omega_8^o + x_{88} = 483.244$, $\omega_9^o = 180.018$, $\omega_{10}^o = 397.712$,

$\omega_{11}^o = 282.612$, $\omega_{12}^o + x_{1212} = 320.039$,

$x_{22} = -19.075$, $x_{24} = -18.239$, $x_{29} = -0.602$, $x_{211} = -3.118$,

$x_{212} = -1.728$,

$x_{34} = 5.509$, $x_{312} = -0.989$,

$x_{44} = -6.959$, $x_{45} = -12.830$, $x_{46} = -1.308$, $x_{47} = -0.340$,

$x_{48} = -3.746$, $x_{49} = -0.472$, $x_{410} = -12.552$, $x_{411} = 0.863$,

$x_{412} = -1.555$,

$x_{66} = 2.032$, $x_{69} = 0.270$,

$x_{79} = -0.431$,

$x_{89} = -1.051$,

$x_{99} = -0.066$, $x_{910} = 12.901$, $x_{911} = -0.114$, $x_{912} = 0.829$,

$x_{1010} = 4.363$, $x_{1011} = 12.338$, $x_{1012} = 7.613$

$x_{1111} = 3.113$, $x_{1112} = 7.041$.

APPENDIX 4

Dependence of $(A-\bar{B})$ on vibrational level in the S_1 state.

	$\alpha_v^{(A-\bar{B})}/cm^{-1}$			
v	HCCCHO	DCCCHO	HCCCDO	DCCCDO
2	-0.059	-0.094	-0.023	0.029
3	-0.021	-	0.014	-0.024
4	0.021	-	0.029	0.020
5	0.024	-	-	-
6	-0.039	-	-0.044	-0.074
8	-0.077	-	-0.046	-
9	-	-	0.021	0.018
10	0.036	0.034	0.030	0.044
11	-0.248	-0.167	-0.112	-
12	0.014	0.027	-0.006	-0.003

REFERENCES

1. K.F.Freed, Topics.Appl.Phys, **15**, 23 (1976).
2. M.Born and R.Oppenheimer, Ann.Physik, **84**, 457 (1927).
3. G.Herzberg, Electronic spectra of polyatomic molecules, Van Nostrand, Princeton (1966).
4. J.Franck, Trans.Faraday.Soc, **21**, 536 (1925).
   E.U.Condon, Phys.Rev, **28**, 1182 (1926).
   E.U.Condon, *ibid*, **32**, 858 (1928).
5. F.Duschinsky, Acta Phys.-Chim URSS, **7**, 551 (1937).
6. G.Herzberg and E.Teller, Z.Physik.Chem, **B21**, 410 (1933).
7. E.Fermi, Z.Physik, **71**, 250 (1931).
8. J.K.G.Watson, Vibrational spectra and structure (Ed. J.R.Durig), **6**, 1 (1977).
9. J.M.Hollas, High resolution spectroscopy, Butterworths, London (1982).
10. I.M.Mills, Molecular spectroscopy, 8th European congress, Butterworths, London (1965).
11. H.A.Jahn, Proc.Roy.Soc (London), **A168**, 469 (1939).
12. C.G.Stevens and J.C.D.Brand, J.Chem.Phys, **58**, 3324 (1973).
13. S.P.McGlynn, T.Azumi and M.Kinoshita, Molecular spectroscopy of the triplet state, Prentice-Hall (1969).
14. J.C.D.Brand, W.H.Chan and D.S.Liu, J.Mol.Spectrosc, **50**, 310 (1974).
15. J.C.Sauer, Org.Synth.Collection, **4**, 813 (1963).
16. M.G.Veliev and M.M.Guseinov, Synthesis, 461 (1980).

17. H.McNab, J.Chem.Soc.Perkin II, 1283 (1981).

18. J.H.Callomon and G.G.Chandler, Applied Optics, **8**, 133 (1969).

19. D.L.Albritton, A.L.Schmeltekopf and R.N.Zare, Molecular spectroscopy: Modern research, **2**, Academic Press (1976).

20. J.A.Howe and J.H.Goldstein, J.Chem.Phys, **23**, 1223 (1955).

21. C.C.Costain and J.R.Morton, *ibid*, **31**, 389 (1959).

22. G.Winnewisser, J.Mol.Spectrosc, **46**, 16 (1973).

23. H.Jones, *ibid*, **81**, 21 (1980).

24. M.Takami and K.Shimoda, *ibid*, **59**, 35 (1976).

25. R.C.Benson, R.S.Scott and W.H.Flygare, J.Phys.Chem, **73**, 4359 (1969).

26. M.Takami, J.Mol.Spectrosc, **80**, 301 (1980).

27. M.Takami and M.Suzuki, J.Chem.Phys, **72**, 4089, (1980).

28. R.D.Brown and P.D.Godfrey, Aust.J.Chem, **37**, 1951 (1984).

29. J.C.D.Brand and J.K.G.Watson, Trans.Faraday.Soc, **56**, 1583 (1960).

30. J.K.G.Watson, PhD Thesis, University of Glasgow (1962).

31. G.W.King and D.Moule, Spectrochim.Acta, **17**, 286 (1961).

32. P.Klaboe and G.Kremer, *ibid*, **33A**, 947 (1977).

33. M.Takami and M.Suzuki, J.Mol.Spectrosc, **73**, 144 (1978).

34. K.Tavladorakis, Ph.D Thesis, University of London (1991).

35. D.R.Williams, J.Chem.Phys, **55**, 4578 (1971).

36. J.A.Howe and J.H.Goldstein, J.Amer.Chem.Soc, **80**, 4846 (1958).

37. J.C.D.Brand, J.H.Callomon and J.K.G.Watson, Can.J.Phys, **39**, 1508, (1961).

38. J.C.D.Brand, J.H.Callomon and J.K.G.Watson, Disc. Faraday. Soc, **35**, 175, (1963).

39. J.C.D.Brand, W.H.Chan, D.S.Liu, J.H.Callomon and J.K.G.Watson, J.Mol.Spectrosc, **50**, 304, (1974).

40. J.C.D.Brand, J.Chem.Soc, 858, (1956).

41. F.W.Birss, R.Y.Dong and D.A.Ramsay, Can.J.Phys, **17**, 1810, (1973).

42. C.T.Lin and D.C.Moule, J.Mol.Spectrosc, **37**, 280, (1971).

43. G.W.King and D.Moule, *ibid*, **20**, 331, (1966).

44. C.T.Lin and D.C.Moule, *ibid*, **38**, 136, (1971).

45. H.Stafast, J.Opitz and J.R.Huber, Chem.Phys, **56**, 63, (1981).

46. U.Brühlmann, P.Russegger and J.R.Huber, Chem.Phys.Lett, **75**, 179, (1980).

47. P.Russegger and J.R.Huber, Chem.Phys, **61**, 205, (1981).

48. D.M.Brenner and K.Brezinsky, Chem.Phys.Lett, **67**, 36, (1979).

49. D.M.Brenner, K.Brezinsky and P.M.Curtis, *ibid*, **72**, 202, (1980).

50. D.M.Brenner, J.Chem.Phys, **74**, 494, (1981).

51. M.L.Lesiecki, G.R.Smith, J.A.Stewart and W.A.Guillory, Chem.Phys, **46**, 321, (1980).

52. C.A.Thayer and J.T.Yardley, J.Chem.Phys, **61**, 2487, (1974).

53. C.A.Thayer and J.T.Yardley, *ibid*, **57**, 3992, (1972).

54. C.A.Thayer, A.V.Pocius and J.T.Yardley, *ibid*, **62**, 3712, (1975).

55. See for example:
U.Brühlmann and J.R.Huber, Chem.Phys, **94**, 273, (1985) and references therein.

56. See for example:
P.Schmidt, H.Bitto and J.R.Huber, J.Chem.Phys, **88**, 696, (1988) and references therein.

57. J.C.D.Brand, W.H.Chan and D.S.Liu, J.Mol.Spectrosc, **50**, 310, (1974).

58. P.Russegger and H.Lischka, Chem.Phys, **86**, 31, (1984).

59. P.Russegger and J.R.Huber, *ibid*, **89**, 33, (1984).

60. N.R.Draper and H.Smith, Applied regression analysis, Willey, New York (1981).

61. H.Stafast, H.Bitto and J.R.Huber, J.Chem.Phys, **79**, 3660 (1983).

62. D.F.Kelley, J.H.English, V.E.Bondybey and P.M.Rentzepis, *ibid*, **77**, 697 (1982).

63. R.Y.Dong and D.A.Ramsay, Can.J.Phys, **51**, 2444 (1973).

64. H.Stafast, H.Bitto and J.R.Huber, Chem.Phys.Lett, **93**, 303 (1982).

65. U.Brühlmann, P.Russegger and J.R.Huber, *ibid*, **84**, 479 (1981).

66. U.Brühlmann and J.R.Huber, Chem.Phys, **68**, 405 (1982).

67. D.Kumar and J.R.Huber, Chem.Phys.Lett, **38**, 537 (1976).

68. D.Kumar and J.R.Huber, Ber.Bunsenges.Physik.Chem, **81**, 216 (1977).

69. H.Bitto, H.Stafast, P.Russegger and J.R.Huber, Chem. Phys, **84**, 249 (1984).

70. J.Mühlbach, M.Dubs, H.Bitto and J.R.Huber, Chem.Phys. Lett, **111**, 288 (1984).

71. M.Dubs, J.Mühlbach, H.Bitto, P.Schmidt and J.R.Huber, J.Chem.Phys, **83**, 3755 (1985).

72. M.Dubs, J.Mühlbach and J.R.Huber, *ibid*, **85**, 1288 (1986).

73. J.P.Pique, M.Lombardi, U.Brühlmann and J.R.Huber, J.Phys.Coll, **C7**, 659 (1987).

74. G.H.Atkinson, J.Price, N.Goldstein, G.Rumbles and W.Pfieffer, unpublished results, quoted in: G.H.Atkinson, S.Speiser, N.Goldstein, J.Price and G.Rumbles, J.Mol.Spectrosc, **136**, 356 (1989).